Design of food grade particles with tailored properties using a crystal engineering approach

Panayiotis Klitou

Submitted in accordance with the requirements for the degree of

Doctor of Philosophy

The University of Leeds

School of Food Science and Nutrition

January 2022

The candidate confirms that the work submitted is his own, except where work that has formed part of jointly-authored publications has been included. The contribution of the candidate and the other authors to this work has been explicitly indicated below. The candidate confirms that appropriate credit has been given within the thesis where reference has been made to the work of others. Details of the jointly-authored publications and the contributions of the candidate and the other authors to the work are outlined on the page iv.

List of publications & corresponding thesis chapters:

Chapter 3

Klitou, P., Rosbottom, I., & Simone, E. (2019). Synthonic Modeling of Quercetin and Its Hydrates: Explaining Crystallization Behavior in Terms of Molecular Conformation and Crystal Packing. *Crystal Growth & Design*, *19*(8), 4774–4783.

Chapter 4

Klitou, P., Pask, C. M., Onoufriadi, L., Rosbottom, I., & Simone, E. (2020). Solid-State Characterization and Role of Solvent Molecules on the Crystal Structure, Packing, and Physiochemical Properties of Different Quercetin Solvates. *Crystal Growth & Design*, *20*(10), 6573–6584.

Chapter 5

Klitou, P., Rosbottom, I., Cuoacci, C., Altomare, A., & Simone E. (2021). Quercetin-ethanol solvate: An elusive structure of the popular flavonoid substance

Manuscript ready to be submitted to *Food Chemistry*

Chapter 6

Klitou, P., Rosbottom, I., Karde, V., Heng, Y.Y.J., & Simone E. (2021). Designing particles with optimal surface properties: A study on quercetin solid forms' morphology and surface chemistry

Manuscript ready to be submitted to *JACS*

Further details of the jointly-authored publications and the contributions of the candidate and the other authors to the work are included below:

Details of authorship contributions:

Panayiotis Klitou: designed all the experiments presented in the following publications and conducted the measurements, carried out molecular modelling using Habit 98 software, data analysis and interpretation as well as drafted and edited the manuscripts and replied to the comments from reviewers.

Elena Simone and Ian Rosbottom: provided supervision, feedback and contributed to the proofreading and editing of the manuscript and to the comments from the reviewers.

Synthonic Modeling of Quercetin and Its Hydrates: Explaining Crystallization Behavior in Terms of Molecular Conformation and Crystal Packing

- Dr Ian Rosbottom: crystallographic information files minimization in Materials Studio 2017 software and quantum chemical calculations for the conformational analysis conducted in Gaussian 09. Wrote the conformational analysis results paragraph.

Solid-State Characterization and Role of Solvent Molecules on the Crystal Structure, Packing, and Physiochemical Properties of Different Quercetin Solvates

- Dr Christopher M. Pask: carried out the Single Crystal X-Ray Diffraction experiment and has written the methodology section on that.
- Larisa Onoufriadi: helped with the DSC-TGA experiments.
- Dr Ian Rosbottom: provided the diagrams for Figure 4.3.

Quercetin-ethanol solvate: An elusive structure of the popular flavonoid substance

- Dr Angela Altomare and Dr Corradi Cuocci: provided help and advice on solving some crystal structures from PXRD data they collected. (This work is still in progress and not included in the paper).

Designing particles with optimal surface properties: A study on quercetin solid forms' morphology and surface chemistry

- Dr Vikram Karde: carried out the Inverse Gas Chromatography and BET experiments and written the methodology sections for those.

Rationale for submitting the thesis in an alternative format:

The thesis will be submitted in an alternative format (thesis by publication) due to the fact that the work done is divided into four chapters, which are published or will be soon published as individual papers in peer reviewed journals. The manuscripts and papers are recognized to be relevant to the field of study of my research, they report findings based on original experimental and modelling work and meet the minimum requirements set by the Faculty of Environment at the University of Leeds for the alternative format thesis. The papers and manuscripts are co-authored with my supervisors and other academics who helped with part of the experimental work or with writing up of small sections. Nevertheless, the work was almost entirely carried out by myself and I wrote all four papers. The thesis was constructed as required by the Faculty of Environment protocol for alternative format. A thesis outline is provided in the Introduction.

List of accepted conference abstracts and awards:

Poster presentations

- Klitou P., Rosbottom I., & Simone E. (2018). Exploring the crystallization behaviour of quercetin, a common flavonoid molecule used in the food and nutraceutical industries. *6th International School of Crystallization: Drugs, Foods, Agrochemicals, Minerals, New Materials*. Granada, Spain
- Klitou P., Rosbottom I., Zembyla M., Sarkar A., Murray B., Roberts K., & Simone E. (2018). Molecular modelling of morphology and surface chemistry of quercetin dihydrate crystals. *BACG Conference, University of Limerick*. Limerick, Ireland.
- Klitou P., Rosbottom I., & Simone E. (2018). Molecular modelling of crystal structure and intermolecular packing energetics of quercetin and its hydrates. *Belfast Crystallographic Meeting*. Belfast, N. Ireland.
- Klitou P., Rosbottom I., & Simone E. (2019). Even crystals can get hydrated! *Showcase Poster Conference, University of Leeds*. Leeds, UK
- Klitou P., Rosbottom I., Onoufriade L., & Simone E. (2019). Molecular modelling and experimental study of the crystal structure and morphology of quercetin and its hydrates. *BACG Conference*. London, UK.
- Klitou P., Rosbottom I., & Simone E. (2020). Molecular modelling and experimental study of the crystal structure and morphology of quercetin structures. *University of Leeds PGR Conference*. Leeds, UK
- Klitou P., Rosbottom I., & Simone E. (2021). Understanding the relationship between the crystal structure of different solid forms of quercetin and their physical properties using synthonic modelling. *21st International Symposium on Industrial Crystallization*. (Online event)

Oral presentations

- Klitou P., Rosbottom I., & Simone E. (2018). Molecular modelling of crystal structure and intermolecular packing energetics of quercetin and its hydrates. *University of Leeds PGR Conference*. Leeds, UK
- Klitou P., Rosbottom I., & Simone E. (2019). Molecular modelling of crystal structure, intermolecular packing energetics, morphology and surface chemistry of quercetin and its hydrates. *The 12th European congress of chemical engineering*. Florence, Italy
- Klitou P., Rosbottom I., Onoufriade L., & Simone E. (2020). Relating crystalline physiochemical properties with bulk chemistry of different solid forms of quercetin using molecular modelling and experimental studies. *CCDC Crystal Conversations*. (Online event)
- Klitou P., Rosbottom I., & Simone E. (2021). Determination of the relationship between the crystal structure of different solid forms of quercetin and their surface properties. *BACG Conference*. (Online event)

Awards

- Travel grant for: *6th International School of Crystallization: Drugs, Foods, Agrochemicals, Minerals, New Materials*. Granada, Spain.
- Travel grant for: *Belfast Crystallographic Meeting*. Belfast, N. Ireland.
- IUCr Journals Student Poster Prize for: Klitou P., Rosbottom I., & Simone E. (2018). Exploring the crystallization behaviour of quercetin, a common flavonoid molecule used in the food and nutraceutical industries. *6th International School of Crystallization: Drugs, Foods, Agrochemicals, Minerals, New Materials*. Granada, Spain

Acknowledgements

This PhD journey would not have been the same if I did not have the support from some very important people. First of all I am grateful to my supervisor Elena Simone for giving me the opportunity and honour to work with her and be her first PhD student. Her advice, motivation and vision inspired me and encouraged me to work harder and made me more confident in my abilities. I truly appreciate all the advice and support she gave me in all aspects of this doctoral project, which has also helped me improve as a scientist and shape my professional career. I cannot imagine doing this PhD project with any other supervisor and it was truly a pleasure being her student!

I want to thank Ian Rosbottom, who helped me as a supervisor from the start until the end of this project and offered valuable advice and support, especially with all the modelling work and writing up of papers. I also want to acknowledge Michael Rappolt and Megan Povey for their help and advice. Many thanks go to the friends and colleagues in the School of Food Science and Nutrition, all the technicians and of course the Food Crystal Engineering group which was my academic family during this time. I particularly like to thank: Lorenzo Metilli, Larisa Onoufriade, Arwen Tyler, Nataricha Phisarnchananan, Neil Rigby and Miles Ratcliffe who made this journey easier and more enjoyable.

I gratefully acknowledge the School of Food Science and Nutrition for the financial support during my studies.

Many thanks also to all of my friends for their support, especially those who had the patience to be listening to me during my emotional breakdowns in the difficult pandemic times. A very special thank you to my good friend Morfo Zembyla who was an important part of this journey.

Lastly, I want to thank my family for their unconditional love and support in every possible way all these years. I want to dedicate this thesis to them.

Abstract

Crystalline materials are ubiquitous in the pharmaceutical, food, chemical and agrochemical industries, to name a few. The development of products and formulations containing crystalline solids requires the in-depth understanding and exploration of the various existing solid forms of these substances. At the same time, crystal engineering aims to design molecular crystals with directed properties, based on the knowledge of hydrogen bonding and intermolecular interactions within the crystal lattice. Such knowledge can enable delivering particles with optimized physiochemical properties, such as stability, morphology and surface chemistry, which can ultimately lead to a faster product development and more efficient formulations for specific applications. Therefore, there is a profound need of understanding how these properties related to the crystallographic characteristics of solids.

In this doctoral project, different solid forms of an important food grade flavonoid substance, quercetin, including quercetin anhydrous (QA), quercetin monohydrate (QMH), quercetin dihydrate (QDH), quercetin DMSO-solvate (QDMSO), quercetin ethanol-solvate (QE) and their respective de-solvated forms, were studied in order to understand how the crystallographic structure affects the macroscopic properties of quercetin particles. The strength and nature of the intermolecular pairwise interactions (synthons) in the different structures were calculated and the lattice was comprehensively examined. The modelling work was integrated and validated with experimental solid-state characterization. It was found that crystallization of quercetin from an aqueous solvent favors the formation of hydrates, with QDH being the structure of highest stability at ambient conditions. This is because the water molecules in the lattice satisfy the hydrogen bonding interactions available in the quercetin molecules, allowing

a more planar conformation of this molecule that enable the formation of stronger π-π interactions. It was, further, demonstrated that the stronger hydrogen bonding network between the quercetin and the DMSO molecules in QDMSO can lead to a higher relative thermal stability for the that structure compared to QDH, for which the hydrogen bonds between the quercetin and the water molecules were weaker.

The attachment energy morphological predictions and surface chemistry analysis of quercetin forms, verified by experimental studies on the structures, demonstrated surface anisotropy and heterogeneous surface energies for the quercetin forms. The facet-specific surface chemistry was explained based on the study of the extrinsic synthons. It was shown that overall QDH has more non-polar surfaces compared to QDMSO, whose dominant surface was found to grow by polar hydrogen bonding interactions.

The solid-form landscape of quercetin was also further explored, and four new structures were discovered: two new solvates (QDMSO and QE) and their de-solvated forms. The transformation conditions between the different solid forms were also established.

The approach presented in this work can be extremely useful when designing products and processes involving different solid forms, specifically solvates, and for understanding and controlling the morphology and surface chemistry of crystalline solids. The interlink established between the crystal lattice and the physiochemical properties of quercetin not only elucidates the underlying chemistry behind many crystallization phenomena, such as the formation of solvates and their anisotropic nature, but also assists in enabling the prediction and design of tailor-made crystals with optimal characteristics.

Contents

List of Figures

List of Tables

List of Abbreviations

API	Active Pharmaceutical Ingredient
BFDH	Bravais, Friedel, Donnay and Harker
CIF	Crystallographic information file
CPCM	Conducting polarisable continuum model
CSD	Cambridge structural database
DMSO	Dimethyl sulfoxide
DSC	Differential Scanning Calorimetry
DVS	Dynamic vapour sorption
FD-IGC	Finite dilution Inverse gas chromatography
HSM	Hot stage microscopy
IGC	Inverse gas chromatography
NMR	Nuclear magnetic resonance
PXRD	Powder X-ray diffraction
QA	Quercetin anhydrous
QDH	Quercetin dihydrate
QDMSO	Quercetin-DMSO solvate
QE	Quercetin-ethanol solvate
QMH	Quercetin monohydrate
RH	Relative humidity
SAX	Small angle X-ray scattering
SCXRD	Single crystal X-ray diffraction
SEM	Scanning electron microscopy
TGA	Thermogravimetric analysis

TZVP	Triple zeta with polarisation
VdWs	Van der Waals
VTPXRD	Variable temperature Powder X-ray diffraction
WAX	Wide angle X-ray scattering
XRD	X-ray diffraction

Nomenclature

E_{att}	Attachment energy
E_{latt}	Lattice energy
E_{sl}	Slice energy
K_G	Overall crystal growth coefficient
M_T	Mass of crystals present in supersaturated solution
T_f	Fusion temperature of the solute
V_N	IGC retention volume
W_s	Specific surface area of stationary phase in IGC
d_{hkl}	Distance between Miller planes (slice thickness)
k_m	Mass transfer coefficient
k_r	Surface integration rate constant
n_o	Order of diffraction pattern
r_c	Critical radius
t_R	IGC retention time
t_i	Induction time
t_o	Dead time in IGC
α_{eq}	Solution activity in saturated state
α_{ss}	Solution activity in supersaturated state
γ_{LV}^{d}	Dispersive component of liquid-vapour surface tension
γ_{SV}^{d}	Dispersive component of a solid surface energy
γ_a	Activity coefficient

ε_{hkl}	Surface anisotropy factor
μ_{eq}	Chemical potential of solute molecules in saturated state
μ_{ss}	Chemical potential of solute molecules in supersaturated state
d/a	Electron donor to acceptor ratio
A	Surface area of crystal
B	Rate of secondary nucleation
G	Gibb's free energy
J	Rate of nucleation
N	Stirrer speed
R	Gas constant
R_{hkl}	Rate of growth of facet
S	Supersaturation ratio
T	Temperature
Z	Number of asymmetric units in the unit cell
Z'	Number of molecules in the asymmetric unit
j	James-Martin pressure drop factor
k	Boltzmann constant
m	Mass of crystals
r	Cluster radius
w	Carrier gas flow rate in IGC
x	Molar fraction of solute in solution
ΔH_f	Molar enthalpy of fusion of the solute
ΔC	Degree of supersaturation
γ	Interfacial tension

θ	Angle of X-ray beam diffraction
λ	Wavelength
σ	Supersaturation
τ	Torsion angle between phenyl and pyrone ring

CHAPTER 1 - INTRODUCTION

1.1 Background

Crystallization is one of the oldest unit operations in the chemical industry and it can be seen as a purification technique, a separation process or a branch of particle technology. [1] Crystallization from solution is widely used in the pharmaceutical, chemical, agrochemical, food and cosmetic industries. [2] In the food industry crystals play an important role in the functionality, quality and consumer enjoyment of many food products. For example, the control of size distribution of ice and fat crystals in ice cream ensures that it provides the desired mouthfeel, and a smooth texture that is acceptable for consumers. [3] More recently, research into the crystallization behaviour of cocoa butter aimed to create novel chocolate products providing healthier and more sustainable alternatives to traditional chocolate, by reducing the high saturated fat content using oleofoams stabilized by cocoa butter crystals. [4][5] In the pharmaceutical and nutraceutical industries, crystal purity, polymorphic state, and crystal size and shape are key properties that can impact other physiochemical properties such as bioavailability, flowability, adhesion and other downstream processes as well as storage and handling. [6] Understanding the mechanisms that govern crystallization and improving the ability to control this operation through a crystal engineering approach, is crucial to obtain the desired crystalline phase and, therefore, to manufacture products with tailored physiochemical properties and functionality. Relating product properties with crystallographic information and designing processes that can deliver crystals with the desired characteristics has always been, and will continue to be, important areas of research.

Understanding nucleation from solution, which is the self-assembly of the solute molecules within a solvent, and the effect of crystallization parameters such as choice of solvent,

supersaturation and temperature profiles on the quality of the final product, is perhaps one of the biggest long-term challenges in the crystallization community. Different solid forms of a substance can exist, including polymorphs, solvates and cocrystals. [7] As a multitude of solvents and processing conditions can be used in the manufacturing of crystalline products, it is important to have a clear understanding of the solid form landscape of the crystallizing compound. Solid form screening, which is the activity of generating and analyzing different solid forms of a substance, is an essential part for product development in many industrial sectors that make use of crystalline materials. Solid form screening aims at finding the optimal form in terms of physiochemical properties and stability for a specific product. [8] For example, in the nutraceutical and pharmaceutical industries, solid form screening is performed to identify the solid form with the best profile in terms of bioavailability, thermodynamic stability and biological efficacy, as well as other related properties such as dissolution rate and surface characteristics. [9]

A significant number of marketed pharmaceutical and nutraceutical products contain solvated active pharmaceutical ingredients (APIs) and excipients. [9] Solvates of a substance are multicomponent crystalline solids that contain both the host molecule (organic molecule) and a guest solvent molecule in the crystal lattice. The incorporation of the solvent molecules in the lattice impacts the intermolecular interactions with the host molecule and generates a new unit cell. Consequently, solvated solid forms of a substance could exhibit different physiochemical properties compared to the anhydrous pure form, in an effect analogous to that of polymorphism. [7] These solvated structures could offer improved physiochemical properties for a specific formulation, thus they are often preferred over the pure forms. In addition, crystalline solids may often come in contact with water and other liquid solvents and vapours during various downstream processing steps such as filtration and storage. [9] Therefore, knowledge of the solid form landscape and transformation conditions between the

various forms of a substance is essential to design storage conditions, and avoid any unexpected transformations during manufacturing.

The anisotropic nature of crystalline substances poses another big challenge for industrial crystallization. This arises due to the fact that crystals are made of multiple facets with different chemical nature, resulting from different orientation of the crystal's molecules at each facet. Understanding crystal surface anisotropy is important in many processes that are typical of the manufacturing of particulate products, including milling, granulation and tabletting. [10] This understanding will enable the control and design of particulate products with optimal properties for a specific product, and has been a subject of research for many scientists.

While solid form screening and experimental studies of crystalline solids and their anisotropic properties is an irreplaceable stage for development and manufacturing, molecular modelling of the crystal structures can provide a faster and more economical route for the prediction of many of those properties. This can complement the screening and experimental studies for the solid form characterization and prediction of their properties, especially during the early stages of development where the availability of the material is usually low, and can ultimately aid in engineering crystals with optimal characteristics.

The ability to relate crystal structure to the physiochemical properties of the solid forms and design particles with tailored properties is the basis of crystal engineering. Crystal engineering requires the understanding of intermolecular interactions, or synthons, within the lattice of the crystal structure. [11] Synthons are more specifically defined by Desiraju as "structural units that convey the essential features of a crystal structure". [11] Computational methods for the prediction of the strength, directivity and dispersive nature of the intermolecular interactions within crystalline structures can be used in the prediction of crystal lattice and surface attachment energies, and subsequently to morphological predictions. [12] These methods

require the use of atomistic forcefields for the accurate calculation of the synthon strength between the molecules in the crystal structures. [13][14][15] Synthonic modelling can be used to predict crystal properties based on the spatial arrangements and interaction energies of the molecules within the crystal lattice. Ultimately, this allows molecular-scale design and control of the physiochemical properties of crystalline materials. [16][17]

What is usually the biggest challenge is the ability to link the synthons' strength, directivity and nature to the crystallization behaviour of a molecule from solution, in terms of molecular conformation and morphology, and finally to the particle properties. This link can aid in the understanding of the underlying chemistry behind many crystallization phenomena such as the formation of solvates and hydrates, the anisotropic nature of the crystals and facet-specific surface properties. This has been the focus of this doctoral project. To the author's knowledge there is no other study that follows a similar systematic procedure that combines a multi-angle modelling and experimental methods to gain insight into the crystallization behaviour of the model molecule.

The model compound used in this thesis is quercetin, an important flavonoid substance popular for its vast range of health benefits, and widely used in the food and nutraceutical industries. [18][19][20] The different solid forms of quercetin were investigated both experimentally and computationally to rationalize how and why the different crystallographic structures varied in terms of relative stability and surface properties, and to better understand its crystallization behaviour. The methodology developed and presented here could also aid in the design of other organic molecular crystals and particulate products.

1.2 The model compound: Quercetin

The model compound used in this thesis is quercetin. Quercetin, 2-(3,4-Dihydroxyphenyl)-3,5,7-trihydroxy-4H-chromen-4-one, is a naturally occurring flavonoid, a polyphenolic compound, found in many fruits and vegetables, including onions, tomatoes, apples and berries, but also ingested from tea, wine and vinegar. [21][22] Flavonoids are natural pigments found in most parts of plants and are particularly attractive in the biological and food sciences, due to their known beneficial effects on health. [20][23] Quercetin has stimulated considerable interest in recent years, and it is the most extensively studied flavonoid, due to its significant association between dietary consumption and various health benefits, including antioxidant, anti-inflammatory and antitumor activities. [21][22][24][25] Due to this vast range of biological effects, quercetin finds use in the nutraceutical industry and food supplements. [22] Nutraceuticals are described as medicinal or nutritional components of food claimed to have a medicinal effect on human health, also termed as functional foods. [20][23]

The quercetin molecule consists of a pyrone ring and a phenyl ring, which constitute the hydrophobic part of the molecule and can form hydrophobic interactions such as Van der Waal's forces of attraction. [22][26] The hydrophilic part of the molecule consists of five hydroxyl groups that determine the molecule's biological activity and can act as hydrogen bond acceptors and/or donors, as well as an ether and carbonyl group acting as acceptors for both intramolecular and intermolecular hydrogen bonding. [26][27][28][29]

Quercetin has received ample interest in scientific research due to the various health benefits that it can provide. It has been shown to be an anticancer agent because it can inhibit cell proliferation and angiogenesis and induce apoptosis and cellular senescence. [20] Furthermore, it exhibits a number of properties that lead to cardiovascular protection, for example it is an antioxidative and antiplatelet. The antioxidant behaviour is due to its ability to scavenge oxygen-derived free radicals. [30] Due to the high reactivity of its hydroxyl groups, quercetin

can stabilize the reactive oxygen species by interacting with the reactive compound of the radical and inactivating it. [21][30] Further to these, quercetin has been reported to inhibit tumour growth due to its high affinity to interact with membrane-bound enzymes. For example, it interacts in an inhibitory way with the cytochrome P-450 isozyme specific for polycyclic aromatic hydrocarbon metabolism. [21] Lastly, Quercetin inhibits inflammatory enzymes cyclooxygenase (COX) and lipoxygenase, thereby decreasing inflammatory mediators such as prostaglandins and leukotrienes. [20]

Quercetin occurs in food mainly as glycosides, in a bounded form, with sugars, phenolic acids, alcohols etc. After ingestion, derivatives of quercetin are hydrolysed in the gastrointestinal tract and are then absorbed and metabolized. [26] The content and form of all quercetin derivatives in food is significant for their bioavailability as aglycone. However, due to its poor aqueous solubility, quercetin is poorly absorbed by the body and the major percentage is excreted out, therefore, the bioavailability of quercetin is relatively low, and this severely limits its potential health benefits. [31] The solubility of quercetin dihydrate in water has been measured and it is reported by Srinivas et al. to be as low as 0.00263 g/L at 25 °C. [22] Other studies have tried to measure the solubility in methanol and ethanol solvents, and aqueous solvent mixtures, where the solubility in those solvents was shown to be enhanced. [32][33][34]

Quercetin can exist as anhydrous, monohydrate and dihydrate crystal structures. [21][28][35][36][18] Quercetin dihydrate has been reported to crystallize from evaporation of an aqueous ethanol solution and an aqueous 1-propanol solution. [21][18] The crystal packing and conformation of quercetin in the different structures have been studied extensively. Souza et al. have compared experimental and theoretical ^{1}H NMR shift patterns calculated using the Density Functional Theory (DFT) to predict the molecular structure and conformation of quercetin in solution. [37] They showed that quercetin adopts a less planar conformation in solution compared to a single molecule in the gas phase, owing to the intermolecular

interactions that take place in the liquid phase. [37] Hanuza et al. in 2016 have determined the vibrational spectra of quercetin using FTIR, Raman Spectra as well as DFT quantum chemical calculations. [29] They discussed the role of hydrogen bonds in the stabilization of the structure and have calculated the stable geometry of the molecule. [29]

Although the crystal structure of quercetin dihydrate was solved back in 1985 by Rossi et al. and also reported by Jin et al. in 1989, the difficulty obtaining single crystals of the anhydrous quercetin and quercetin monohydrate of sufficient size and quality for single crystal X-ray diffraction is highlighted in literature. [21][18][38][39] Olejniczak et al. confirmed the existence of an anhydrous form by several experimental techniques such as PXRD, DSC, TGA and NMR, and discussed the impact of the water molecule on the hydrogen bonding network, comparing the anhydrous and dihydrate forms and emphasizing its crucial role in determining the molecular geometry of quercetin. [38] Filip et al. in 2013 followed a multi-technique approach, combining PXRD data with information from ss-NMR and molecular modelling to elucidate the conformation of quercetin in the anhydrous structure and gain insight into the relationship between the hydrogen bonding network and the crystal packing pattern. [39] For quercetin monohydrate, the PXRD pattern was determined in 2011 by Domagata et al. and the multipolar atom model was applied to analyse the structure in terms of its geometry, molecular packing and intra- and intermolecular interactions. [35] The monohydrate structure was nucleated from an acetonitrile solution, however exact experimental procedures remain unclear. The PXRD patterns for the solved quercetin anhydrous, monohydrate, and dihydrate structures are shown in Figure 1.1.

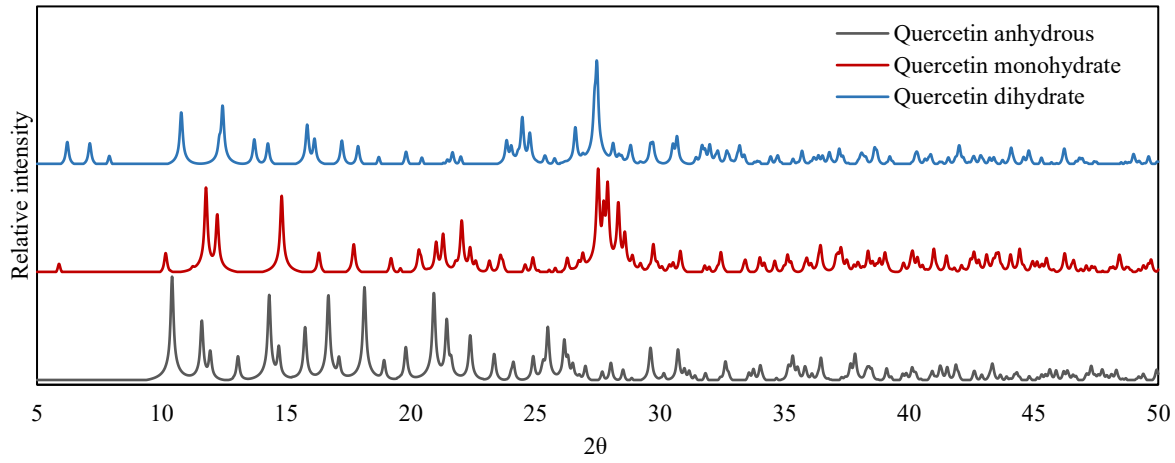

Figure 1.1 PXRD patterns for the known quercetin structures. [21][28][35]

It is reported in literature that often quercetin is commercially available as a mixture of the anhydrous and dihydrate forms, or in mixtures of crystalline structures with a different degree of hydration. [38][40] Borghetti et al. have employed a range of experimental techniques including VTPXRD, DSC/TGA and SEM to study the physiochemical properties and thermal stability of quercetin hydrates. They identified quercetin dihydrate as being the most thermodynamically stable structure compared to samples containing quercetin at different degrees of hydration. They also report that the water molecules in the dihydrate form lead to a lower energy state structure with a minimal potential for transition. [40] Furthermore, a study on the solubilities of quercetin anhydrous and quercetin dihydrate by Srinivas et al. has shown the aqueous solubility of quercetin anhydrous up to 100°C to be higher than that of quercetin dihydrate, implying that quercetin dihydrate is a more stable crystal structure at those conditions. [22]

Quercetin often finds use in numerous applications in the food and nutraceutical industries. [22] Quercetin dihydrate is marketed as a dietary supplement in capsule form, to help improve anti-inflammatory and immune response. [19] In 2018, Zembyla et. al have used quercetin

crystals as a Pickering stabilizer to stabilize water in oil emulsions. They observed that the quercetin crystals absorb at the interface and provide stabilization of water droplets for several days. [41][42] The ability of quercetin to act as a Pickering stabilizer may lead to various soft matter applications where stabilization using biocompatible particles is necessary. [43] More recently, Ma et al. have studied the oral bioavailability of quercetin encapsulated in zein-based Pickering emulsions using a simulated gastrointestinal track. [44] The quercetin-loaded zein colloid particles were prepared from the simultaneous precipitation of quercetin and zein from an aqueous ethanol solution. [44][45] Owing to its poor aqueous solubility and consequently reduced bioavailability, crystal engineering approaches have been followed recently to enhance the solubility and bioavailability of this important flavonoid substance, through the formation of cocrystals. [28][46][47][48] Smith et al. have managed to produce four cocrystals of quercetin with caffeine, caffeine and methanol, isonicotinamide, and theobromine dihydrate. The four cocrystal structures exhibited enhanced degree of solubility when compared to quercetin dihydrate, and therefore improved pharmacokinetic properties. [46]

In this doctoral thesis, the specific model compound has been chosen because it can form a range of intermolecular interactions, including hydrogen bonding and π-π stacking interactions, and due to the fact that it readily forms solvated structures, which has been the focus of the work. The different solid forms of quercetin were investigated both experimentally and computationally to rationalize how and why the different crystallographic structures varied in terms of relative stability and surface properties, and to better understand its crystallization behaviour. The methodology developed and presented here could also aid in the design of other organic molecular crystals and particulate products.

1.3 Aims of the thesis

The present study will try to address the following research questions:

1. What is the solid-form landscape of this important flavonoid substance, and what are the physiochemical properties and transformation conditions of the different solid forms?
2. Rationalize how the level of hydration/solvation of a solid form affects the crystal structure, packing and conformation energetics, in particular: how do the type and strength of the synthons in the lattice change and how does this affect the conformation and packing of the host molecules?
3. Elucidate the role of solvent molecules on the molecular packing and type of synthons in different solvated structures: do different solvent molecules in the lattice form interactions of different strength and polarity? How do these affect the crystal structure and molecular packing?
4. How do the solvent molecules relate to the crystallization behaviour and the physiochemical properties of different solvates?
5. How does surface chemistry vary for the different facets and between different solvates of the same substance? How does the predicted surface chemistry compare to the experimental one?

1.4 Delivery plan

The delivery plan to tackle the aims mentioned above includes both computational and experimental techniques as follow:

1. Crystallization of quercetin from a range of solvents and solvent mixtures, including water, ethanol, and dimethyl sulfoxide, through a range of crystallization techniques including cooling, anti-solvent, and evaporation crystallization.
2. Solid-state characterization of the solid forms using various techniques to assess solid-state stability, surface characteristics and transformation conditions between the different forms.
3. Calculation of the strength, directivity and dispersive nature of the bulk intrinsic intermolecular interactions (synthons) in the different quercetin structures. Characterisation and identification of the important synthons in the lattice.
4. Calculation of the type, strength and direction of the extrinsic synthons. Identification of the important synthons that contribute to the growth of the different facets of the quercetin solid forms. Prediction of surface chemistry of the facets of each form, based on the characterisation of the extrinsic synthons.
5. Prediction of the particle morphology of each quercetin solid form, based on the pair wise intermolecular interactions.

1.5 Thesis Outline

Chapter 2 – *Theoretical Background*

This chapter provides a theoretical background on the basics of crystallization and synthonic modelling.

Chapter 3 - *Synthonic Modelling of Quercetin and Its Hydrates: Explaining Crystallization Behaviour in Terms of Molecular Conformation and Crystal Packing*

The aim of this study was to evaluate the effect of water molecules on the structure, packing energetics and conformation of the model molecule, quercetin. Synthonic modelling was used to compare the type and strength of intermolecular interactions in the structures of the compound at different levels of hydration. The multi-angle modelling methodology proposed here provides insight into hydrate formation and can be extremely valuable when designing products, processes and storage conditions for particulate products with known hydrates. This chapter was published in the peer-reviewed journal *Crystal Growth & Design, vol. 19, no. 8, pp. 4774–4783, Aug. 2019.*

Chapter 4 - *Solid-State Characterization and Role of Solvent Molecules on the Crystal Structure, Packing and Physiochemical Properties of Different Quercetin Solvates*

In this work a novel solvated structure of quercetin was discovered and characterized using a range of experimental and computational techniques. The findings were compared to other known solvated structures of quercetin to evaluate the effect of the solvent molecules on the type and strength of intermolecular interactions, conformation and packing arrangements in the solvated crystal. This information was then related to the physiochemical properties of these structures. This proposed working framework can assist when designing particulate products with known solvated forms. This chapter was published in the peer-reviewed journal *Crystal Growth & Design, vol. 20, no. 10, pp. 6573–6584, Oct. 2020.*

Chapter 5 – *Quercetin-ethanol solvate: An elusive structure of the popular flavonoid substance*

In this chapter the crystallization behaviour of quercetin in different ethanol-water solvent mixtures was investigated. Two novel solid forms, a weak quercetin-ethanol solvate and its de-solvated structure, were discovered and characterised by a range of analytical techniques. The work assisted in building up the solid form landscape and transformation conditions of

quercetin, which is widely used in many formulations. This chapter will be submitted to the peer-reviewed journal, *Food Chemistry*.

Chapter 6 – *Designing particles with tailor-made surface properties: A study on quercetin solid forms*

In this chapter the aim was to study the facet specific surface properties of different solid forms of quercetin, using molecular modelling and experimental techniques. The main goal was to determine the relationship between crystallographic structure and the surface anisotropic properties. The extrinsic synthons and surface energies of the different solid forms were calculated and related to the facet specific polarity. This chapter will help in understanding and controlling the morphology and surface chemistry of crystalline solids, to enable engineering particles with the most desirable characteristic and interfacial behaviour. This chapter will be submitted to the peer-reviewed journal, *JACS*.

Chapter 7 – *Conclusion and future studies*

This chapter consists of a summary and discussion of the main results as well as conclusions in relation to the main research problems and areas for future studies.

Appendices – Appendices A, B and C provide the supporting information for Chapters 4, 5 and 6, respectively.

References

[1] John Garside and Roger Davey, *From Molecules to Crystallizers An Introduction to Crystallization*. Oxford Science Publications, 2000.

[2] E. Simone, "Application of process analytical technology (PAT) tools for the better understanding and control of the crystallization of polymorphic and impure systems Certificate of originality," no. December, 2015.

[3] R. W. Hartel, "Advances in Food Crystallization," *Annu. Rev. Food Sci. Technol.*, vol. 4, no. 1, pp. 277–292, 2013, doi: 10.1146/annurev-food-030212-182530.

[4] L. Metilli, A. Lazidis, M. Francis, S. Marty-Terrade, J. Ray, and E. Simone, "The Effect of Crystallization Conditions on the Structural Properties of Oleofoams Made of Cocoa Butter Crystals and High Oleic Sunflower Oil," *Cryst. Growth Des.*, vol. 21, no. 3, pp. 1562–1575, Mar. 2021, doi: 10.1021/acs.cgd.0c01361.

[5] H. Ewens, L. Metilli, and E. Simone, "Analysis of the effect of recent reformulation strategies on the crystallization behaviour of cocoa butter and the structural properties of chocolate," *Curr. Res. Food Sci.*, vol. 4, pp. 105–114, 2021, doi: https://doi.org/10.1016/j.crfs.2021.02.009.

[6] M. A. Lovette, A. R. Browning, D. W. Griffin, J. P. Sizemore, R. C. Snyder, and M. F. Doherty, "Crystal shape engineering," *Ind. Eng. Chem. Res.*, vol. 47, no. 24, pp. 9812–9833, 2008, doi: 10.1021/ie800900f.

[7] S. R. Vippagunta, H. G. Brittain, and D. J. W. Grant, "Crystalline solids," vol. 48, pp. 3–26, 2001.

[8] J. Aaltonen, M. Allesø, S. Mirza, V. Koradia, K. C. Gordon, and J. Rantanen, "Solid

form screening – A review," *Eur. J. Pharm. Biopharm.*, vol. 71, no. 1, pp. 23–37, 2009, doi: https://doi.org/10.1016/j.ejpb.2008.07.014.

[9] A. M. Healy, Z. A. Worku, D. Kumar, and A. M. Madi, "Pharmaceutical solvates, hydrates and amorphous forms: A special emphasis on cocrystals," *Adv. Drug Deliv. Rev.*, vol. 117, pp. 25–46, 2017, doi: 10.1016/j.addr.2017.03.002.

[10] E. Hadjittofis, M. A. Isbell, V. Karde, S. Varghese, C. Ghoroi, and J. Y. Y. Heng, "Influences of Crystal Anisotropy in Pharmaceutical Process Development," 2018.

[11] G. R. Desiraju, "Crystal engineering: From molecule to crystal," *J. Am. Chem. Soc.*, vol. 135, no. 27, pp. 9952–9967, 2013, doi: 10.1021/ja403264c.

[12] G. Clydesdale, K. J. Roberts, and R. Docherty, "HABIT95 — a program for predicting the morphology of molecular crystals as a function of the growth environment," *J. Cryst. Growth*, vol. 166, no. 1–4, pp. 78–83, Sep. 1996, doi: 10.1016/0022-0248(96)00056-5.

[13] S. L. Mayo, B. D. Olafson, and W. A. Goddard, "DREIDING: a generic force field for molecular simulations," *J. Phys. Chem.*, vol. 94, no. 26, pp. 8897–8909, Dec. 1990, doi: 10.1021/j100389a010.

[14] A. T. Hagler, S. Lifson, and P. Dauber, "Consistent force field studies of intermolecular forces in hydrogen-bonded crystals. 2. A benchmark for the objective comparison of alternative force fields," *J. Am. Chem. Soc.*, vol. 101, no. 18, pp. 5122–5130, Aug. 1979, doi: 10.1021/ja00512a002.

[15] F. A. Momany, L. M. Carruthers, R. F. Mcguire, and H. A. Scheraga, "Intermolecular Potentials from Crystal Data . III . Determination of Empirical Potentials and Application to the Packing Configurations and Lattice Energies in Crystals of

Hydrocarbons , Carboxylic Acids , Amines , and Amides1," vol. 78, no. 16, pp. 1595–1620, 1974, doi: 10.1021/j100609a005.

[16] J. Pickering, R. B. Hammond, V. Ramachandran, M. Soufian, and K. J. Roberts, "Synthonic Engineering Modelling Tools for Product and Process Design," in *Engineering Crystallography: From Molecule to Crystal to Functional Form*, K. J. Roberts, R. Docherty, and R. Tamura, Eds. Dordrecht: Springer Netherlands, 2017, pp. 155–176.

[17] I. Rosbottom and K. J. Roberts, "Crystal Growth and Morphology of Molecular Crystals BT - Engineering Crystallography: From Molecule to Crystal to Functional Form," K. J. Roberts, R. Docherty, and R. Tamura, Eds. Dordrecht: Springer Netherlands, 2017, pp. 109–131.

[18] G. Z. Jin, Y. Yamagata, and K. Tomita, "Structure of quercetin dihydrate," *Acta Crystallogr. Sect. C Cryst. Struct. Commun.*, vol. 46, no. 2, pp. 310–313, 1990, doi: 10.1107/S0108270189006682.

[19] Y. Li *et al.*, "Quercetin, inflammation and immunity," *Nutrients*, vol. 8, no. 3, pp. 1–14, 2016, doi: 10.3390/nu8030167.

[20] A. V. Anand David, R. Arulmoli, and S. Parasuraman, "Overviews of biological importance of quercetin: A bioactive flavonoid," *Pharmacogn. Rev.*, vol. 10, no. 20, pp. 84–89, 2016, doi: 10.4103/0973-7847.194044.

[21] M. Rossi, L. F. Rickles, and W. A. Halpin, "The crystal and molecular structure of quercetin: A biologically active and naturally occurring flavonoid," *Bioorg. Chem.*, vol. 14, no. 1, pp. 55–69, 1986, doi: 10.1016/0045-2068(86)90018-0.

[22] K. Srinivas, J. W. King, L. R. Howard, and J. K. Monrad, "Solubility and solution

thermodynamic properties of quercetin and quercetin dihydrate in subcritical water," *J. Food Eng.*, vol. 100, no. 2, pp. 208–218, 2010, doi: 10.1016/j.jfoodeng.2010.04.001.

[23] P. M. Shah, V. Vishnu Priya, and R. Gayathri, "Quercetin – A flavonoid:A systematic review," *J. Pharm. Sci. Res.*, vol. 8, no. 8, pp. 878–880, 2016.

[24] Z. Luo, B. S. Murray, A. Yuso, M. R. a Morgan, M. J. W. Povey, and A. J. Day, "Particle-Stabilizing Effects of Flavonoids at the Oil - Water Interface," *J. Agric. ...*, vol. 59, pp. 2636–2645, 2011.

[25] M. Ay, A. Charli, H. Jin, V. Anantharam, A. Kanthasamy, and A. G. Kanthasamy, "Quercetin," *Nutraceuticals*, pp. 447–452, Jan. 2016, doi: 10.1016/B978-0-12-802147-7.00032-2.

[26] M. MATERSKA, "Quercetin and Its Derivatives : Chemical Structure and Bioactivity -a Review," *Polish J. food Nutr. Sci.*, vol. 58, no. 4, pp. 407–413, 2008.

[27] E. Grotewold, *The science of flavonoids*. 2006.

[28] K. Vasisht, K. Chadha, M. Karan, Y. Bhalla, A. K. Jena, and R. Chadha, "Enhancing biopharmaceutical parameters of bioflavonoid quercetin by cocrystallization," *CrystEngComm*, vol. 18, no. 8, pp. 1403–1415, 2016, doi: 10.1039/C5CE01899D.

[29] J. Hanuza *et al.*, "Vibrational Spectroscopy Molecular structure and vibrational spectra of quercetin and quercetin-5 ' -sulfonic acid," vol. 88, pp. 94–105, 2017, doi: 10.1016/j.vibspec.2016.11.007.

[30] P. Kavuru, "Crystal Engineering of Flavonoids," *Cryst. Eng. Flavonoids*, 2008.

[31] A. D. Gilley *et al.*, "Novel cellulose-based amorphous solid dispersions enhance quercetin solution concentrations in vitro," *Carbohydr. Polym.*, vol. 157, pp. 86–93, 2017, doi: https://doi.org/10.1016/j.carbpol.2016.09.067.

[32] L. Chebil, C. Humeau, J. Anthony, F. Dehez, J. M. Engasser, and M. Ghoul, "Solubility of flavonoids in organic solvents," *J. Chem. Eng. Data*, vol. 52, no. 5, pp. 1552–1556, 2007, doi: 10.1021/je7001094.

[33] M. H. Abraham and W. E. Acree, "On the solubility of quercetin," *J. Mol. Liq.*, vol. 197, pp. 157–159, 2014, doi: 10.1016/j.molliq.2014.05.006.

[34] R. S. Razmara, A. Daneshfar, and R. Sahraei, "Solubility of Quercetin in Water + Methanol and Water + Ethanol from (292.8 to 333.8) K," vol. 2, no. 2, pp. 3934–3936, 2010.

[35] S. Domagała, P. Munshi, M. Ahmed, B. Guillot, and C. Jelsch, "Structural analysis and multipole modelling of quercetin monohydrate - A quantitative and comparative study," *Acta Crystallogr. Sect. B Struct. Sci.*, vol. 67, no. 1, pp. 63–78, 2011, doi: 10.1107/S0108768110041996.

[36] E. E. Nifant'ev *et al.*, "On the problem of identification of the dihydroquercetin flavonoid," *Russ. J. Gen. Chem.*, vol. 76, no. 1, pp. 161–163, Jan. 2006, doi: 10.1134/S1070363206010324.

[37] L. A. De Souza, W. M. G. Tavares, A. P. M. Lopes, M. M. Soeiro, and W. B. De Almeida, "Structural analysis of flavonoids in solution through DFT 1 H NMR chemical shift calculations : Epigallocatechin , Kaempferol and Quercetin," *Chem. Phys. Lett.*, vol. 676, pp. 46–52, 2017, doi: 10.1016/j.cplett.2017.03.038.

[38] S. Olejniczak and M. J. Potrzebowski, "Solid state NMR studies and density functional theory (DFT) calculations of conformers of quercetin†," pp. 2315–2322, 2004.

[39] X. Filip, I. Grosu, and M. Micla, "NMR crystallography methods to probe complex hydrogen bonding networks : application to structure elucidation of anhydrous

quercetin 3," pp. 4131–4142, 2013, doi: 10.1039/c3ce40299a.

[40] G. S. Borghetti, J. P. Carini, S. B. Honorato, A. P. Ayala, J. C. F. Moreira, and V. L. Bassani, "Thermochimica Acta Physicochemical properties and thermal stability of quercetin hydrates in the solid state," *Thermochim. Acta*, vol. 539, pp. 109–114, 2012, doi: 10.1016/j.tca.2012.04.015.

[41] M. Zembyla, B. S. Murray, and A. Sarkar, "Water-in-Oil Pickering Emulsions Stabilized by Water-Insoluble Polyphenol Crystals," *Langmuir*, vol. 34, no. August, pp. 1–7, 2018, doi: 10.1021/acs.langmuir.8b01438.

[42] M. Zembyla, A. Lazidis, B. S. Murray, and A. Sarkar, "Water-in-Oil Pickering Emulsions Stabilized by Synergistic Particle − Particle Interactions," 2019, doi: 10.1021/acs.langmuir.9b02026.

[43] M. Zembyla, B. S. Murray, and A. Sarkar, "Water-in-oil emulsions stabilized by surfactants , biopolymers and / or particles : a review," *Trends Food Sci. Technol.*, vol. 104, no. July, pp. 49–59, 2020, doi: 10.1016/j.tifs.2020.07.028.

[44] J. Ma, X. Huang, S. Yin, Y. Yu, and X. Yang, "Bioavailability of quercetin in zein-based colloidal particles-stabilized Pickering emulsions investigated by the in vitro digestion coupled with Caco-2 cell monolayer model," *Food Chem.*, vol. 360, no. April, p. 130152, 2021, doi: 10.1016/j.foodchem.2021.130152.

[45] A. R. Patel, P. C. M. Heussen, J. Hazekamp, E. Drost, and K. P. Velikov, "Quercetin loaded biopolymeric colloidal particles prepared by simultaneous precipitation of quercetin with hydrophobic protein in aqueous medium," *Food Chem.*, vol. 133, no. 2, pp. 423–429, 2012, doi: 10.1016/j.foodchem.2012.01.054.

[46] A. J. Smith, P. Kavuru, L. Wojtas, M. J. Zaworotko, and R. D. Shytle, "Cocrystals of

Quercetin with Improved Solubility and Oral Bioavailability," *Mol. Pharm.*, vol. 8, no. 5, pp. 1867–1876, Oct. 2011, doi: 10.1021/mp200209j.

[47] J. O'Mahony, S. Wei, A. Molinelli, and B. Mizaikoff, "Imprinted Polymeric Materials. Insight into the Nature of Prepolymerization Complexes of Quercetin Imprinted Polymers," *Anal. Chem.*, vol. 78, no. 17, pp. 6187–6190, Sep. 2006, doi: 10.1021/ac060446j.

[48] H. He, Y. Huang, Q. Zhang, J.-R. Wang, and X. Mei, "Zwitterionic Cocrystals of Flavonoids and Proline: Solid-State Characterization, Pharmaceutical Properties, and Pharmacokinetic Performance," *Cryst. Growth Des.*, vol. 16, no. 4, pp. 2348–2356, Apr. 2016, doi: 10.1021/acs.cgd.6b00142.

CHAPTER 2 – THEORETICAL BACKGROUND

2.1 Crystal structures and Miller Indices

Crystallization is a process of solid formation which results in a highly organized 3D structure, in which the constituent atoms, molecules or ions are characterized by long range order. [1] The smallest repeating unit in a crystal structure is known as the "asymmetric unit". Several asymmetric units are related to each other by symmetry to complete the unit cell, which is then repeated infinitely in three dimensions to create a crystal lattice. The unit cell is described by the unit cell parameters, which consist of three axis a, b, c and three angles α, β, γ. [1]

Crystals are classified into specific crystal systems according to the degree of symmetry. There are seven different crystal systems, which are characterized with specific axis lengths and angles between the axis. Within some crystal systems the molecules can be arranged into different positions in the lattice, resulting in four different space lattice types. The combination of the lattice type and the seven crystal systems forms the 14 Bravais lattices to one of which all crystal structures belong. [2] The classification of the 14 Bravais lattices is shown in Figure 2.1. Highly symmetric crystal systems are more likely to crystallize in simple atomic systems. Increasing the complexity of the molecular species can result in the molecules crystallizing in lower symmetry classes. [2]

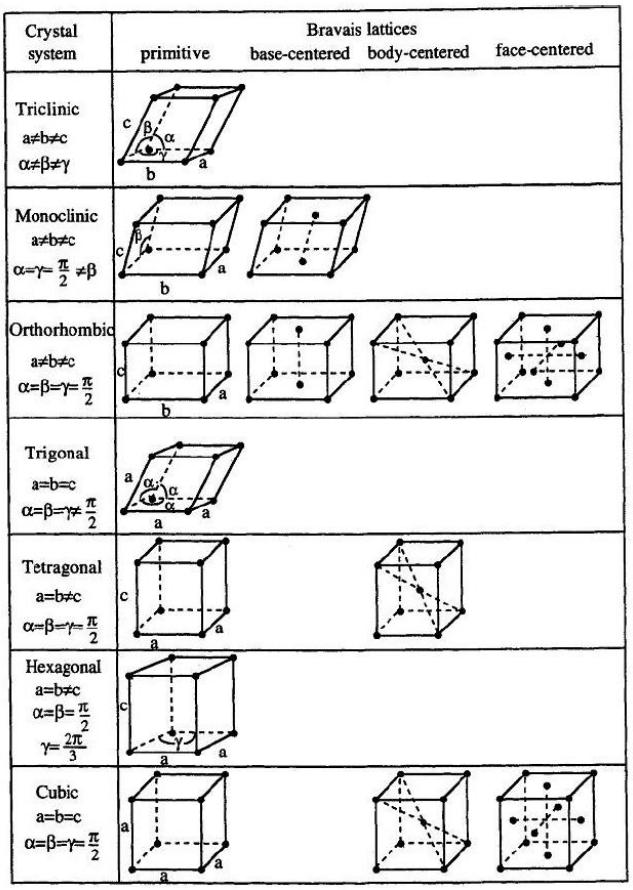

Figure 2.1 Classification of the fourteen Bravais lattices into the seven crystal systems. [2]

In 1839, W. H. Miller introduced the concept of Miller indices (hkl), suggesting that each face of a crystal could be represented by the indices h, k and l. The surface, or plane, was defined as the reciprocal of where the plane intercepts the crystallographic axis. The intercepts are defined as A, B and C. If the plane cuts the axis at a distance equal to a full lattice parameter from the origin X,Y or Z, then the integer h, k or l is 1. If the plane cuts the axis at half the lattice parameter, then the integer is 2, and so on. If the plane is parallel to a crystallographic axis then the intercept is infinity, and the Miller index is 0. [1] This is demonstrated in Figure 2.2. The distance between the planes in a direction is known as the interplanar spacing d_{hkl}.

$$h = \frac{a}{X}, \quad k = \frac{b}{Y} \quad \text{and} \quad l = \frac{c}{Z}$$

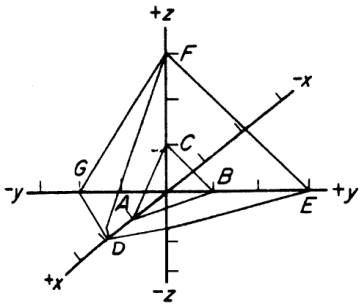

Figure 2.2 Intercepts of planes on the crystallographic axis and definition of Miller indices. [1]

2.2 Solubility and Supersaturation

A solution is defined as a homogeneous mixture of two or more substances. The selection of the "best" solvent for a particular crystallization process is not an easy matter, and sometimes a mixture of two or more solvents may be found to possess the best properties for the particular crystallization. The solute to be crystallized should be readily soluble in the solvent, and should be easily precipitated from the solution, in the desired crystalline form, after cooling, evaporation or antisolvent addition. [1] Solvents are usually classified as polar or non-polar.

Solubility is defined as the amount of a substance that can be dissolved in a specific solvent at a given temperature. It is worth noting that for a given solute in a given solvent, the solubility curve can usually be affected by temperature. Impurities or additives dissolved in solution can affect the solubility. [3]

Experimentally, solubility curves as a function of temperature can be obtained using a technique known as thermo-gravimetric method, or by using turbidimetry to detect the clear

point of a suspension upon heating. [4][5] It can also be calculated using the modified Van't Hoff Equation, which incorporates the activity coefficient, γ, to account for non-ideal solutions:

$$\ln(x\gamma) = \frac{\Delta H_f}{R}\left[\frac{1}{T_f} - \frac{1}{T}\right] \qquad (2.1)$$

where, x is the mole fraction of the solute in solution (molar solubility), ΔH_f is the molar enthalpy of fusion of the solute (J/mol), R is the gas constant, T_f is the fusion temperature of the solute (K), T is the solution temperature (K).

Knowing the solubility curve in a given solvent is required for the understanding and optimal design of a crystallization process. Figure 2.3 shows a hypothetical solubility curve (solid line). Below the solid line, Region I, the solution is undersaturated and any crystals cannot exist in equilibrium with the solution, thus, they dissolve. Above the solubility curve, the solution is in a supersaturated state where crystals can nucleate and grow.

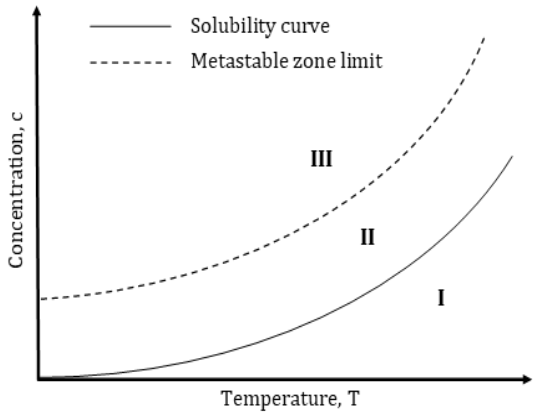

Figure 2.3 Phase diagram of concentration versus temperature showing the various regions within a crystallization process

Region II, the metastable zone, below the dashed line, is a region of lower supersaturation, where existing crystals can grow but spontaneous nucleation cannot happen. The width of the metastable zone depends both on kinetic and thermodynamic factors including agitation,

cooling rates, the type of solvent, pH and the presence of impurities. [6] Region III, above the dashed line, is called the labile region where the solution possesses the critical degree of supersaturation required for spontaneous nucleation to occur. Supersaturation is, therefore, the driving force for nucleation and growth.

Strictly speaking supersaturation is defined as the difference between the chemical potential of the solute molecules in the supersaturated (μ_{ss}) and saturated (μ_{eq}) state respectively. [1]

Supersaturation can be expressed as:

$$\sigma = \frac{\mu_{ss} - \mu_{eq}}{kT} \quad (2.2)$$

where k is the Boltzmann constant and T is the temperature.

Using the Gibbs-Duhem equation, the chemical potentials can be related to the solution activities, and supersaturation can be also related to the solution concentrations:

$$\sigma = \ln\left(\frac{\alpha_{ss}}{\alpha_{eq}}\right) \rightarrow \ln\left(\frac{x_{ss}}{x_{eq}}\right) \approx \frac{x_{ss} - x_{eq}}{x_{eq}} \quad (2.3)$$

Where x_{ss} and x_{eq} refer to the molar fraction of solute in a supersaturated and saturated solution, respectively.

In practise supersaturation is usually expressed as Supersaturation ratio, S, (equation 2.4), or as the degree of supersaturation, ΔC, (equation 2.5):

$$S = c_{ss}/c_{eq} \quad (2.4)$$

$$\Delta C = c_{ss} - c_{eq} \quad (2.5)$$

The aim in a crystallization from solution is to create supersaturation; this can be achieved by different methods, including cooling, evaporation, or addition of an anti-solvent.

Cooling crystallization is used for compounds whose solubilities increase with temperature. As the temperature is lowered there is a decrease in the solubility of the solute in solution for this type of crystallization; hence the equilibrium concentration, c_{eq}, decreases and there is an increase in the degree of supersaturation. Evaporation involves the removal of solvent from the solution and increases the concentration of the solute in the solution, thus increasing supersaturation. Finally, anti-solvent addition relies on the addition of a second solvent that reduces the solubility of the solute in the resultant mixture. [7] In cases where the solubility of a solute is not strongly dependent on temperature, cooling crystallization would not be an effective method; alternatively evaporation or anti-solvent methods could be used. An advantage of anti-solvent crystallization is that it can be used in cases where substances are heat sensitive and large temperature alterations would not be appropriate. Anti-solvent crystallization can also create high degrees of supersaturation, which allows fast precipitation of small size particles. [6]

2.3 Nucleation

Nucleation is the appearance of a crystalline nucleus and is the process of creating a new solid phase from a supersaturated liquid phase. [8] It can be classified into either primary or secondary.

2.3.1 Primary Nucleation

When nucleation happens in the absence of existing crystals is defined as “primary”. Primary nucleation can be homogeneous if it is spontaneous in solution, or heterogeneous if it is induced by the presence of an external surface (e.g., foreign particles). Homogeneous nucleation rarely occurs since solutions often contain random impurities that may induce nucleation. Generally,

heterogeneous nucleation takes place at lower supersaturations as impurities tend to reduce the energy required for nucleation. [7]

Homogeneous primary nucleation can be explained by two theories: the Classical Nucleation Theory (CNT), and the Two-Step Nucleation theory. The CNT states that the free energy, required for the formation of a stable cluster that can grow, is the sum of the volume excess free energy, ΔG_V, and the surface excess free energy, ΔG_S. ΔG_S is a positive quantity, the magnitude of which is proportional to r^2. In a supersaturated solution, ΔG_V is a negative quantity proportional to r^3. [1]

$$\Delta G = \Delta G_V + \Delta G_S = -\frac{4}{3}\pi r^3 \Delta G_v + 4\pi r^2 \gamma \qquad (2.6)$$

where r is the cluster radius and γ is the interfacial tension and ΔG_v is the free energy change of the transformation per unit volume.

In a supersaturated solution the solid state is more stable than the solution, so ΔGv tends to decrease the energy barrier for nucleation. The ΔGs instead is associated with the presence of a discontinuity of concentration at the solution-crystal boundary, thus tends to increase the total ΔG.

The critical nucleus is the minimum size of a stable nucleus. For clusters of molecules of size less than this, the clusters are unstable. For nucleus sizes greater than this, the clusters are stable and can grow. As the supersaturation increases, the value of the energy barrier and the value of the critical radius both decrease. With increasing supersaturation, the barrier eventually becomes small enough for nucleation to become spontaneous. [1]

The critical size, r_c, (equation 2.7) and the critical Gibbs free energy, ΔG_{crit}, are given by:

$$r_c = -\frac{2\gamma}{\Delta G_V} \qquad (2.7)$$

$$\Delta G_{crit} = \frac{4}{3}\pi\gamma\, r_c^2 \qquad (2.8)$$

The rate of nucleation is defined as the rate at which clusters grow through this critical size to become crystals, and it is an Arrhenius type of equation:

$$J = A\exp[-\frac{16\pi\gamma^3 v^2}{3k^3T^2(lnS)^2}] \qquad (2.9)$$

The delay between the attainment of supersaturation and the detection of the first newly created crystal in solution is called induction time, and is inversely proportional to the rate of nucleation, as estimated by Mullin[1]:

$$\frac{1}{t_i} \propto \exp\left(\frac{\gamma^3}{T^3(\ln S)^3}\right) \qquad (2.10)$$

For some proteins and a few organic and inorganic molecules, the two-step theory seems to describe crystal nucleation better than the CNT. [9] The theory states that the formation of a nucleus is preceded by the formation of a stable liquid cluster at higher density than the solution. The high concentration of molecules in this cluster favours the formation of the solid nuclei, which then grow in ordered crystalline structures. [8]

2.3.2 Secondary Nucleation

Nucleation of new crystals, induced only because of the prior presence of seed crystals of the material being crystallized, is defined as secondary nucleation. [8] Seed crystals catalyse the nucleation, which can take place at a lower supersaturation as compared to primary nucleation. [7] There are different mechanisms that can induce secondary nucleation; the most significant one is contact nucleation, also referred to as collision breeding, caused by the collisions between the growing crystals and the walls of the crystallizer, a stirrer or impeller or contact between crystals themselves. [8] Other mechanisms include initial breeding, caused by crystalline dust from dry seeds that introduces new centres for growth, needle or polycrystalline breeding, and shear nucleation caused by fluid shear on growing crystal faces. [3]

Secondary nucleation is the most important type of nucleation happening in industry, where seeding is performed. . [6] The rate of secondary nucleation (B) can be expressed empirically by a power law function in the form:

$$B = k_B M_T^j N^k \Delta C^b \qquad (2.11)$$

The rate of secondary nucleation is affected by three main factors: the degree of supersaturation (ΔC), the mass of seed crystals present in the supersaturated solution (M_T), and the interactions between the crystals and solution, expressed as stirrer speed (N). The rate constants k_B, j, k and b can be predicted by semi-empirical models of contact nucleation in crystallizers. [8]

2.4 Crystal Growth

What follows crystal nucleation is crystal growth, which involves the addition of solute molecules from a supersaturated solution to the crystal surface. [7] Crystal growth is a two-step process consisting of mass transfer (by diffusion) of solute molecules from the bulk to the surface of the nuclei, followed by a surface reaction (surface integration) where the molecules attach to the surface. [9] The rates of solute diffusion through the boundary layer adjacent to the crystal surface, and the surface integration onto the crystal are given by:

Diffusion: $\frac{dm}{dt} = k_m A(C - C_i)$ (2.12)

Integration: $\frac{dm}{dt} = k_r A(C_i - C^*)$ (2.13)

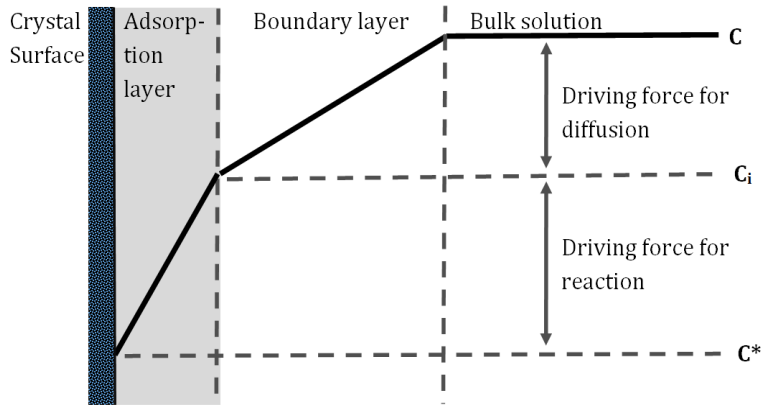

Figure 2.4 Concentration driving forces in crystallization from solution according to the simple diffusion-reaction model. [1]

Where m is the mass of crystal deposited in time t, A is the surface area of the crystal, k_m is the mass transfer coefficient, k_r is the surface integration rate constant, C is the solute concentration in bulk liquid, C_i is the solute concentration at the interface between the crystal and the solution, and C^* is the saturation concentration. Figure 2.4 depicts the concentration profiles during crystal growth.

Since C_i is difficult to measure, the two equations are normally combined to equation 2.14, where $\Delta C = C - C^*$ is the overall driving force, and K_G is the overall crystal growth coefficient.

$$\frac{dm}{dt} = K_G A(\Delta C)^g \qquad (2.14)$$

with g that is the overall growth rate order.

If g=1, then:

$$\frac{1}{K_G} = \frac{1}{k_r} + \frac{1}{k_d} \qquad (2.15)$$

If the surface integration resistance, $\frac{1}{k_r}$, is low, then K_G is equal to k_m and the process is diffusion controlled. If the diffusion resistance, $\frac{1}{k_d}$, is low, then K_G is equal to k_r and the process is controlled by the surface integration step.

2.5 Polymorphism

A substance capable of crystallizing into different, but chemically identical, crystalline forms is said to exhibit polymorphism. Polymorphs can have different physical properties such as density, melting point, solubility, reactivity, thermal and optical properties. [1] Polymorphism arises due to alternative ways in which molecules or ions can pack in a crystal structure to minimise their free energy. Different packing is driven by differences in intermolecular interactions between polymorphs of the same substance. [8]

Together with polymorphs there are other different classes of solid forms, known as hydrates, solvates and amorphous. In solvates, both solute and solvent molecules are part of the crystal structure that make up the solid phase, and if the solvent molecule is water then the crystalline form is referred to as hydrate. [6][8] In amorphous solids, molecules are arranged in a disorderly manner. Solvate, hydrate and amorphous forms are sometimes referred to as pseudo-polymorphs. [6] Polymorphs and solvates can be identified and characterised by several analytical techniques including powder X-Ray diffraction, Infrared (IR), and Near Magnetic Resonance (NMR) spectroscopy. Differential Scanning Calorimetry (DSC) can be used to monitor phase transformations. [1]

The nucleation of a certain polymorph and the transition between one form to another is an important factor to control during crystallization due to the different properties of the polymorphs. A polymorphic transformation can be brought about by changes in pressure,

temperature, composition and pH, and can occur in the solid state, it can be solution mediated, melt mediated or interface mediated. The kinetics of transformation also depend on conditions such as temperature and pressure. [9]

Crystallization from solution is widely used in the food and pharmaceutical industries and there is a great interest in understanding and controlling this mechanism. Ostwald's rule of stages states that upon crystallization, the metastable form will nucleate first and will then transform into other more stable forms until the most stable structure appear, in order to minimize the Gibb's free energy of the system and reach equilibrium. [7] The difference in Gibb's free energy, ΔG, between the two forms acts as the driving force for the polymorphic transformation, and the most stable form is therefore that with the lower G. [7] The most stable form will always be the least soluble in every solvent at a given temperature and pressure, and for a dimorphic system there are two possible scenarios: (1) Where the solubility curves of the two polymorphs cross each other at a temperature (called the transition temperature) lower than the melting point of both forms (2) Where the solubility curves do not cross each other in solution. [9] The first type of system is called enantiotropic while the latter is defined as monotropic. This is schematically illustrated in Figure 2.5.

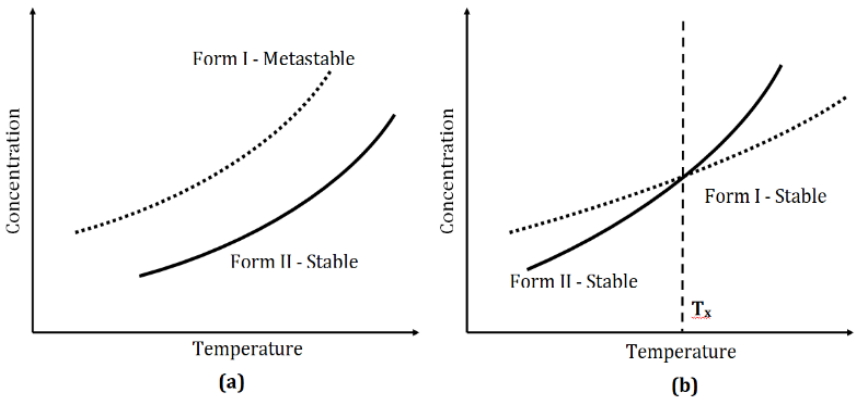

Figure 2.5 Phase diagrams for a compound containing two polymorphic forms (dimorphic) showing a (a) monotropic and (b) enantiotropic system.

The mechanism of solvent mediated polymorphic transformation typically involves three steps: (1) dissolution of the metastable phase into solution; (2) nucleation of the stable form; (3) crystal growth of the new stable nuclei. [7] Any of these steps could be the rate-limiting step to influence the rate of polymorphic transformation. The rate of transformation can be controlled by introducing specific additives that act as inhibitors. [1]

It should be noted that transformation is not certain even if a system enters a zone that would theoretically allow it. It will depend on conditions such as temperature and pressure, which can alter the transformation kinetics. [1] Furthermore, control over the polymorph nucleated can be achieved by the choice of solvent or presence of additives: solvent has a strong effect on the nucleation of one polymorph or another because of the kind of bonds that can form with solute. Similarly, additives can direct the nucleation towards a specific polymorph rather than others, by forming interactions with the solute molecule and therefore interfering with the molecular preassembly route to nucleation, favouring the nucleation of a specific form. [10][11] Also, the level of supersaturation affects the polymorph to be nucleated; generally, a high supersaturation favours the nucleation of the metastable form. [9]

2.6 Crystal Engineering

Crystal engineering aims the design organic solids and it is defined by Desiraju as "the understanding of intermolecular interactions in the context of crystal packing and in the utilization of such understanding in the design of new solids with desired physical and chemical properties". [12] Crystalline materials are held together by non-covalent interactions of varying strength, including hydrogen bonding interactions and van der Waals forces of attraction. A detailed understanding of these interactions is required in order to apply crystal engineering for the design of new solid forms.

Hydrogen bonds are usually exploited in crystal engineering because of its strong and directional nature, and it is often the dominant intermolecular interaction in many molecular crystals. Hydrogen bonds are defined by IUPAC as “an attractive interaction between a hydrogen atom from a molecule or a molecular fragment X-H in which X is more electronegative than H, and an atom or a group of atoms in the same or different molecule, in which there is evidence of bond formation.” [13] Hydrogen bonds can vary in strength and can be classified in terms of bond distance between donor and acceptor atoms. In crystal engineering it is often challenging to predict where hydrogen bonds will form due to the multi donor and acceptor sites contained in a system. [14]

Another type of interaction usually found in organic crystals is known as π-π stacking interactions, and are often formed in structures that contain two or more aromatic rings that lie adjacent to each other. These interactions can occur when attractive interactions between π-electrons and the σ-framework are more favourable than the repulsions between π-electrons. The neighbouring aromatic rings can arrange themselves in different geometries, including face-to-face π-stacking and offset π-stacking. [15][16][17]

Finally, van der Waals interactions are defined as “the attractive or repulsive forces between molecular entities (or between groups within the same molecular entity) other than those due to bond formation or to the electrostatic interaction of ions with one another or with neutral molecules”. Van der Waals interactions are much weaker compared to the hydrogen bonding and π-π stacking interactions. [18]

The knowledge of these intermolecular interactions permits approaches such as crystal engineering to be used in order to predict ways in which molecules will interact and link together for the formation of crystalline solids.

2.7 Synthonic Modelling

The term "synthon" is used to describe a growth unit of a crystalline material. The strength of the intermolecular synthons that are directed in a particular direction are believed to govern the growth rates in that direction, and therefore the overall shape of the crystal. Synthonic Engineering (SE), or Synthonic Modelling draws upon the molecular and crystallographic structure of a material and involves the analysis of the spatial arrangement and energy of the synthons (intermolecular interactions) that hold a crystal together, using the atom-atom approach. [19] SE tools, such as HABIT 98, can calculate the nature, strength and directionality of these synthons. [20] Hence, they can be used to predict crystal morphologies and facet specific surface chemistry, in terms of the strengths of their intermolecular interactions, as well as predict physiochemical properties of the crystalline material. SE can therefore provide a guide to the experimental conditions required to produce a pre-defined crystal morphology and physiochemical properties. [21]

The intermolecular interactions in a crystalline structure are often calculated using empirical interatomic potentials derived from experimental data. [22][23] The lattice energy for the structure under study can be calculated and be compared to the experimentally obtained sublimation enthalpy, according to equation 2.16.

$$E_{cr} = \Delta H_S - 2RT \qquad (2.16)$$

Where E_{cr} is the experimental lattice energy calculated from the sublimation enthalpy, ΔH_S, R is the universal gas constant and T is the temperature. A good agreement between the lattice energy predicted by the modelling software and the experimentally calculated lattice energy suggests that the potential is suitable to predict the strength of the interatomic interaction for the atoms involved, and hence predict the strength of the intermolecular interactions. [19][21]

The calculation of a pairwise intermolecular interaction is often achieved through the "atom-atom" method, which sums the individual atom-atom interactions between the two molecules. A Lennard-Jones potential is used, which contains terms to calculate the van der Waals interactions and the Coulombic term to calculate electrostatic interactions, as in equation 2.17.

$$V_{ij} = -\frac{A}{r_{ij}^6} + \frac{B}{r_{ij}^{12}} + \frac{q_i q_j}{D r_{ij}} \qquad (2.17)$$

Where A and B are atom-atom interaction specific parameters, q_i and q_j are fractional charges on atoms i and j separated by distance r and D is the dielectric constant. [24]

The SE tool used in this doctoral project is HABIT 98. [20][21] HABIT 98 constructs a series of unit cells in three dimensions and calculates the non-bonded energy between a central molecule and all other molecules in the central and surrounding unit cells, within a sphere of a limiting radius set by the user, beyond which the energy of interaction between a molecule and the central molecule is negligible. [20][21] The intermolecular interactions can be ranked by strength or distance and outputted for analysis, along with the atom by atom contribution to the lattice energy, summed over the asymmetric unit. The ranking of the intermolecular interactions by strength can be outputted using the DEBUG-1 function, while the breakdown of lattice energy per molecule, atom type and functional group can be achieved using the DEBUG-2 function. The energy of interactions is broken down into van der Waals attractive, van der Waals repulsive, hydrogen bonding attractive, hydrogen bonding repulsive and electrostatic. Intermolecular interactions that are present within the bulk of the material are termed as "intrinsic synthons". These interactions are "fully satisfied", in the sense that all the interactions are formed between a molecule in the bulk of the crystal and other bulk molecules around it. "Extrinsic synthons" are "unsaturated" intermolecular interactions exposed at the surface of a crystal; these are the interactions that a molecule on the surface of the crystal can form with the surroundings. [21] Face-specific information can be outputted for analysis. The

nature and strength of these interactions, combined with molecular scale modelling of the predicted surfaces using a molecular visualization software, can be used to provide important information on the surface chemistry of the dominant faces. Crystal growth involves the creation and breakage of solvent/solvent, solute/solvent and solute/solute interactions. [21]

Crystal morphology is predicted from the calculation of the strength and directionality of the intermolecular interactions within the crystal structure. By identifying those interactions that are exposed at the growth surfaces it is possible to establish which of them govern the relative facet-specific growth rates through the attachment energy model.

2.7.1 The Attachment Energy model

The attachment energy model, developed by Hartmann and Perdok in 1955, states that the rate of growth perpendicular to a crystal surface (*hkl*) is proportional to the attachment energy for that surface. [25] Relative to any crystal plane (*hkl*) the lattice energy, E_{cr}, can be partitioned into slice energy, E_{sl}, and the attachment energy for the slice, E_{att}, as in equation 2.18. [21]

$$E_{cr} = E_{sl} + E_{att} \qquad (2.18)$$

The lattice energy, E_{cr}, is the sum of all atom-atom interactions between a central molecule and all the surrounding molecules within a summation radius limit beyond which the lattice energy increases by negligible amount. The slice energy, E_{sl}, is the summation of all the atom-atom interactions within a slice layer of thickness, d_{hkl}, whereas the attachment energy, E_{att}, is the energy released on the addition of a growth slice to the surface of the growing crystal. In this model it is assumed that the attachment energy is proportional to the growth rate, in a direction perpendicular to that facet, according to equation 2.19. [25][26]

$$R \propto E_{att} \qquad (2.19)$$

The attachment energies can be converted into centre to face distances and then used to construct a Wulff plot prediction of the crystal morphology. [21] Based on the attachment energy model, a face of higher attachment energy will have a faster growth rate. It is often observed that the slow growing surfaces of a crystal, those having a lower attachment energy, dominate the final morphology, and the fast growing faces, of higher attachment energies, are small, or can be "faceted out" and not be present in the final morphology. In general, the attachment energy morphological predictions give the best match to the morphology of crystals grown in the vapour phase or at low driving force in solution. [19]

The surface anisotropy factor, ε_{hkl}, can provide a measure as to how satisfied the possible intermolecular interactions of the molecules at a growing surface are, when compared to those within the bulk.

$$\varepsilon_{hkl} = \frac{E_{sl}}{E_{cr}} \qquad (2.20)$$

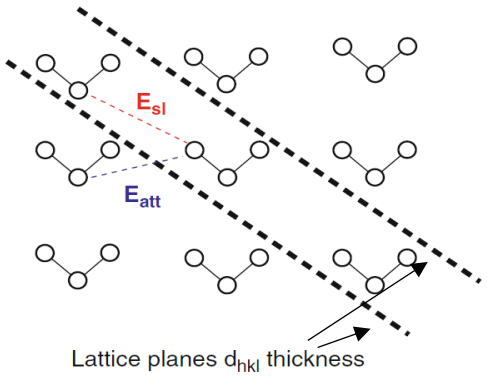

Figure 2.6 Schematic representation of how attachment energy is calculated at the molecular level.

2.7.2 Attachment Energy morphological predictions

Early relationships of interplanar spacing to morphological importance, linked with lattice geometry, lead to Bravais, Friedel, Donnay and Harker model (BFDH). [27] This model is still used to identify the morphologically dominant faces *(hkl)*. The model suggests that, after

allowances have been made for space group symmetry, the crystallographic forms with greatest interplanar spacing, d_{hkl}, will be the most morphologically important at the surface of the crystalline particle. [1] Computer programs, such as Morang, can calculate the interplanar spacing in specific crystallographic directions. Morang utilises the unit cell information and calculates the interplanar spacing in each crystallographic direction and then ranks them in descending order. Therefore, the likely morphologically important surfaces are efficiently predicted. [19] The biggest limitation of the BFDH model is that it fails to take into account the effect of the intermolecular forces on face specific crystal growth in a molecular crystal.

Alternatively, the attachment energies calculated from the attachment energy model discussed previously can be converted into centre to face distances and then used to construct a Wulff plot prediction of the crystal morphology, using routine molecular drawing programs such as Mercury. [21][19] The Wulff plots are based on the Wulff theory which states that "the equilibrium crystal habit would consist of crystal faces whose distance from the origin, in a specific (*hkl)* direction, is proportional to the specific surface energies of the faces and the crystal growth rates away from the nucleation centre". [1] This is based on Gibbs' theory that the three-dimensional shape of a crystal will be the one in which the total free energy is at minimum, according to equation 2.21.

$$\Sigma_i \gamma_i A_i \qquad (2.21)$$

Where γ_i and A_i are the surface energy and surface area, respectively, of the ith face.

The morphological predictions from the attachment energy model assume the crystals to be grown in the vapour phase at a low driving force. However, it should be considered that the majority of crystallization processes take place in a solution phase, and that interactions of the growing crystal with the surrounding solvent as well as the crystal growth kinetics are going to affect the final crystal morphology.

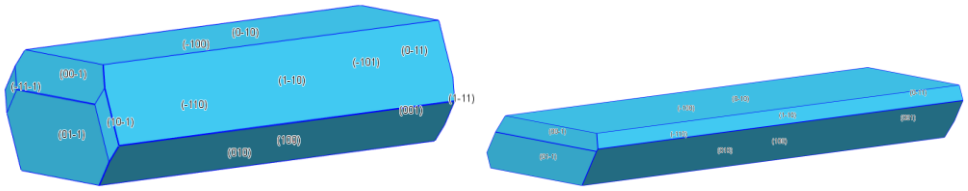

(a) (b)

Figure 2.7 Morphological predictions for quercetin dihydrate from (a) the BFDH model, (b) the attachment energy model.

2.8 Solid-state characterization techniques

Solid-state characterization techniques are analytical techniques used to characterize the crystal products, providing information such as the polymorphic form and stability. [28] The analytical techniques further provide information that can help understand the crystallization process of a compound as well as identifying transformation conditions between different solid forms. [29] The techniques discussed here are DSC, TGA, PXRD, DVS and IGC.

2.8.1 Differential Scanning Calorimetry (DSC)

Differential scanning calorimetry is a thermal analysis technique used for solid state analysis of crystalline solids. The operation involves the heating of two cells, one containing the reference material and the other the sample. The two cells are kept at the same temperature by a constant heating rate. Any changes within the system that occur during the heating process will result in a change in the heat flow rate to the sample. The measurements take place at a controlled flow of nitrogen to prevent degradation of the sample. [30]

The measurements provide quantitative and qualitative information about the physiochemical changes involving exothermic or endothermic processes such as melting or boiling points, heats of fusion and reaction, oxidative and thermal stability and specific heat. The technique can be used to detect the presence of solvates and study polymorphic transitions. On a typical DSC

diagram, as in Figure 2.8, the transformations can be recognized by the sign of heat flow absorbed by the sample. In this thesis, endothermic events are indicated as negative and exothermic events as positive.

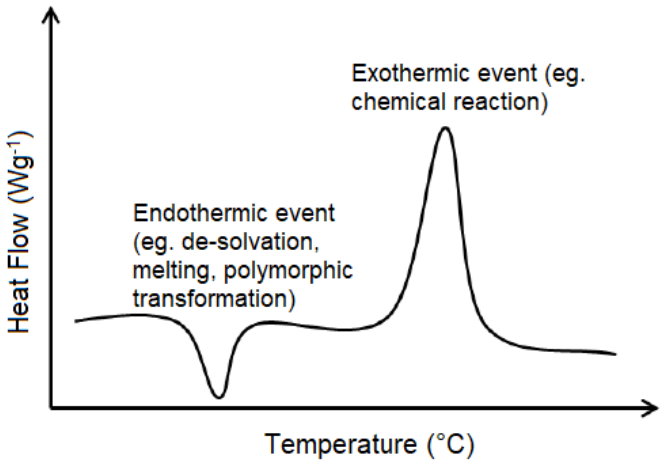

Figure 2.8 DSC diagram example representing endothermic events as negative and exothermic as positive.

2.8.2 Thermogravimetric analysis (TGA)

Thermogravimetric analysis is a thermal technique used in the identification and characterization of solvate crystal structures. During the analysis, the sample is heated at a constant rate and the mass of the sample is monitored against temperature and time. An observed decreased in mass can indicate loss of solvent, which can be either from the surface of the particles (physisorption) or from the internal structure of the crystal in a de-solvation event. A weight loss at higher temperatures usually indicates loss of solvent from the lattice as a higher amount of energy needs to be supplied to break the intermolecular bonds. TGA data can be used to determine the stoichiometry of solvates and hydrates. [30]

2.8.3 Dynamic Vapour Sorption (DVS)

Dynamic Vapor Sorption is a gravimetric sorption technique that measures the rate and amount of solvent sorbed and released by a sample. The DVS accomplishes this by varying the vapour concentration surrounding the sample and measuring the change in mass which this produces, at constant temperature. The technique can be used to determine the hygroscopicity of solids, detect different hydrate forms and measure the kinetic stability of solids at different conditions of relative humidity (RH). [30][31]

2.8.4 X-Ray Diffraction (XRD)

Due to their long range order, crystalline materials have the ability to diffract X-Rays to produce regular patterns, which can be used to provide structural information such as discrimination between polymorphs and determination of unit cell dimensions.

An X-Ray cathode tube (typically Cu or Mo of X-ray wavelengths 1.5418Å and 0.71073Å, respectively) generates the X-rays which are filtered to produce monochromatic radiation, and are directed towards the sample. Interaction of the incident X-ray beam with the electrons in each atom of the sample causes the X-rays to diffract at certain angles depending on the arrangement of atoms within the crystal lattice. [15]

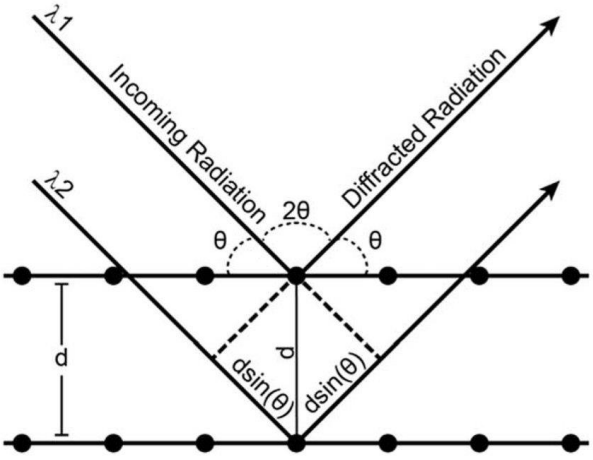

Figure 2.9 X-rays diffracted by a crystalline lattice following Bragg's law [32]

Diffraction occurs when an X-ray interacts with lattice planes known as Miller planes with a characteristic spacing, d. Miller planes refer to families of parallel planes that are described by Miller indices, (hkl), and their separation is termed as d_{hkl}. The path difference between the incident and diffracted X-rays can be calculated by considering X-rays reflected by two adjacent Miller planes separated by a distance of d_{hkl}, as shown in Figure 2.9. The measured angles of diffraction are used to determine the arrangement and spacing between the atoms within the lattice according to Braggs Law:

$$n_o\lambda = 2d \sin(\theta) \qquad (2.22)$$

Where θ is the angle of beam diffraction from the sample, d is the distance between the Miller planes in the crystal, λ is the wavelength of the incident beam and n_o is the order of the diffraction pattern. [15]

The diffracted X-rays are detected by the detector and then processed and counted. The different angles of diffraction are presented on an X-ray pattern by the presence of different peaks. Each diffraction peak can thus be identified with an hkl value since each peak represents diffraction from a specific Miller plane. It is possible to obtain all diffraction directions of the crystal lattice by scanning the sample through a range of 2θ angles. [32]

Powder X-ray diffraction (PXRD) is usually used to determine the different polymorphs within a given system. If the sample is subjected to a controlled temperature programme during scanning, the technique is called variable temperature powder X-ray diffraction (VT-PXRD). If a single crystal is used (SC-XRD), the technique can identify the specific positions of the atoms within a crystal structure, by yielding an electron density map. Hence, the crystal structure can be produced.

2.8.5 Inverse Gas Chromatography (IGC)

Inverse gas chromatography has been demonstrated as a practical technique for measuring surface energy and surface energy heterogeneity. [33] It operates in the opposite way to conventional chromatography, where the stationary phase is the unknown component and solvent probes with known properties are the mobile phase. For heterogeneous materials, the relationship between the measured surface energy and the surface coverage provide information about the surface energy distribution of the material. [34] During the analysis, known solute molecules are carried by an inert gas through a packed column of the unknown solid substance, and the physiochemical characteristics of the solid-solute system can be determined from the retention times and retention volumes of these known solute molecules. At infinite dilution IGC (IFD-IGC), small amounts of solvent are injected, covering only the high surface energy sites of the stationary phase, while in the finite mode (FD-IGC), higher amounts of solvent are injected covering larger sections of the stationary phase. [35][36] Dispersive interactions can be determined from nonpolar solute molecules, such as alkanes (eg. heptane, octane, nonane and decane), while the acid-base (polar) interactions' identification requires a polar solute molecule, eg. ethanol or water. The retention time (t_R) of each injected probe vapour depends on the strength of interaction with the sample surface. [35][36] The retention volume (V_N) can be calculated as follow:

$$V_N = \frac{j}{W_s} w(t_R - t_o)\left(\frac{T}{T_{ref}}\right) \qquad (2.23)$$

Where j is the James-Martin pressure drop factor accounting for the compressibility of the injected probes, W_s stands for the specific surface area of stationary phase, w is the carrier gas flow rate, t_o is the dead time, the time required for an inert molecule to travel through the stationary phase, T is the experiment's temperature and T_{ref} is the reference temperature of 273.15 K.

The dispersive component of a solid surface energy, γ_{SV}^{d}, can be obtained using approaches described by Schultz et al. and Dorris and Gray, using the retention volume data of the alkane probes. [37][38] Figure 2.10 is a graphical representation of how the Schultz method can be used to calculate the surface energy. From the slope of the line formed by the alkane probes, the dispersive van der Waals component surface energy, γ_{SV}^{d}, can be calculated. The retention volume data of the polar probes consist of both a dispersive and an acid-base component. With knowledge of the dispersive component for the polar probes used, the acid-base component can also be calculated, as the difference between the change in the Gibbs free energy of adsorption of a polar solvent data point and the chain alkanes' regression line. [35][36][39][40][41]

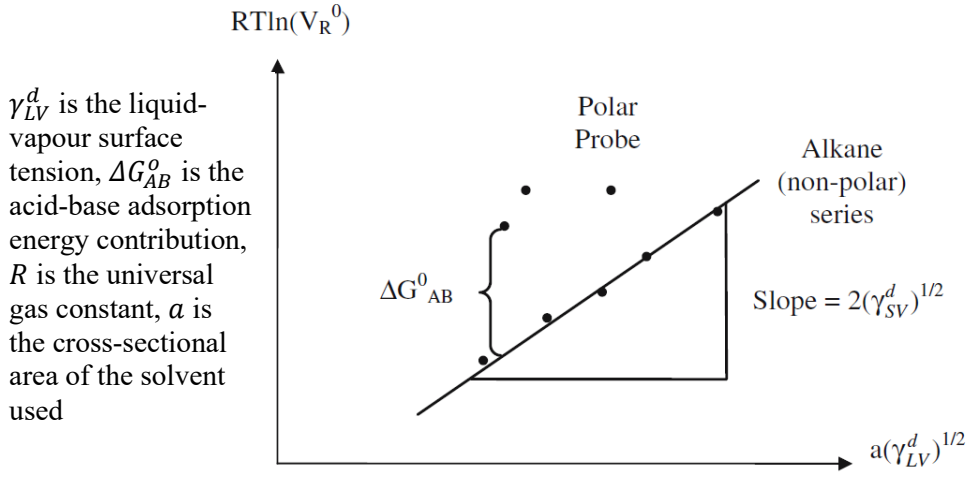

Figure 2.10 Schematic representation of the Schultz method for the determination of surface energy, using IGC analysis. [36]

References

[1] J.W. Mullin, “Crystallization.”

[2] G. Grosso and G. P. B. T.-S. S. P. (Second E. Parravicini, Eds., “Preface to the first edition,” Amsterdam: Academic Press, 2014, pp. xiii–xiv.

[3] A. N. Saleemi, “Strategic feedback control of pharmaceutical crystallization systems,” 2011.

[4] D. M. Camacho Corzo *et al.*, “Nucleation mechanism and kinetics from the analysis of polythermal crystallisation data: Methyl stearate from kerosene solutions,” *CrystEngComm*, vol. 16, no. 6, pp. 974–991, 2014, doi: 10.1039/c3ce41098f.

[5] A. Chianese and H. J. Kramer, *Industrial Crystallization Process Monitoring and Control*. 2012.

[6] K. Howard, “Institutional Repository Process analytical technology investigation of the crystallization of pharmaceutical polymorphs , salts and hydrates,” no. July, 2011.

[7] M. R. Abu Bakar, “Process analytical technology based approaches for the monitoring and control of size and polymorphic form in pharmaceutical crystallization processes,” 2010.

[8] John Garside and Roger Davey, *From Molecules to Crystallizers An Introduction to Crystallization*. Oxford Science Publications, 2000.

[9] E. Simone, “Application of process analytical technology (PAT) tools for the better understanding and control of the crystallization of polymorphic and impure systems Certificate of originality,” no. December, 2015.

[10] E. Simone, G. Steele, and Z. K. Nagy, “Tailoring crystal shape and polymorphism using combinations of solvents and a structurally related additive,” *CrystEngComm*, vol. 17, no. 48, pp. 9370–9379, 2015, doi: 10.1039/C5CE01878A.

[11] P. L. Kaskiewicz *et al.*, “Understanding and Designing Tailor-Made Additives for Controlling Nucleation: Case Study of p-Aminobenzoic Acid Crystallizing from Ethanolic Solutions,” *Cryst. Growth Des.*, vol. 21, no. 4, pp. 1946–1958, Apr. 2021, doi: 10.1021/acs.cgd.0c01209.

[12] G. R. Desiraju, “Crystal engineering: From molecule to crystal,” *J. Am. Chem. Soc.*,

vol. 135, no. 27, pp. 9952–9967, 2013, doi: 10.1021/ja403264c.

[13] E. Arunan *et al.*, “Definition of the hydrogen bond (IUPAC Recommendations 2011): ,” *Pure Appl. Chem.*, vol. 83, no. 8, pp. 1637–1641, 2011, doi: doi:10.1351/PAC-REC-10-01-02.

[14] J. J. Dannenberg, “An Introduction to Hydrogen Bonding By George A. Jeffrey (University of Pittsburgh). Oxford University Press: New York and Oxford. 1997. ix + 303 pp. $60.00. ISBN 0-19-509549-9.,” *J. Am. Chem. Soc.*, vol. 120, no. 22, p. 5604, Jun. 1998, doi: 10.1021/ja9756331.

[15] L. Ooi, *Principles of x-ray crystallography*. Oxford; New York: Oxford University Press, 2010.

[16] P. W. Atkins, J. De Paula, and P. W. Atkins, *Atkins’ Physical chemistry.* Oxford; New York: Oxford University Press, 2002.

[17] C. A. Hunter and J. K. M. Sanders, “The nature of .pi.-.pi. interactions,” *J. Am. Chem. Soc.*, vol. 112, no. 14, pp. 5525–5534, Jul. 1990, doi: 10.1021/ja00170a016.

[18] P. Muller, “Glossary of terms used in physical organic chemistry (IUPAC Recommendations 1994): ,” *Pure Appl. Chem.*, vol. 66, no. 5, pp. 1077–1184, 1994, doi: doi:10.1351/pac199466051077.

[19] J. Pickering, R. B. Hammond, V. Ramachandran, M. Soufian, and K. J. Roberts, “Synthonic Engineering Modelling Tools for Product and Process Design,” in *Engineering Crystallography: From Molecule to Crystal to Functional Form*, K. J. Roberts, R. Docherty, and R. Tamura, Eds. Dordrecht: Springer Netherlands, 2017, pp. 155–176.

[20] G. Clydesdale, K. J. Roberts, and R. Docherty, “HABIT95 — a program for predicting the morphology of molecular crystals as a function of the growth environment,” *J. Cryst. Growth*, vol. 166, no. 1–4, pp. 78–83, Sep. 1996, doi: 10.1016/0022-0248(96)00056-5.

[21] I. Rosbottom and K. J. Roberts, “Engineering Crystallography: From Molecule to Crystal to Functional Form,” 2017, doi: 10.1007/978-94-024-1117-1.

[22] F. A. Momany, L. M. Carruthers, R. F. Mcguire, and H. A. Scheraga, “Intermolecular Potentials from Crystal Data . III . Determination of Empirical Potentials and

Application to the Packing Configurations and Lattice Energies in Crystals of Hydrocarbons , Carboxylic Acids , Amines , and Amides1," vol. 78, no. 16, pp. 1595–1620, 1974, doi: 10.1021/j100609a005.

[23] S. L. Mayo, B. D. Olafson, and W. A. Goddard, "DREIDING: a generic force field for molecular simulations," *J. Phys. Chem.*, vol. 94, no. 26, pp. 8897–8909, Dec. 1990, doi: 10.1021/j100389a010.

[24] D. E. Williams, "Nonbonded Potential Parameters Derived from Crystalline Hydrocarbons," *J. Chem. Phys.*, vol. 47, no. 11, pp. 4680–4684, Dec. 1967, doi: 10.1063/1.1701684.

[25] P. Hartman, "The attachment energy as a habit controlling factor. III. Application to corundum," *J. Cryst. Growth*, vol. 49, no. 1, pp. 166–170, 1980, doi: 10.1016/0022-0248(80)90077-9.

[26] R. B. Hammond, K. Pencheva, and K. J. Roberts, "A structural-kinetic approach to model face-specific solution/crystal surface energy associated with the crystallization of acetyl salicylic acid from supersaturated aqueous/ethanol solution," *Cryst. Growth Des.*, vol. 6, no. 6, pp. 1324–1334, 2006, doi: 10.1021/cg0505618.

[27] R. Docherty, G. Clydesdale, K. J. Roberts, and P. Bennema, "Application of Bravais-Friedel-Donnay-Harker, attachment energy and Ising models to predicting and understanding the morphology of molecular crystals," *J. Phys. D. Appl. Phys.*, vol. 24, no. 2, pp. 89–99, 1991, doi: 10.1088/0022-3727/24/2/001.

[28] E. J. Munson, "Chapter 3 - Analytical Techniques in Solid-state Characterization," Y. Qiu, Y. Chen, G. G. Z. Zhang, L. Liu, and W. R. B. T.-D. S. O. D. F. Porter, Eds. San Diego: Academic Press, 2009, pp. 61–74.

[29] T. D. Turner, P. J. Halfpenny, and K. J. Roberts, "Pharmaceutical Solid-State Characterisation Techniques BT - Engineering Crystallography: From Molecule to Crystal to Functional Form," K. J. Roberts, R. Docherty, and R. Tamura, Eds. Dordrecht: Springer Netherlands, 2017, pp. 367–393.

[30] D. Q. M. Craig, "Characterization of Polymorphic Systems Using Thermal Analysis," *Polymorphism*. pp. 43–79, Feb. 06, 2006, doi: https://doi.org/10.1002/3527607889.ch3.

[31] "DVS Resolution," *Surface measurement systems*. https://www.surfacemeasurementsystems.com/wp-content/uploads/2014/05/DVS-Resolution-brochure-v1.0.pdf.

[32] C. V Stan, C. M. Beavers, M. Kunz, and N. Tamura, "X-Ray Diffraction under Extreme Conditions at the Advanced Light Source," *Quantum Beam Science* , vol. 2, no. 1. 2018, doi: 10.3390/qubs2010004.

[33] R. Ho and J. Y. Y. Heng, "A review of inverse gas chromatography and its development as a tool to characterize anisotropic surface properties of pharmaceutical solids," *KONA Powder Part. J.*, vol. 30, no. 30, pp. 164–180, 2012, doi: 10.14356/kona.2013016.

[34] A. E. Jefferson, D. R. Williams, and J. Y. Y. Heng, "Computing the Surface Energy Distributions of Heterogeneous Crystalline Powders," vol. 25, pp. 339–355, 2011, doi: 10.1163/016942410X525506.

[35] P. P. Yla, J. Y. Y. Heng, F. Thielmann, and D. R. Williams, "Inverse Gas Chromatographic Method for Measuring the Dispersive Surface Energy Distribution for Particulates," 2008.

[36] J. Y. Y. Heng, F. Thielmann, and D. R. Williams, "The Effects of Milling on the Surface Properties of Form I Paracetamol Crystals," vol. 23, no. 8, pp. 1918–1927, 2006, doi: 10.1007/s11095-006-9042-1.

[37] J. Schultz, L. Lavielle, and C. Martin, "The Role of the Interface in Carbon Fibre-Epoxy Composites," *J. Adhes.*, vol. 23, no. 1, pp. 45–60, Sep. 1987, doi: 10.1080/00218468708080469.

[38] G. M. Dorris and D. G. Gray, "Adsorption of n-alkanes at zero surface coverage on cellulose paper and wood fibers," *J. Colloid Interface Sci.*, vol. 77, no. 2, pp. 353–362, 1980, doi: https://doi.org/10.1016/0021-9797(80)90304-5.

[39] R. R. Smith, U. V Shah, J. V Parambil, D. J. Burnett, F. Thielmann, and J. Y. Y. Heng, "The Effect of Polymorphism on Surface Energetics of D-Mannitol Polymorphs," vol. 19, no. 1, 2017, doi: 10.1208/s12248-016-9978-y.

[40] J. Y. Y. Heng, K. Campus, and U. Kingdom, "Determining Surface Energetics of Solid Surfaces," pp. 1–14.

[41] R. Ho and J. Y. Y. Heng, “A Review of Inverse Gas Chromatography and its Development as a Tool to Characterize Anisotropic Surface Properties of Pharmaceutical Solids,” vol. 30, no. 30, pp. 164–180, 2013.

CHAPTER 3 - SYNTHONIC MODELLING OF QUERCETIN AND ITS HYDRATES: EXPLAINING CRYSTALLIZATION BEHAVIOUR IN TERMS OF MOLECULAR CONFORMATION AND CRYSTAL PACKING

Abstract

Hydrated structures of a specific compound can often have different physiochemical properties compared to the anhydrous form. Therefore, being able to predict and understand these properties, especially the stability, is critical. In this study quercetin, a flavonoid molecule, is modelled in three different states of hydration to gain an understanding of the effect of water molecules on the structure, packing and conformation energetics of the three forms. Conformational analysis and modelling of intermolecular interactions (synthonic modelling) have been performed. It was found that in the anhydrous form hydrogen bonding is the strongest type of interaction while in the two hydrate structures, the incorporation of water within the lattice leads to the formation of hydrogen bonds between the quercetin and water molecules. Within hydrates quercetin molecules adopt a more planar conformation which allows them to pack more closely by strong π-π stacking interactions, thus resulting in a higher relative stability. The modelling results highlight the importance of water in the stabilization of the lattice and explain the preferential nucleation of the dihydrate form. It is further demonstrated how synthonic modelling can be a predictive tool for the product's properties, leading to more efficient product design and faster development.

3.1 Introduction

Hydrates are multicomponent crystalline solids that contain both the host molecule and one or more water molecules incorporated in the crystal lattice, whereby it is thought that approximately a third of organic compounds can form hydrated structures. [1][2] Understanding organic molecules' propensity to form hydrates and mapping their thermodynamic stability is of critical importance when formulating particulate products, particularly for the pharmaceutical, food and agrochemical industries. [3]

Exposing anhydrous structures to conditions of high relative humidity can induce hydration, whilst some hydrates precipitate in water or aqueous solutions, after the dissolution of the formulated product in the desired media (stomach or digestive tract for drugs, wet soil for agrochemicals). [4] Since hydrates can present significantly different physical and chemical properties (solubility, density, bioavailability etc.) compared to their anhydrous counterparts, their unexpected formation can dramatically affect the quality and efficiency of a particulate product. [5][6][7] In some cases the hydrated forms of molecular crystals exhibit properties that are desired for a particulate product, for example improved release rate or higher stability. [3][7][8][9] Understanding how the water interacts with the host molecules in crystalline solids, as well as how the pathway from solution to hydrated structure can become preferential over the pathway to pure form, is essential to predict the relative stability and crystallisability of hydrated crystal forms. [1]

Different crystal forms, whether they are single or multi component, can vary in terms of molecular conformation or crystal packing. [10] The presence of water molecules within a crystal lattice can affect the type and strength of intermolecular interactions within the bulk, which in turn could stabilise molecular conformations that may not be accessible within the pure crystal forms. [11] This in turn not only can influence the properties of the solid-state, but also the kinetic pathway from the solution to the crystalline state.

Unsatisfied hydrogen bond donors and acceptors within an anhydrous crystal structure, those that could potentially form hydrogen bonds, is the main driving force for hydrate formation. [9][12] The incorporation of water molecules in the crystal lattice provides additional H-bond donor and acceptor sites that can potentially compensate for the unsatisfied hydrogen bonding between the donors and acceptors of the host molecule. [6][9][12] In 1991 Desiraju reported that hydrate formation is more favourable when the hydrogen bond donor/acceptor ratio (d/a ratio) for the host molecule is low, and usually <0.5. [13] The d/a ratio is a ratio between the hydrogen bond donors and acceptors that could potentially participate in a hydrogen bond, and represents a measure of the imbalance between the two in the structure. [13] The incorporation of water molecules within the crystal structure increases the number of available bond donors and shifts the donor/acceptor ratio towards unity. [14] The polarity of the functional groups of the molecules or atoms that form a crystalline structure can also influence hydrate formation, as compounds with charged or polar groups or atoms have a high tendency to form hydrated structures. [1] Finally, the formation of hydrates tends to decrease the void space in a crystal structure and leads to more efficient packing. [9][15]

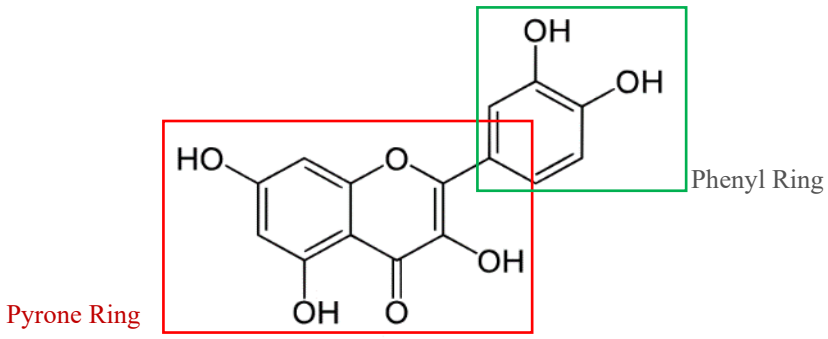

Figure 3.1 The molecular structure of quercetin

In this work, quercetin, 2-(3,4-Dihydroxyphenyl)-3,5,7-trihydroxy-4H-chromen-4-one, is chosen as the model compound. The molecule is a polyphenolic compound found in many

fruits and vegetables, including onions, tomatoes, apples and berries. [16][17][18] Due to this vast range of biological effects, having antioxidant, anti-inflammatory, anti-bacterial and anti-hypertensive properties as well as the ability to inhibit the growth of human cancer cell lines, quercetin finds use in the nutraceutical industry and as food supplement or ingredient. [19][20][21][22][23][24][25]

The molecular structure of quercetin can be observed in Figure 3.1.[27][28] Quercetin can exist as anhydrous (QA), monohydrate (QMH) and dihydrate (QDH) forms. [29][30] It is sparingly soluble in water, which results in difficulties when crystallizing the hydrated forms from aqueous solvents.

While the crystal structure of QDH was solved in the late 80s, crystals of QA and QMH of suitable size and quality have not been obtained to be solved by single crystal X-ray diffraction (SCXRD). [30][31][32] The existence of the QA form was confirmed using several experimental techniques such as powder X-Ray diffraction (PXRD) and nuclear magnetic resonance (NMR), while for QMH the PXRD pattern was determined in 2011 by Domagata et al. [8][31][32]

Experimental characterisation of the physiochemical properties and thermal stability of the quercetin hydrates has been conducted by Borghetti et al., employing a range of experimental techniques including variable temperature PXRD (VTPXRD), differential scanning calorimetry coupled with thermogravimetric analysis (DSC/TGA) and scanning electron microscopy (SEM). The authors have identified QDH as the most thermodynamically stable form. [33] A study on the solubilities of QA and QDH by Srinivas et al. has shown the aqueous solubility of QA up to 100°C to be higher than that of QDH, implying that QDH is a more stable crystal structure at those conditions. [17] While experimental studies could be laborious, time consuming and expensive, molecular modelling can provide an alternative route to gain

insight into the properties and propensity of formation of hydrates, minimizing the required laboratory work needed. [34][35][36][37]

Synthonic modelling and computational methods can utilize atomistic force fields drawn from empirical data, to calculate the strength, directionality and dispersive nature of the intermolecular interactions (synthons) within a crystalline structure. This information can help in predicting the physiochemical properties of crystals. [34][36] In the past synthonic modelling has been used to study crystalline structures and estimate their properties, by calculating the lattice energy and identifying the dominant intermolecular interactions. [38][39][40][41][42][43][44][45][46][47][48][49][50][51][52][53][54]

Synthonic modelling allows studying more complex multi-component systems, including those of hydrated structures. [55][56][57] Characterisation and comparison of the bulk intermolecular interactions within the anhydrous and hydrated structures of a specific compound can provide evidence on how water molecules can affect the intermolecular interactions among the different forms, and direct properties such as crystal shape, thermodynamic stability and surface chemistry. As an example, Clydesdale et al. (1995) have used synthonic modelling to simulate the morphology of the α-lactose monohydrate crystal structure and identified that the water molecules in the structure play a space-filling role during the growth process. [56] More recently, D.E. Braun et al. have studied the intermolecular interactions in 1,10-phenanthroline anhydrate and monohydrate, and explained the higher stability of the monohydrate form, identifying the lack of hydrogen bond donor groups of the molecule as the reason leading to hydrate formation. [57]

The structure and conformation of the quercetin molecules in the three forms have been studied individually both by experimental and theoretical techniques, and the effect of water on the molecular geometry of quercetin in the hydrated structures has been discussed. [28][58] However, it is still unclear from these studies what is the effect of water on intermolecular

packing energetics and conformational energy of each structure and how this link to the experimentally observed physiochemical properties of each form, including thermodynamic stability, crystallization behaviour of the compound and the preferential nucleation of one form to the other. [59][60]

In the presented work, the effect of water molecules on the structure, packing energetics and conformation of a multi-component system characterised by a model molecule, quercetin, and water in different ratios is investigated using a multi-angle modelling approach. Synthonic modelling is used here to compare the type and strength of intermolecular interactions in the structures of a compound at different levels of hydration. A systematic procedure is developed to gain insight of hydrate formation of quercetin and its hydrates, and to explain the crystallization behaviour of the compound. This proposed modelling methodology can be extremely valuable when designing products, processes and storage conditions for particulate products with known hydrates. [61][62]

The intermolecular interactions in the solid state of quercetin and two of its hydrated crystalline forms have been estimated and studied in this work. The knowledge of such interactions can elucidate the different mechanisms of crystal growth for these structures and explain the crystallization behaviour in different solvents, particularly water. Additionally, comparing the main intermolecular interactions can explain differences in the properties (e.g., relative stability and solubility) of crystals structures of the same compound at different hydration levels.

3.2 Computational Modelling Methodology

3.2.1 Structure file preparation and minimisation

The crystallographic information files (.cif) for the three quercetin structures were obtained from the Cambridge Structural Database (CDS): quercetin anhydrous (REFCODE: NAFZEC),

quercetin monohydrate (REFCODE: AKIJEK), quercetin dihydrate (REFCODE: FEFBEX). [8][16][27]

The crystal structures were minimised using the Forcite module in Materials Studio 2017. [63][64] The torsion angle around the phenyl and pyrone rings of the quercetin molecule was kept rigid while the hydroxyl group torsion angles were allowed to obtain the most energetically favourable configuration according to the packing of each structure. The unit cell parameters were kept constant. The SMART algorithm was selected for the structural minimisation and the DREIDING forcefield was used as this is one of the most suitable force-fields for treating organic molecules and it was proved to work effectively with quercetin. [65][66][67][68]

The files were exported as .car files (Cartesian coordinates) and then converted to fractional coordinates.

3.2.2 Conformational Analysis

The quantum chemical calculations were carried out in Gaussian09. [69] The cartesian coordinates of the quercetin molecules from the anhydrous, monohydrate and dihydrate crystal structures were extracted and used as the starting point for the geometry optimization. The energy of the molecules was calculated at the density functional level of theory, utilising the triple zeta with polarisation (TZVP) basis set of Alrich and co-workers. [70] The exchange correlation energy was calculated using the Becke three parameter Lee Yang Parr (B3LYP) functional, with the Grimme D3 dispersion energy function added to account for any intra- or inter-molecular dispersion energy. [71] The aqueous environment was simulated using the conducting polarisable continuum model (CPCM). [72]

To represent the crystal conformer in solution, the central torsion was frozen using the redundant coordinate option, whilst the rest of the molecule was relaxed to reduce any possible

energetic inconsistencies due to bond lengths from the crystal structures. To calculate the favoured conformation of each crystal structure conformer in the solution environment, the molecule was relaxed without any constraints.

All energies were normalised to the lowest energy molecular conformer to calculate the relative energy differences between the conformers.

3.2.3 Bulk Intrinsic Synthon analysis

The bulk intrinsic synthon analysis was carried out using the HABIT98 software developed at the University of Leeds. [73] HABIT98 takes in structural information from existing crystallographic data to construct a series of unit cells in three dimensions, and calculates the pairwise intermolecular interaction between a molecule in the origin unit cell and all the other molecules within a fixed radius from the central molecule. [35][36] In all three structures, the quercetin molecule of the first asymmetric unit of the unit cell was taken as the centre molecule and all intermolecular interaction were calculated within a sphere of 30Å radius. The calculation of intermolecular interaction energies was performed using the Momany force-field, which contains a Lennard-Jones potential for the VdW interactions, a specific 10-12 H-bonding potential and a Coulombic term with respect to the electrostatic interactions. [74] The contributions per functional group and per atom type to the total lattice energy of each structure were calculated using the DEBUG-2 function, and were summed over the asymmetric unit. The ranking of the intermolecular interactions by strength was outputted using the DEBUG-1 function. All visualization of molecular and crystal packing were carried out in Mercury CSD 3.10. [75]

The unit cell density was calculated using Equation 3.1:

$$Unit\ cell\ density = \frac{Molecular\ formula\ weight \times Z}{Unit\ cell\ volume} \qquad (3.1)$$

where Z is the number of asymmetric units in the unit cell.

The sequence of calculations followed for the conformational and bulk intrinsic synthon analysis are illustrated in Figure 3.2.

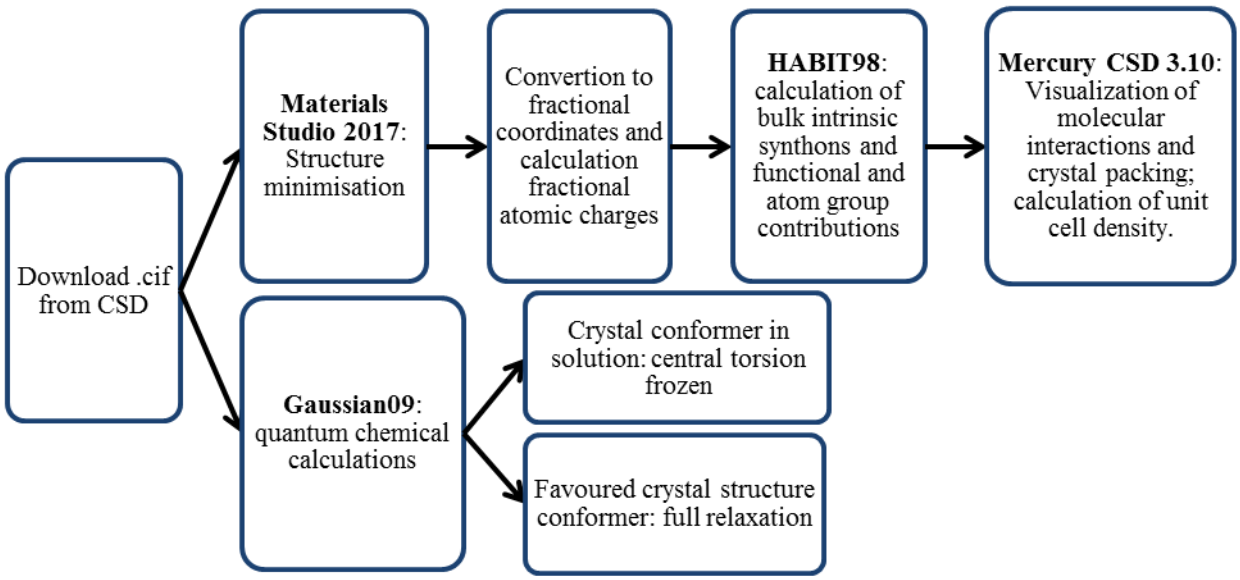

Figure 3.2 Flow diagram for the structure files preparation and sequence of calculations for the conformational and bulk intrinsic synthon analysis.

3.3 Results and Discussion

3.3.1 Unit Cell and Donor/Acceptor ratio Analysis

The unit cell packing and crystallographic data for quercetin anhydrous, monohydrate and dihydrate, as obtained from the Materials Studio optimised files, are illustrated in Figure 3.3 and Table 3.1. QA crystallizes with 4 quercetin molecules, and QMH with 4 quercetin and 4 water molecules, in orthorhombic and monoclinic unit cells respectively. QDH crystallizes with 2 quercetin molecules and 4 water molecules in a triclinic unit cell.

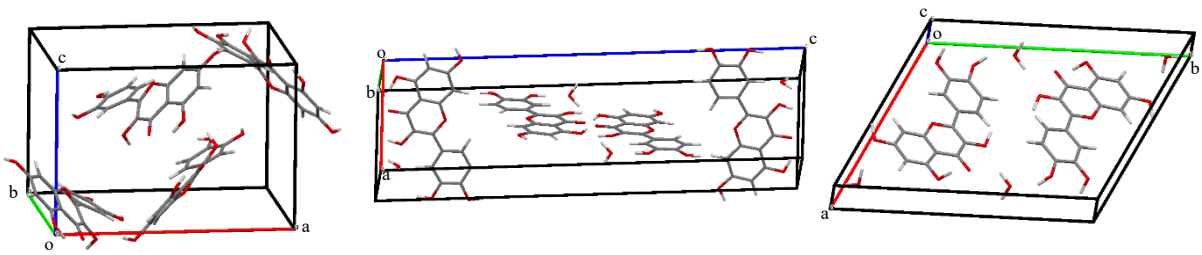

Figure 3.3 Unit cells of (a) Quercetin anhydrous (b) Quercetin monohydrate (c) Quercetin dihydrate

The density of the unit cell for each structure was calculated and it was found that the QMH and QDH structures present very similar values, whereas that of the QA structure is significantly lower. It is generally assumed that denser crystal forms are more thermodynamically stable than their less dense counterparts, for the same host molecules. [76]

Table 3.1. Unit cells parameters of quercetin structures. Z is the number of asymmetric units and Z' the number of molecules in each asymmetric unit.

Name	Quercetin anhydrous	Quercetin monohydrate	Quercetin dihydrate
Formula	$C_{15}H_{10}O_7$	$C_{15}H_{10}O_7.H_2O$	$C_{15}H_{10}O_7.2H_2O$
Space Group	$P2_1/a$ Orthorhombic	$P\ 2_1/c$ Monoclinic	P 1 Triclinic
Cell Lengths (Å)	**a** 14.7998 **b** 11.2379 **c** 10.3512	**a** 8.7370 **b** 4.8520 **c** 30.1600	**a** 13.109 **b** 17.026 **c** 3.67
Cell Angles (°)	**α** 90.0000 **β** 90.0000 **γ** 90.0000	**α** 90.0000 **β** 95.5200 **γ** 90.0000	**α** 98.18 **β** 90.342 **γ** 119.638
Cell Volume ($Å^3$)	1721.6	1272.61	701.931
Cell Density ($u/Å^3$)	0.702	1.007	0.964
Z, Z'	4, 1	4, 2	2, 3
Donor/acceptor ratio	0.357	0.438	0.500

A donor/acceptor ratio (d/a ratio) analysis was carried out for the quercetin structures, as described by Desiraju. [13] This analysis allows the identification of all the donors and

acceptors of the asymmetric unit that could potentially be involved in a hydrogen bond interaction, and not only those that actually form hydrogen bonds.

The d/a ratio is a ratio between all the hydrogen bond donors and acceptors in the asymmetric unit of the considered structure (QA, QMH, and QDH) that could potentially be involved in a hydrogen bond interaction. Since the quercetin molecule is made of only C, O, and H atoms, it contains five potential hydrogen bond donors (the H atoms in the hydroxyl groups) and 14 hydrogen bond acceptors (the two lone pairs of electrons each O atom of the hydroxyl groups, the carbonyl bond, and the keto group), as shown in Figure 3.4. Table 3.1 shows that the d/a ratio for the quercetin structures follows the trend QA < QMH < QDH. The inclusion of one water molecule in the lattice introduces two additional donors (hydrogen atoms) and two additional acceptors (two lone pairs of electrons on the oxygen atom) in the asymmetric unit, which reduces the imbalance of donors to acceptors and pushes the d/a ratio toward unity.

QA has a d/a ratio of 0.357, below the characteristic value of 0.5, which has been identified as the threshold below which organic molecules have a high tendency to form hydrated crystal structures. [13]

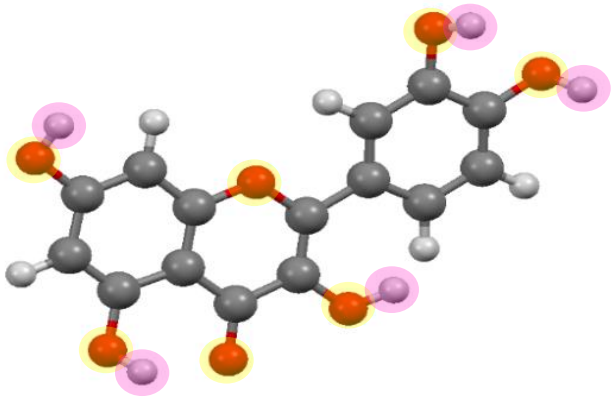

Figure 3.4 Hydrogen bond donors (highlighted in pink) and hydrogen bond acceptors (highlighted in yellow), for the quercetin molecule. Colour code: Grey- carbon atoms, red-oxygen atoms, white-hydrogen atoms.

3.3.2 Conformational analysis

The geometry and conformation of the quercetin molecule in the three solid forms has been studied and results were compared. The torsion angle of the phenyl to the pyrone ring of the quercetin molecules in each solid form has been calculated and it is illustrated in Figure 3.5. It is observed that the torsion angle is greatest (31.5°) for the anhydrous structure. This torsion angle leaves the molecule much less planar compared to the monohydrate and dihydrate structures, which present torsion angles of -1.0° and 6.7° respectively. [32]

The energy of the quercetin molecules in their different crystal structure conformations was calculated, to compare the impact that the change in molecular conformation has on molecule stability. It was found that their energy ranking was of the order QDH > QA > QMH. However, upon optimisation of the structures in the aqueous environment, the quercetin molecules both in the QMH and QDH structures optimised to almost the same conformation, which has a torsion angle of close to 17° about the central degree of freedom. In contrast, quercetin in QA optimised to a more twisted conformation which was calculated to be approximately 2.6 kcal/mol less stable than the conformer found from optimisation of the QMH and QDH crystal structure quercetin molecules.

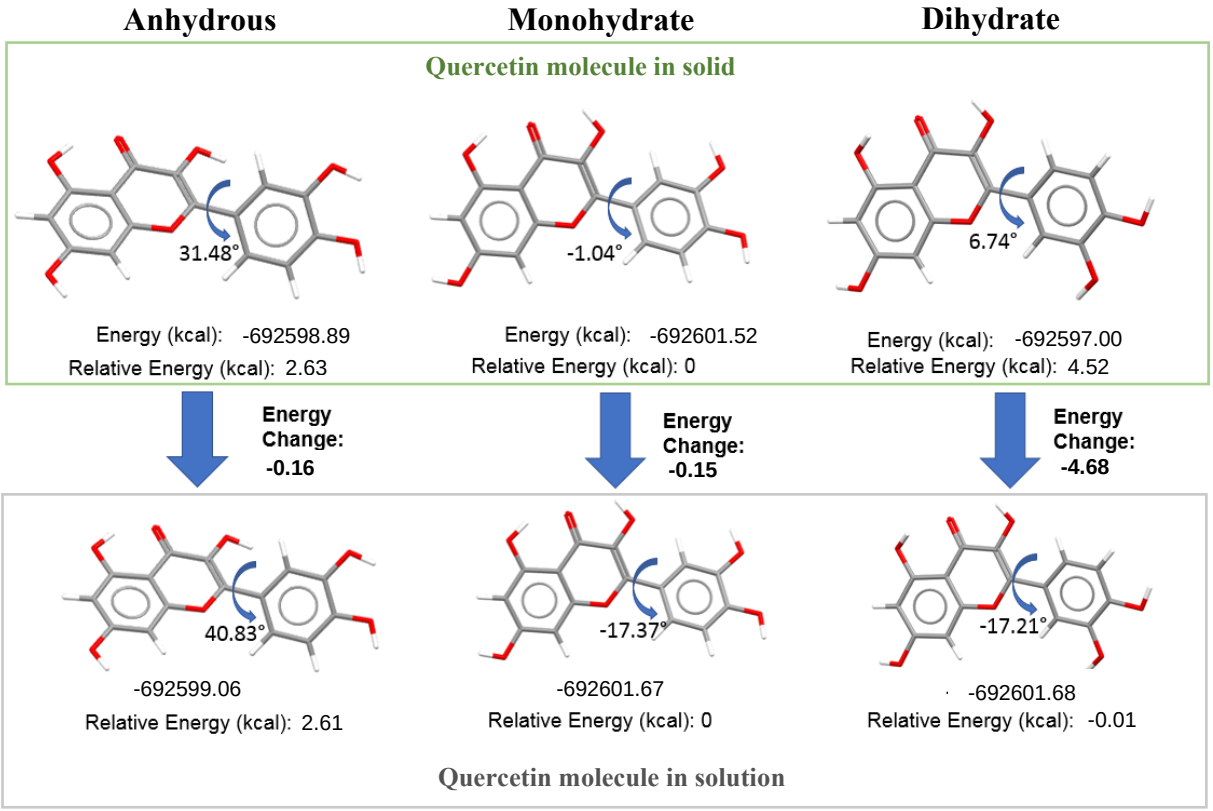

Figure 3.5 DFT geometry optimisation in an aqueous environment of the anhydrous, monohydrate and dihydrate crystal structure conformers of quercetin. The monohydrate and dihydrate optimise to almost the same twist about the central torsion, whilst the anhydrous optimises to a significantly different conformation.

These results suggest that that QMH quercetin molecular conformation is closest to the most stable conformation in the solution, with it only showing a small energy penalty to go from its optimised conformer to its crystal structure conformer. Despite the QDH molecule doing more energetic work to go from optimised conformer to crystal structure conformer, it should be observed that it is optimised to the same conformer as the QMH conformer, suggesting there is a low energy pathway between the crystal structure conformer and optimised conformer.

In comparison, the QA conformer optimised to a completely different structure, suggesting that the crystal structure conformation is not close to the most stable solution conformation and instead it optimises to a local stable minimum. Hence, one would assume that if the conformation is fluctuating in the dynamic solution state, it is more likely that the conformation would fluctuate to conformers which are close to its global minimum, such as the local minimum found from the QA geometry optimisation or the QMH and QDH conformers. Therefore, it can be postulated it is less energetically likely for the quercetin molecule to randomly fluctuate into the QA conformation, in favour of the local minimum found from the QA optimisation or the QMH or QDH conformers, suggesting that this would provide an energetic barrier to crystallisation.

Literature solubility studies indicates that the QDH structure is thermodynamically more stable than the QMH form below 100°C. [33] However, the conformational analysis presented here indicates that the QDH needs to do more energetic work to transition into its crystal structure conformation, in comparison to QMH. It is possible that, during nucleation from solution, the smaller amount of de-solvation necessary for the formation of QDH and a more energetically favourable intermolecular packing play a greater role than the conformation, driving the crystallisation of the QDH form over the monohydrate. This is further corroborated by the results of the synthonic analysis shown in the following paragraphs.

3.3.3 Bulk Intrinsic Synthon Analysis

The main bulk intrinsic intermolecular synthons in the three structures were computed using HABIT98 and ranked by strength using the DEBUG-1 function. The three strongest intermolecular synthons in each structure, those having the lowest energy value in kcal mol^{-1}, were calculated and are illustrated in Figure 3.6, Figure 3.7 and Figure 3.8, for QA, QMH and QDH respectively. Table 3.2 summarises the information for these synthons.

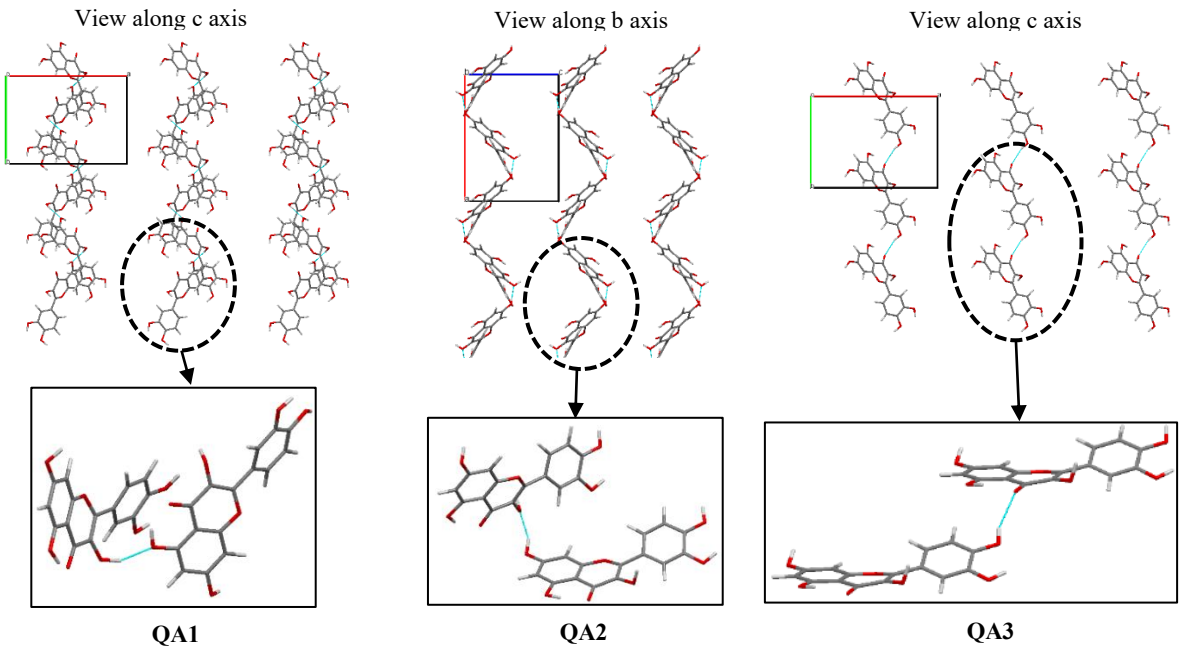

Figure 3.6 Key intermolecular synthons in quercetin anhydrous ordered by synthon strength. Light blue dotted lines indicate hydrogen bonding

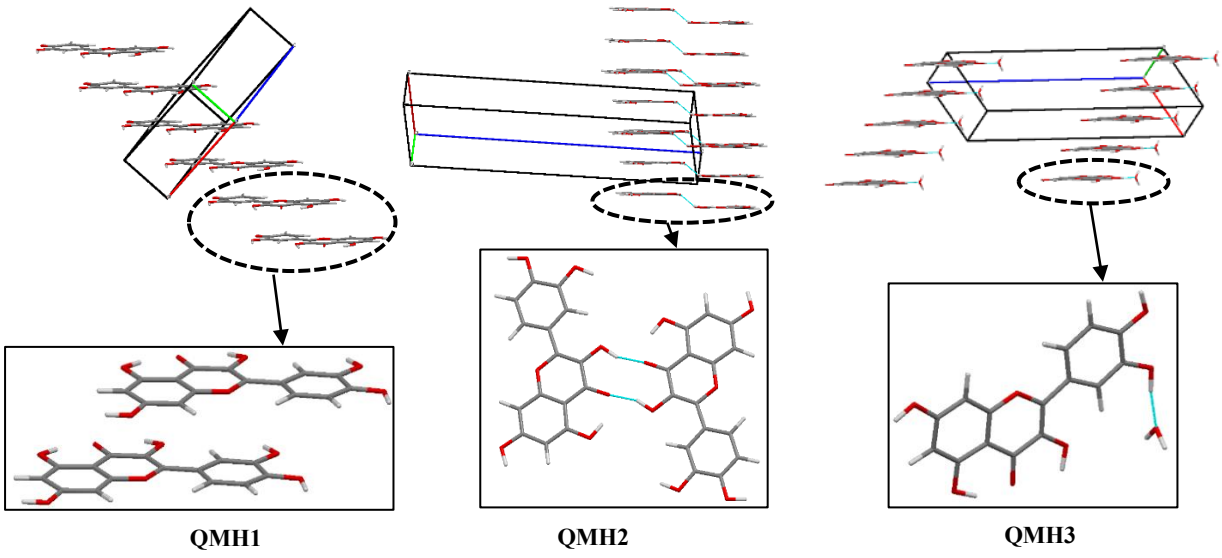

Figure 3.7 Key intermolecular synthons in quercetin monohydrate ordered by synthon strength. Light blue dotted lines indicate hydrogen bonding

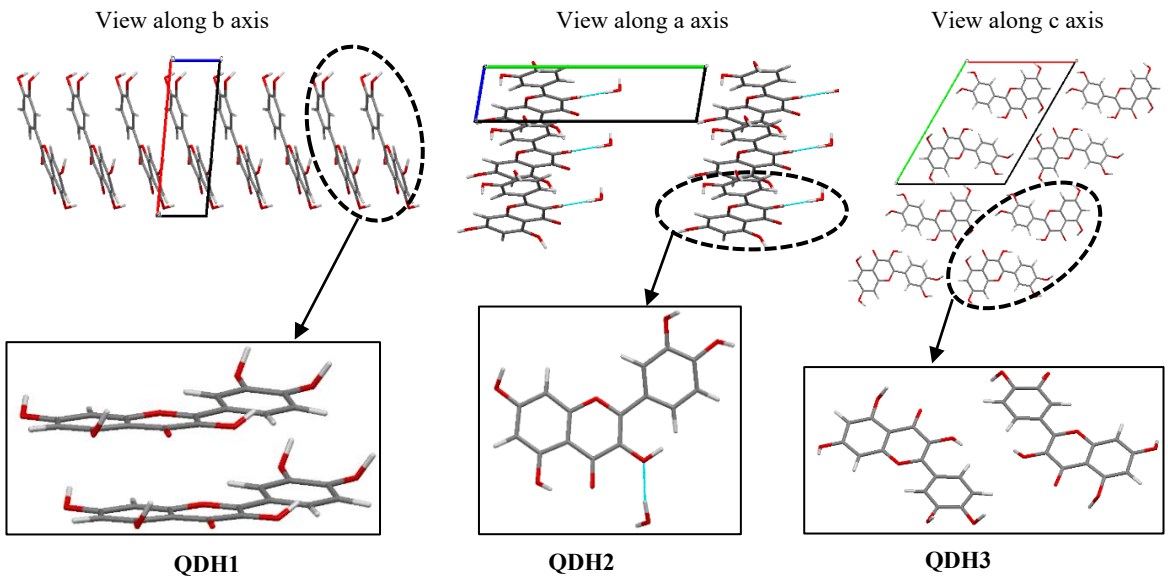

Figure 3.8 Key intermolecular synthons in quercetin dihydrate ordered by synthon strength. Light blue dotted lines indicate hydrogen bonding.

Table 3.2. Summary of intermolecular synthons in QA, QMH and QDH structures.

Quercetin structure	**Synthon**	**Molecules involved**	**Main synthon type**	**Inter-molecular distance (Å)**	**Atom-atom distance for H-bond (Å)**	**Synthon energy (Kcal mol^{-1})**	**% contribution to lattice energy**
Anhydrous	QA1	Quercetin - Quercetin	Hydrogen bond	6.93	1.89	-4.26	38.4%
	QA2	Quercetin - Quercetin	Hydrogen bond	7.57	1.88	-2.86	25.8%
	QA3	Quercetin - Quercetin	Hydrogen bond	11.24	2.28	-1.57	14.1%
Monohydrate	QMH1	Quercetin – Quercetin	π-π stacking	4.85	-	-6.39	24.5%
	QMH2	Quercetin – Quercetin	Hydrogen bond	7.99	1.92	-5.33	10.2%
	QMH3	Quercetin - Water	Hydrogen bond	5.93	1.76	-2.55	9.8%
Dihydrate	QDH1	Quercetin – Quercetin	π-π stacking	3.67	-	-7.66	37.8%
	QDH2	Quercetin – Water	Hydrogen bond	5.64	2.02	-1.61	7.9%

	QDH3	Quercetin - Quercetin	Permanent dipole-dipole	9.14	-	-1.43	3.5%

In QA, the three strongest interactions in the lattice are found to be mainly hydrogen bonds between quercetin molecules, whereby the QA2 forms an unbroken chain of quercetin molecules running along the a-direction of the lattice.

Table 3.3 shows that a quercetin molecule is found to form hydrogen bonds with six other quercetin molecules. The carbonyl bond and hydroxyl groups of the quercetin molecule are involved in the hydrogen bonding. The non-planar conformation of the quercetin molecule facilitates close contact between the hydroxyl and carbonyl groups, in order to maximize the number and strength in energy of these interactions. This is demonstrated in Figure 3.6, where the twisted conformation of quercetin allows for the close contacts between the hydroxyl and carbonyl groups to form the QA3 synthon.

However, the non-planar conformation of the molecule does not allow the formation of strong π-π stacking interactions which can be observed in the two hydrates structures, as shown in Figure 3.7 and Figure 3.8. Stacking interactions of such small intermolecular distance, as in the two hydrates, are not found to be among the three strongest interactions in the lattice of the anhydrous form, explaining the less closely packed nature of the quercetin molecules in the anhydrous structure.

Table 3.3. Hydrogen bonding interactions in QA, QMH and QDH

Quercetin structure	***Number of quercetin-quercetin hydrogen bonds***	***Number of quercetin-water hydrogen bonds***
Anhydrous	6	0
Monohydrate	6	4
Dihydrate	0	6

The strongest intermolecular synthons in the QMH and QDH structures, named QMH1 and QDH1 respectively, are π-π stacking interaction between quercetin molecules. The main contribution to this type of interaction comes from the aromatic carbon atoms of the phenyl and pyrone rings of the quercetin molecules, which interact via Van der Waal forces of attraction. In both hydrated structures, these interactions promote the formation of uninterrupted chains of stacked quercetin molecules packed in an offset orientation, thought to maximise the interaction between the negative central aromatic π-system and the positively charged hydrogens on the outer ring. [77] These strong interactions promote the close packing (shorter intermolecular distances) of the quercetin molecules in the two hydrates.

Comparison of the QDH1 to QMH1 shows that the π-π stacking interaction in the dihydrate form is stronger, with shorter intermolecular distances compared to that of the monohydrate. The π-π stacking interaction in the dihydrate is the dominant synthon, contributing to almost 38% of the total lattice energy. Clearly, the addition of the second water molecule in the unit cell of QDH indirectly influences the interactions among quercetin molecules, allowing them to pack closer together by forming stronger bonds.

In the two hydrated forms, synthons QMH3 and QDH2 are both hydrogen bond interactions between a hydroxyl group of a quercetin molecule and a water molecule. In both cases the interaction creates a channel of water molecules running parallel to the stacked chain of quercetin molecules. Under conditions which promote dehydration of the hydrated structures, the packing of water molecules in the two hydrates is expected to influence the dehydration mechanism. [78][79]

Unlike the anhydrous form, in both hydrates all of the hydroxyl groups of the quercetin molecules are forming at least one hydrogen bond, indicating that water compensates for unsatisfied hydrogen bonding. As presented in Table 3.3, in the QMH structure hydrogen bonding is partly satisfied by interactions among quercetin molecules and partly by quercetin-

water interactions, whereas in the dihydrate form all hydrogen bonding is satisfied exclusively by interactions between quercetin and water molecules. The contribution of the quercetin and water molecule interaction energies to the total lattice energy of each structure were calculated. As shown in Figure 3.9, the contribution of water to the total lattice energy increases with the number of water molecules per unit cell, indicating the tendency of incorporation of water molecules into the lattice, and that the formation of interactions between quercetin and water is favoured. The water molecules are found to contribute to 23% of the total lattice energy of QDH, highlighting the significance of the quercetin-water interactions in this structure.

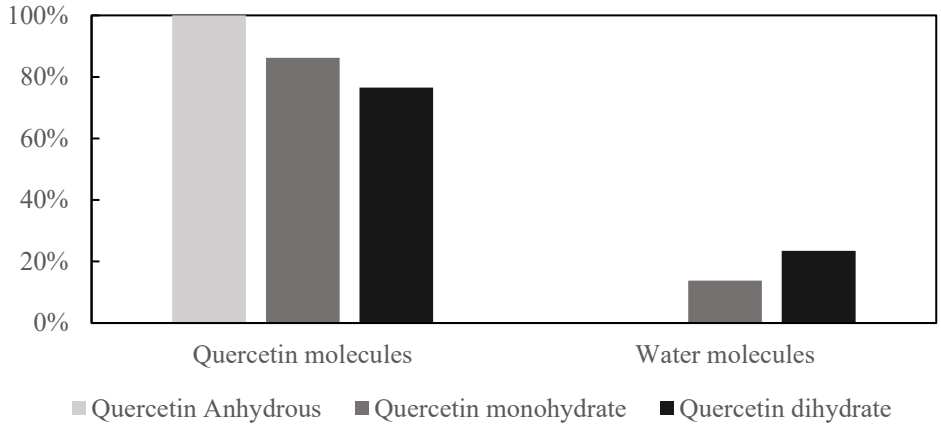

Figure 3.9 % contributions of quercetin and water molecules' interactions to total lattice energy of the three structures

In conclusion, the results of the present modelling analysis show that, as the degree of hydration and the number of water molecules in the unit cell increases for the three quercetin structures:

(1) hydrogen bonding in the lattice is more satisfied by interaction with the incorporated water molecules, allowing a more planar conformation for the quercetin molecules in the two hydrate structures

(2) the contribution of the π-π stacking interactions between quercetin molecules to the stabilization of the crystal lattice increases.

It is obvious from literature that crystallization of quercetin from an aqueous solvent always produces the dihydrate form. [16][30] This behaviour is explained by the modelling results is as follows:

- During crystallization from an aqueous solvent, the water molecules being much smaller in size compared to quercetin molecules, can be positioned close to the polar groups of the quercetin molecule forming hydrogen bonds;
- Once hydrogen bonding is satisfied, the quercetin molecules, having a more planar configuration, can pack more closely and efficiently via strong π-π stacking interactions;
- The smaller amount of de-solvation and conformational rearrangement in the dihydrate structure probably results in the easier crystallisation of this form from aqueous solution. This agrees with the higher calculated unit cell density which predicts a greatest stability;
- Quercetin in QA must take an energetically unfavourable conformation to satisfy its hydrogen bonding groups, thus ends up having a lower thermodynamic stability, and is not preferentially nucleated from an aqueous solvent.

From the points above, we summarise that the favourable packing of the quercetin-water H-bonding and quercetin-quercetin π-π stacking, rather than the conformational stability, results in the dominant crystallisation of the dihydrate form. We do however believe that the unfavourable conformation of the anhydrous form plays some role in making this structure especially challenging to nucleate.

The modelling results shown here highlight the importance of the water molecules in the stabilization of the crystal structures of QMH and QDH, as they can influence the hydrogen bonding pattern and affect the strength and nature of intermolecular interactions formed. These

results agree with experimental studies on the relative stability of quercetin and its hydrated forms. [17][28][31][32][33]

In conclusion, this works can explain why quercetin preferentially crystallizes as hydrated form from aqueous solvents and why polymorphic transitions from the QA to a hydrate are favourable in environments with high humidity. [17][33]

3.4 Conclusions

In this work, synthonic modelling and molecular conformational analysis were used to study three different crystalline structures of quercetin: the anhydrous, monohydrate and dihydrate forms. The role of water molecules within the structures was studied to understand how it affects the packing and conformation energetics of quercetin crystals. By analysing the bulk chemistry of QA, it was found that all key synthons are polar interactions, involving hydrogen bonds and permanent dipole-dipole interactions, while in the QMH and QDH structures the synthon contributing more to the lattice energy is a non-polar π-π stacking interaction. The hydrogen bonding interactions in the two hydrates are satisfied partly (QMH) or exclusively (QDH) by interaction with the water molecules.

The results of the synthonic modelling can explain the crystallization behaviour of quercetin reported in literature and its tendency to crystallize or transform in the dihydrated form in the presence of water molecules. A conformational analysis was also performed and revealed that the quercetin molecules within QA are organized in a less planar arrangement, thus being unable to pack as efficiently as in the hydrated crystals and resulting in a lower unit cell density. The quercetin molecules in the QMD and QDH are arranged in a more planar way, since quercetin hydrogen bonding is satisfied by the presence of water molecules.

In conclusion, this work shows how synthonic modelling and conformational analysis can be used as a predicting tool to better understand the relationship between crystal structure and

product properties (particularly stability), leading to a more efficient product formulation and faster development, but also as a tool to predict and design crystallization processes in order to obtain crystals with desired physiochemical properties.

Acknowledgements

The authors gratefully acknowledge Professor K. J. Roberts for the use of Habit98 synthonic modelling software, which was used in this work. Financial support was provided by the School of Food Science and Nutrition, University of Leeds, United Kingdom.

References

[1] Healy, A. M.; Worku, Z. A.; Kumar, D.; Madi, A. M. Pharmaceutical Solvates, Hydrates and Amorphous Forms: A Special Emphasis on Cocrystals. *Adv. Drug Deliv. Rev*. 2017, 117, 25–46. https://doi.org/10.1016/j.addr.2017.03.002.

[2] Threlfall, T. L. Analysis of Organic Polymorphs. A Review. *Analyst* 1995, 120 (10), 2435–2460. https://doi.org/10.1039/AN9952002435.

[3] Takieddin, K.; Khimyak, Y. Z. Prediction of Hydrate and Solvate Formation Using Statistical Models. *Cryst. Growth Des*. 2016, 16(1), 70-81. https://doi.org/10.1021/acs.cgd.5b00966.

[4] Sung, H.; Fan, Y.; Yeh, K.; Chen, Y.; Chen, L. A New Hydrate Form of Diflunisal Precipitated from a Microemulsion System. *Colloids Surf. B* 2013, 109, 68–73.

[5] Tilbury, C. J.; Chen, J.; Mattei, A.; Chen, S.; Sheikh, A. Y. Combining Theoretical and Data-Driven Approaches To Predict Drug Substance Hydrate Formation. *Cryst. Growth Des*. 2018, 18(1), 57-67. https://doi.org/10.1021/acs.cgd.7b00517.

[6] Price, C. P.; Glick, G. D.; Matzger, A. J. Dissecting the Behavior of a Promiscuous Solvate Former. *Angew. Chem. Int. Ed.* 2006, 45(13), 2062-2066. https://doi.org/10.1002/anie.200503533.

[7] Griesser, U. J. The Importance of Solvates. Polymorphism in the Pharmaceutical Industries (Chapter 8). 2006 Wiley-VCH Verlag GmbH & Co. KGaA. https://doi.org/doi:10.1002/3527607889.

[8] Domagała, S.; Munshi, P.; Ahmed, M.; Guillot, B.; Jelsch, C. Structural Analysis and Multipole Modelling of Quercetin Monohydrate - A Quantitative and Comparative Study. *Acta Crystallogr. Sect. B Struct. Sci*. 2011, 67 (1), 63–78. https://doi.org/10.1107/S0108768110041996.

[9] Trimdale, A. Detailed Analysis of Packing E Ffi Ciency Allows Rationalization of Solvate Formation Propensity for Selected Structurally Similar Organic Molecules. *Cryst. Growth Des*. 2018, 22–27. https://doi.org/10.1021/acs.cgd.7b01457.

[10] Vippagunta, S. R.; Brittain, H. G.; Grant, D. J. W. Crystalline Solids. *Adv. Drug Deliv. Rev.* 2001, 48, 3–26.

[11] Thompson, H. P. G.; Day, G. M. Which Conformations Make Stable Crystal Structures? Mapping Crystalline Molecular Geometries to the Conformational Energy Landscape. *Chem. Sci.* 2014, 5 (8), 3173–3182. https://doi.org/10.1039/C4SC01132E.

[12] Streek, J. Van De; Motherwell, S. New Software for Searching the Cambridge Structural Database for Solvated and Unsolvated Crystal Structures Applied to Hydrates *CrystEngComm* 2007, 9, 55-64. https://doi.org/10.1039/b613332k.

[13] Desiraju, G. R. Hydration in Organic Crystals: Prediction from Molecular Structure. *J. Chem. Soc. Chem. Commun*. 1991, 6, 426–428. https://doi.org/10.1039/C39910000426.

[14] Infantes, L. Organic Crystal Hydrates : What Are the Important Factors for Formation *CrystEngComm*, 2007, 9, 65-71. https://doi.org/10.1039/b612529h.

[15] Kons, A.; Be, A.; Actin, A. Polymorphs and Hydrates of Sequifenadine Hydrochloride : Crystallographic Explanation of Observed Phase Transitions and Thermodynamic Stability. Cryst. Growth Des. 2017, 17(3), 1146-1158. https://doi.org/10.1021/acs.cgd.6b01534.

[16] Rossi, M.; Rickles, L. F.; Halpin, W. A. The Crystal and Molecular Structure of Quercetin: A Biologically Active and Naturally Occurring Flavonoid. *Bioorg. Chem*. 1986, 14 (1), 55–69. https://doi.org/10.1016/0045-2068(86)90018-0.

[17] Srinivas, K.; King, J. W.; Howard, L. R.; Monrad, J. K. Solubility and Solution Thermodynamic Properties of Quercetin and Quercetin Dihydrate in Subcritical Water. *J. Food Eng.* 2010, 100 (2), 208–218. https://doi.org/10.1016/j.jfoodeng.2010.04.001.

[18] Luo, Z.; Murray, B. S.; Yuso, A.; Morgan, M. R. a; Povey, M. J. W.; Day, A. J. Particle-Stabilizing Effects of Flavonoids at the Oil - Water Interface. *J. Agric. Food Chem.* 2011, 59, 2636–2645.

[19] Ay, M.; Charli, A.; Jin, H.; Anantharam, V.; Kanthasamy, A.; Kanthasamy, A. G. Quercetin. *Nutraceuticals* 2016, 447–452. https://doi.org/10.1016/B978-0-12-802147-7.00032-2.

[20] Zembyla, M.; Murray, B. S.; Sarkar, A. Water-in-Oil Pickering Emulsions Stabilized by Water-Insoluble Polyphenol Crystals. *Langmuir* 2018, 34, 1–7. https://doi.org/10.1021/acs.langmuir.8b01438.

[21] Laughton, M. J.; Halliwell, B.; Evans, P. J.; Robin, J.; Hoult, S. Antioxidant and pro-Oxidant Actions of the Plant Phenolics Quercetin, Gossypol and Myricetin: Effects on Lipid Peroxidation, Hydroxyl Radical Generation and Bleomycin-Dependent Damage to DNA. *Biochem. Pharmacol.* 1989, 38 (17), 2859–2865. https://doi.org/https://doi.org/10.1016/0006-2952(89)90442-5.

[22] Oršolić, N.; Knežević, A. H.; Šver, L.; Terzić, S.; Bašić, I. Immunomodulatory and Antimetastatic Action of Propolis and Related Polyphenolic Compounds. *J. Ethnopharmacol*. 2004, 94 (2), 307–315. https://doi.org/https://doi.org/10.1016/j.jep.2004.06.006.

[23] Cushnie, T. P. T.; Lamb, A. J. Antimicrobial Activity of Flavonoids. *Int. J. Antimicrob. Agents* 2005, 26 (5), 343–356. https://doi.org/https://doi.org/10.1016/j.ijantimicag.2005.09.002.

[24] Duarte, J.; Pérez-Palencia, R.; Vargas, F.; Ocete, M. A.; Pérez-Vizcaino, F.; Zarzuelo, A.; Tamargo, J. Antihypertensive Effects of the Flavonoid Quercetin in Spontaneously Hypertensive Rats. *Br. J. Pharmacol.* 2001, 133 (1), 117–124. https://doi.org/10.1038/sj.bjp.0704064.

[25] Larocca, L. M.; Piantelli, M.; Leone, G.; Sica, S.; Teofili, L.; Panici, P. B.; Scambia, G.; Mancuso, S.; Capelli, A.; Ranelletti, F. O. Type II Oestrogen Binding Sites in Acute Lymphoid and Myeloid Leukaemias: Growth Inhibitory Effect of Oestrogen and Flavonoids. *Br. J. Haematol.* 1990, 75 (4), 489–495. https://doi.org/10.1111/j.1365-2141.1990.tb07787.x.

[26] Grotewold, E. The Science of Flavonoids; Springer Editions 2006. https://doi.org/10.1007/978-0-387-28822-2.

[27] Vasisht, K.; Chadha, K.; Karan, M.; Bhalla, Y.; Jena, A. K.; Chadha, R. Enhancing Biopharmaceutical Parameters of Bioflavonoid Quercetin by Cocrystallization. *CrystEngComm* 2016, 18 (8), 1403–1415. https://doi.org/10.1039/C5CE01899D.

[28] Hanuza, J.; Godlewska, P.; Kucharska, E.; Ptak, M.; Kopacz, M.; Ma, M.; Hermanowicz, K.; Macalik, L. Molecular Structure and Vibrational Spectra of Quercetin and Quercetin-5 ' -Sulfonic Acid. *Vibrational Spectroscopy* 2017, 88, 94–105. https://doi.org/10.1016/j.vibspec.2016.11.007.

[29] Nifant'ev, E. E.; Koroteev, M. P.; Kaziev, G. Z.; Uminskii, A. A.; Grachev, A. A.; Men'shov, V. M.; Tsvetkov, Y. E.; Nifant'ev, N. E.; Bel'skii, V. K.; Stash, A. I. On the Problem of Identification of the Dihydroquercetin Flavonoid. *Russ. J. Gen. Chem*. 2006, 76 (1), 161–163. https://doi.org/10.1134/S1070363206010324.

[30] Jin, G. Z.; Yamagata, Y.; Tomita, K. Structure of Quercetin Dihydrate. *Acta Crystallogr. Sect. C Cryst. Struct. Commun.* 1990, 46 (2), 310–313. https://doi.org/10.1107/S0108270189006682.

[31] Olejniczak, S.; Potrzebowski, M. J. Solid State NMR Studies and Density Functional Theory (DFT) Calculations of Conformers of Quercetin. *Org Biomol Chem*. 2004, 2315–2322.

[32] Filip, X.; Grosu, I.; Micla, M. NMR Crystallography Methods to Probe Complex Hydrogen Bonding Networks : Application to Structure Elucidation of Anhydrous Quercetin. *CrystEngComm* 2013, 3, 4131–4142. https://doi.org/10.1039/c3ce40299a.

[33] Borghetti, G. S.; Carini, J. P.; Honorato, S. B.; Ayala, A. P.; Moreira, J. C. F.; Bassani, V. L. Thermochimica Acta Physicochemical Properties and Thermal Stability of Quercetin Hydrates in the Solid State. *Thermochim. Acta* 2012, 539, 109–114. https://doi.org/10.1016/j.tca.2012.04.015.

[34] Nguyen, T. T. H.; Rosbottom, I.; Marziano, I.; Hammond, R. B.; Roberts, K. J. Crystal Morphology and Interfacial Stability of RS -Ibuprofen in Relation to Its Molecular and Synthonic Structure. Cryst. Growth and Des. 2017, 17(6), 3088-3099. https://doi.org/10.1021/acs.cgd.6b01878.

[35] Pickering, J.; Hammond, R. B.; Ramachandran, V.; Soufian, M.; Roberts, K. J. Synthonic Engineering Modelling Tools for Product and Process Design. In Engineering Crystallography: From Molecule to Crystal to Functional Form; Springer Netherlands: Dordrecht, 2017; pp 155–176. https://doi.org/10.1007/978-94-024-1117-1_10.

[36] Rosbottom, I.; Roberts, K. J.; Docherty, R. The Solid State, Surface and Morphological Properties of P -Aminobenzoic Acid in Terms of the Strength and Directionality of Its Intermolecular Synthons. *CrystEngComm* 2015, 17 (30), 5768–5788. https://doi.org/10.1039/C5CE00302D.

[37] Desiraju, G. R. Crystal Engineering: From Molecule to Crystal. *J. Am. Chem. Soc.* 2013, 135 (27), 9952–9967. https://doi.org/10.1021/ja403264c.

[38] Rosbottom, I.; Roberts, K. J. Crystal Growth and Morphology of Molecular Crystals. In Engineering Crystallography: From Molecule to Crystal to Functional Form; Springer Netherlands: Dordrecht, 2017; pp 109–131. https://doi.org/10.1007/978-94-024-1117-1_7.

[39] Momany, F. A.; Carruthers, L. M.; McGuire, R. F.; Scheraga, H. A. Intermolecular Potentials from Crystal Data. III. Determination of Empirical Potentials and Application to the Packing Configurations and Lattice Energies in Crystals of Hydrocarbons, Carboxylic Acids, Amines, and Amides. *J. Phys. Chem*. 1974, 78 (16), 1595–1620. https://doi.org/10.1021/j100609a005.

[40] Hagler, A. T.; Lifson, S.; Dauber, P. Consistent Force Field Studies of Intermolecular Forces in Hydrogen-Bonded Crystals. 2. A Benchmark for the Objective Comparison of Alternative Force Fields. *J. Am. Chem. Soc.* 1979, 101 (18), 5122–5130. https://doi.org/10.1021/ja00512a002.

[41] Lifson, S.; Hagler, A. T.; Dauber, P. Consistent Force Field Studies of Intermolecular Forces in Hydrogen-Bonded Crystals. 1. Carboxylic Acids, Amides, and the C:O.cntdot..cntdot..cntdot.H- Hydrogen Bonds. *J. Am. Chem. Soc.* 1979, 101 (18), 5111–5121. https://doi.org/10.1021/ja00512a001.

[42] Nemethy, G.; Pottle, M. S.; Scheraga, H. A. Energy Parameters in Polypeptides. 9. Updating of Geometrical Parameters, Nonbonded Interactions, and Hydrogen Bond Interactions for the Naturally Occurring Amino Acids. *J. Phys. Chem.* 1983, 87 (11), 1883–1887. https://doi.org/10.1021/j100234a011.

[43] Poornachary, S. K.; Shan, P.; Tan, R. B. H. Impurity Effects on the Growth of Molecular Crystals : Experiments and Modeling. *Adv. Powder Technol.* 2008, 19 (5), 459–473. https://doi.org/10.1016/S0921-8831(08)60912-7.

[44] Yani, Y.; Chow, P. S.; Tan, R. B. H. Molecular Simulation Study of the Effect of Various Additives on Salbutamol Sulfate Crystal Habit. *Mol. Pharmaceutics* 2011, 1910–1918. https://doi.org/10.1021/mp200277u.

[45] Fan, H.; Song, X.; Liu, T.; Xu, Y.; Yu, J. Effect of Al 3 + on Crystal Morphology and Size of Calcium Sulfate Hemihydrate : Experimental and Molecular Dynamics Simulation Study. J. *Cryst. Growth* 2018, 495, 29–36. https://doi.org/10.1016/j.jcrysgro.2018.05.013.

[46] Tong, Z.; Xie, Y.; Zhang, Y. Molecular Dynamics Simulation on the Interaction between Polymer Inhibitors and β -Dicalcium Silicate Surface. *J. Mol. Liq.* 2018, 259, 65–75. https://doi.org/10.1016/j.molliq.2018.03.018.

[47] Poornachary, S. K.; Chia, V. D.; Yani, Y.; Han, G.; Chow, P. S.; Tan, R. B. H. Anisotropic Crystal Growth Inhibition by Polymeric Additives : Impact on Modulation of Naproxen Crystal Shape and Size. *Cryst. Growth and Des.* 2017, 17(9), 4844-4854. https://doi.org/10.1021/acs.cgd.7b00802.

[48] Cai, Z.; Liu, Y.; Song, Y.; Guan, G.; Jiang, Y. The Effect of Tailor-Made Additives on Crystal Growth of Methyl Paraben : Experiments and Modelling. *J. Cryst. Growth* 2017, 461, 1–9. https://doi.org/10.1016/j.jcrysgro.2016.12.103.

[49] Yang, X.; Qian, G.; Zhang, X.; Duan, X.; Zhou, X. Effects of Solvent and Impurities on Crystal Morphology of Zinc Lactate Trihydrate. *Chinese J. Chem. Eng.* 2014, 22 (2), 221–226. https://doi.org/https://doi.org/10.1016/S1004-9541(14)60026-4.

[50] Turner, T. D.; Hatcher, L. E.; Wilson, C. C.; Roberts, K. J. Habit Modification of the Active Pharmaceutical Ingredient Lovastatin Through a Predictive Solvent Selection Approach. *J. Pharm. Sci.* 2019, 108(5), 1–9. https://doi.org/10.1016/j.xphs.2018.12.012.

[51] Rosbottom, I.; Ma, C. Y.; Turner, T. D.; Connell, R. A. O.; Loughrey, J.; Sadiq, G.; Davey, R. J.; Roberts, K. J. Influence of Solvent Composition on the Crystal Morphology and Structure of P‐Aminobenzoic Acid Crystallized from Mixed Ethanol and Nitromethane Solutions. Cryst. Growth Des. 2017, 17(8), 4151–4161. https://doi.org/10.1021/acs.cgd.7b00425.

[52] Toroz, D.; Rosbottom, I.; Turner, T. D.; Corzo, D. M. C.; Hammond, R. B.; Lai, X.; Roberts, K. J. Towards an Understanding of the Nucleation of Alpha-Para Amino Benzoic Acid from Ethanolic Solutions: A Multi-Scale Approach. *Faraday Discuss*. 2015, 179 (0), 79–114. https://doi.org/10.1039/C4FD00275J.

[53] Han, D.; Karmakar, T.; Bjelobrk, Z.; Gong, J.; Parrinello, M. Solvent-Mediated Morphology Selection of the Active Pharmaceutical Ingredient Isoniazid: Experimental and Simulation Studies. *Chem. Eng. Sci.* 2018, 204, 320-328 https://doi.org/https://doi.org/10.1016/j.ces.2018.10.022.

[54] Lukman, Z.; Anuar, N.; Bakar, N. F. A.; Rahman, N. A. Alpha Lactose Monohydrate Morphology: Molecular Modelling and Experimental Approach. *Int. J. Eng. Technol.* 2018, 7 (4), 107–112.

[55] Moldovan, A. A.; Rosbottom, I.; Ramachandran, V.; Pask, C. M.; Olomukhoro, O.; Roberts, K. J. Crystallographic Structure , Intermolecular Packing Energetics , Crystal Morphology and Surface Chemistry of Salmeterol Xinafoate (Form I). *J. Pharm. Sci.* 2017, 106 (3), 882–891. https://doi.org/10.1016/j.xphs.2016.11.016.

[56] Clydesdale, G.; Roberts, K. J.; Telfer, G. B.; Grant, D. J. W. Modeling the Crystal Morphology of α-Lactose Monohydrate. *J. Pharm. Sci*. 1997, 86 (1), 135–141. https://doi.org/10.1021/js950496w.

[57] Braun, D. E.; Schneeberger, A.; Griesser, U. J. Understanding the Role of Water in 1,10-Phenanthroline Monohydrate. CrystEngComm 2017, 41, 6133–6145. https://doi.org/10.1039/c7ce01371j.

[58] Souza, L. A. De; Tavares, W. M. G.; Lopes, A. P. M.; Soeiro, M. M.; Almeida, W. B. De. Structural Analysis of Flavonoids in Solution through DFT 1 H NMR Chemical Shift Calculations : Epigallocatechin , Kaempferol and Quercetin. *Chem. Phys. Lett.* 2017, 676, 46–52. https://doi.org/10.1016/j.cplett.2017.03.038.

[59] Thompson, H.P.G.; Day G.M. Which conformations make stable crystal structures? Mapping crystalline molecular geometries to the conformational energy landscape. *Chem. Sci.*, 2014, 5, 3173-3182.

[60] Rosbottom, I.; Toroz, D; Hammond, R.B.; Roberts, K.J., Conformational and Structural Stability Calculations of the Single Molecule and Hydrogen Bonded Clusters of Para

Aminobenzoic Acid in the Gas and Solution Phases, *CrystEngComm* 2018, 20, (46), 7543-7555.

[61] Desiraju, G. R. Supramolecular Synthons in Crystal Engineering—A New Organic Synthesis. *Angew. Chemie Int. Ed*. 1995, 34 (21), 2311–2327. https://doi.org/10.1002/anie.199523111.

[62] Desiraju, G. R. Crystal Engineering: Structure, Property and beyond. *IUCrJ* 2017, 4 (Pt 6), 710–711. https://doi.org/10.1107/S2052252517014853.

[63] Groom, C. R.; Bruno, I. J.; Lightfoot, M. P.; Ward, S. C. The Cambridge Structural Database. *Acta Crystallogr. Sect. B* 2016, 72 (2), 171–179. https://doi.org/10.1107/S2052520616003954.

[64] AS, I. Discovery Studio Modeling Environment, Release 7.0 [Software Program]. Accelrys Software Inc.: San Diego 2013.

[65] Mayo, S. L.; Olafson, B. D.; Goddard, W. A. DREIDING: A Generic Force Field for Molecular Simulations. *J. Phys. Chem*. 1990, 94 (26), 8897–8909. https://doi.org/10.1021/j100389a010.

[66] Grančič, P.; Bylsma, R.; Meekes, H.; Cuppen, H.M. Evaluation of All-Atom Force Fields for Anthracene Crystal Growth. Cryst. Growth Des. 2015, 15(4), 1625-1633. https://doi.org/10.1021/cg5013507

[67] Nguyen, T. T. H.; Rosbottom, I.; Marziano, I.; Hammond, R. B.; Roberts, K. J., Crystal Morphology and Interfacial Stability of RS-Ibuprofen in Relation to Its Molecular and Synthonic Structure. *Cryst. Growth Des*. 2017, 17, (6), 3088-3099

[68] Rosbottom, I.; Roberts, K. J.; Docherty, R., The solid state, surface and morphological properties of p-aminobenzoic acid in terms of the strength and directionality of its intermolecular synthons. *CrystEngComm* 2015, 17, (30), 5768-5788

[69] Frisch, M. J.; Trucks, G. W.; Schlegel, H. B.; Scuseria, G. E.; Robb, M. A.; Cheeseman, J. R.; Scalmani, G.; Barone, V.; Mennucci, B.; Petersson, G. A.; et al. Gaussian 09, Revision B.01. Gaussian, Inc., Wallingford CT 2009.

[70] Schäfer, A.; Horn, H.; Ahlrichs, R. Fully Optimized Contracted Gaussian Basis Sets for Atoms Li to Kr. *J. Chem. Phys*. 1992, 97 (4), 2571–2577. https://doi.org/10.1063/1.463096.

[71] Becke, A. D. Density-functional Thermochemistry. IV. A New Dynamical Correlation Functional and Implications for Exact-exchange Mixing. *J. Chem. Phys.* 1996, 104 (3), 1040–1046. https://doi.org/10.1063/1.470829.

[72] Takano, Y.; Houk, K. N. Benchmarking the Conductor-like Polarizable Continuum Model (CPCM) for Aqueous Solvation Free Energies of Neutral and Ionic Organic Molecules. *J. Chem. Theory Comput.* 2005, 1 (1), 70–77. https://doi.org/10.1021/ct049977a.

[73] Clydesdale, G.; Roberts, K. J.; Docherty, R. HABIT95 — a Program for Predicting the Morphology of Molecular Crystals as a Function of the Growth Environment. *J. Cryst. Growth* 1996, 166 (1–4), 78–83. https://doi.org/10.1016/0022-0248(96)00056-5.

[74] Momany, F. A.; Carruthers, L. M.; Mcguire, R. F.; Scheraga, H. A. Intermolecular Potentials from Crystal Data . III . Determination of Empirical Potentials and Application to the Packing Configurations and Lattice Energies in Crystals of Hydrocarbons , Carboxylic Acids , Amines , and Amides. *J. Phys. Chem.* 1974, 78 (16), 1595–1620. https://doi.org/10.1021/j100609a005.

[75] van de Streek, J.; Motherwell, S. New Software for Searching the Cambridge Structural Database for Solvated and Unsolvated Crystal Structures Applied to Hydrates. *CrystEngComm* 2007, 9 (1), 55–64. https://doi.org/10.1039/B613332K.

[76] Kitaigorodskii, A. I. Organic Chemical Crystallography; Consultants Bureau: New York, 1961.

[77] Martinez, C. R.; Iverson, B. L. Rethinking the Term “pi-Stacking.” *Chem. Sci.* 2012, 3 (7), 2191–2201. https://doi.org/10.1039/C2SC20045G.

[78] Skarbulis, E.; Actin, A. Structural Characterization and Rationalization of Formation , Stability , and Transformations of Benperidol Solvates Agris Be Rzin. *Cryst. Growth Des*. 2015, 15(5), 2337-2351. https://doi.org/10.1021/acs.cgd.5b00138.

[79] Garnier, S.; Petit, S.; Coquerel, G. Dehydration Mechanism and Crystallisation Behaviour of Lactose. *J. Therm. Anal. Calorim.* 2002, 68 (2), 489–502. https://doi.org/10.1023/A:1016087702409.

CHAPTER 4 - SOLID-STATE CHARACTERIZATION AND ROLE OF SOLVENT MOLECULES ON THE CRYSTAL STRUCTURE, PACKING AND PHYSIOCHEMICAL PROPERTIES OF DIFFERENT QUERCETIN SOLVATES

Abstract

In this work a novel quercetin and dimethyl sulfoxide (DMSO) solvate (QDMSO) crystal structure was grown from a mixture of DMSO and water as solvent. Quercetin is a naturally occurring bioflavonoid widely used in the nutraceutical industry due to its many health benefits. Understanding quercetin solvates formation is essential for the design of novel particulate products with tailored quality attributes, including solubility, thermal resistance and bioavailability.

Here, the physiochemical properties and phase transitions of QDMSO were characterized by a wide range of experimental techniques, and the crystal structure, molecular packing and intermolecular interactions (synthons) within the crystal lattice were modelled. Modelling and experimental results were compared to those of other known quercetin crystal structures, an anhydrous, a monohydrate and a dihydrate form, to elucidate the role of the solvent molecules on the molecular packing and intermolecular interactions and, ultimately, on the physiochemical properties of each crystal form. It was found that in QDMSO, hydrogen bonds and dipole-dipole interactions had a greater contribution to the total lattice energy, and quercetin-solvent hydrogen bonds were stronger in energy compared to those of the other quercetin structures. These findings were used to explain the superior thermal stability of the QDMSO structure as well as its moisture-dependent behavior. This work demonstrates a

coupled modelling and experimental methodology that relates intermolecular interactions and molecular packing in different solvated forms to physiochemical properties and can help in a better prediction and design of particulate products via rational choice of the solid form.

4.1 Introduction

Solvates and hydrates are multicomponent crystalline solids that comprise a host molecule and a guest solvent molecule in the crystal lattice. [1] Many active pharmaceutical ingredients (APIs) and food grade substances can form these structures. [1][2] The presence of guest solvent molecules within the crystal can affect the molecular conformation of the host molecule within the structure, as well as the type and strength of intermolecular interactions that characterize the crystal lattice, resulting in different physiochemical properties, such as thermodynamic stability, solubility, dissolution rate and bioavailability. [3][4][5][6]

Hydrate/solvate formation can then be exploited to safely manipulate the physiochemical properties of crystals in order to achieve desired quality attributes such as improved solubility and bioavailability. [7] In fact, many pharmaceutical products are marketed as solvated crystal forms, for example amoxicillin trihydrate and darunavir ethanolate. [8][9] De-solvation of a solvated crystal form can also provide an alternative pathway to the formation of polymorphic forms that would otherwise be difficult or impossible to crystallize by conventional crystallization techniques. [6] These are typical examples of crystal engineering approaches, which focus on controlling the way that molecules crystallize to produce materials and final products with tailored properties. [10]

In some cases, unexpected transformations of the unsolvated crystals to their solvated forms, or even between different solvated forms, can happen during manufacturing or storage.

[11][12] These transformations can cause undesired physiochemical properties of the final marketed products, compromising their quality and thus incurring extra costs and safety risks for the consumers. [6][11] It is, therefore, imperative to know how crystallization parameters, for example choice of solvent, or environmental conditions during storage, like temperature and relative humidity, could induce any phase transitions between the different crystal forms of a crystalline material. [13]

Quercetin, 2-(3,4-Dihydroxyphenyl)-3,5,7-trihydroxy-4H-chromen-4-one, is a naturally occurring flavonoid found in many fruits and vegetables (e.g., onions, berries and tomatoes) as well as in tea, wine and vinegar. [14][15] Quercetin has recently stimulated considerable interest within the nutrition and food science communities due to its significant association between dietary consumption and various health benefits, including antioxidant, anti-inflammatory and antitumor activities. [14][15][16][17] Due to this vast range of biological effects, quercetin finds use in the nutraceutical industry and as a food supplement product. [15]

Quercetin has been reported to exist as anhydrous, monohydrate and dihydrate crystal forms. [14][18][19][20][21] A previous study identified how water molecules in the hydrated structures of quercetin could impact significantly upon packing and conformation energetics of these forms, as compared to the anhydrous form. [22] Quercetin dihydrate, the commercial form of this compound, has been studied experimentally using a wide range of techniques, and has been identified as the most thermodynamically stable form at ambient conditions. [23][24] However, there has been relatively little work to explore other possible solvated forms of quercetin, which could have superior physical properties for formulation in food products.

In this work, we further explored the solid-state landscape of quercetin by crystallizing this molecule in mixtures of dimethyl sulfoxide (DMSO) and water. Quercetin is characterized by a very low water solubility, which results in difficulties in growing quercetin crystals from

water. [15] Therefore, mixtures of DMSO and water were used to improve yield of crystallization as well as to achieve larger crystals, since DMSO has the ability to solubilize a wide range of otherwise insoluble or sparingly soluble substances. [25]

A novel crystal structure of quercetin, a quercetin-DMSO solvate (QDMSO), was discovered and comprehensively characterized by a range of analytical techniques. This was underpinned by molecular modelling of the molecular conformation and packing energetics to discover the role of the DMSO solvent molecule. The modelling work was compared to that of other quercetin structures – quercetin dihydrate (QDH), quercetin monohydrate (QMH), and quercetin anhydrous (QA), to evaluate the effect of the solvent molecules on the type and strength of intermolecular interactions, conformation and packing arrangements in the crystals. This information was then related to the physiochemical properties of these structures, for example the thermal and moisture-dependent stabilities. [22][24] This proposed working framework for the analysis of solvated structures can be extremely valuable when designing products, processes and storage conditions for particulate products with known solvated forms. [26][27]

4.2 Experimental section

Materials. Quercetin dihydrate with a purity of 97% w/w was obtained from Alfa Aesar (Port of Heysham Industrial Park, Lancashire, England) while dimethyl sulfoxide (DMSO) solvent was purchased from Fisher Scientific (Bishop Meadow Road, Loughborough, England). Water purified by treatment with a Milli-Q apparatus was used. Quercetin dihydrate was used as received for the solid-state characterization.

Preparation of Quercetin-DMSO solvate (QDMSO). QDMSO was obtained by preparing several 70g solutions of different DMSO/water ratios, ranging from 50%(w/w) to 80%(w/w) DMSO. Each solution was made to be saturated at around 55°C by continuously dissolving quercetin dihydrate crystals at such temperature, until further dissolution was not possible. The temperature of the solutions was then reduced to 15 °C at a cooling rate of -0.1 °C/min. This procedure has allowed plate-like crystals of QDMSO, of sizes ranging from 50μm to 300μm depending on the conditions of crystallization, to be obtained. The temperature of the 70%(w/w) DMSO solution was then cycled from 15 °C to 23 °C at a cooling/heating rate of -0.5 °C/min for three days, to promote growth of the crystals to a final size of approximately 500μm, which was suitable for single crystal X-ray diffraction (SCXRD). The temperature was controlled using a Huber Ministat 230 thermoregulator connected to a 100mL jacketed vessel. The crystals were then filtered using filter paper and dried without any further washing.

Single Crystal X-ray Diffraction (SCXRD). Measurements were carried out at 120K on an Agilent SuperNova diffractometer equipped with an Atlas CCD detector and connected to an Oxford Cryostream low temperature device using mirror monochromated Cu Kα radiation (λ = 1.54184 Å) from a Microfocus X-ray source. Crystals of dimensions 0.55 × 0.36 × 0.06 mm^3 were used. The structure was solved by intrinsic phasing using SHELXT and refined by a full matrix least squares technique based on F2, using SHELXL2014. [28][29] All non-hydrogen atoms were located in the Fourier Map and refined anisotropically. All carbon-bound hydrogen atoms were placed in calculated positions and refined isotropically using a “riding model”. All oxygen-bound hydrogen atoms were located in the Fourier Map and refined isotropically. The structure exhibited disorder where one molecule of DMSO was modelled across two positions in an 85:15 ratio. For the purposes of the computational studies shown in this work the minor component was disregarded and a modified cif file was generated that only modelled the 85%

position of the DMSO molecule. For the new QDMSO structure the crystallographic .cif file (CCDC No. 1971580) is available free of charge at https://www.ccdc.cam.ac.uk/structures/.

Variable Temperature Powder X-ray Diffraction (VT-PXRD). PXRD patterns were collected on a Panalytical X'Pert PRO, which was set up in Bragg -Brentano mode, using Cu Kα radiation (λ = 1.54184 Å), in a scan between 5° to 90° in 2θ with a step size of 0.032° and time per step 25 seconds. Temperature was varied from 25 °C to 180 °C.

Thermogravimetric Analysis coupled with Differential Scanning Calorimetry (TGA/DSC). TGA and DSC experiments were performed on a Mettler Toledo TGA/DSC 3+ Stare System equipment. The samples (around 10-15mg) were placed in 70µl aluminium pans, covered with a lid, and heated from 25 to 600°C at a heating rate of 10 °C.min^{-1}. Nitrogen was used as the purge gas at 50 mL min^{-1}. The measurements were repeated three times for each sample.

Hot Stage Microscopy (HSM). All HSM experiments were performed on a Leitz Dialux 22 Polarized microscope (Leica, Germany) equipped with a controlled heating and cooling stage CSS450 (Linkam, Surrey, UK) controlled by the Linksys 32 software (Linkam, Surrey UK) and an imaging system (Canon EOS 7D Mark II DSLR Camera) at 40X magnifications. The samples were heated over a temperature range of 25−150 °C at a constant heating rate of 10 °C min^{-1}.

Dynamic Vapour Sorption (DVS). Dynamic vapour sorption experiments were performed on a Surface Measurement Systems DVS Resolution equipment. Measurements were carried out over a humidity range of 0%-90% relative humidity (RH) at 25°C. Each humidity step was terminated when less than 0.02% sample weight change was observed or when a maximum hold time of 360 mins was reached. Each measurement was repeated at least twice.

Scanning Electron Microscopy (SEM). The dry samples were imaged using a Carl Zeiss EVO MA15 scanning electron microscope at magnifications from 50X to 200X. Samples were arranged on Leit tabs attached to SEM specimen stubs and an Iridium coating was applied before measurement.

4.3 Computational Analysis

As mentioned earlier, for the purposes of computational modelling the modified .cif file of the QDMSO structure that modelled only the 85% position of the DMSO molecule was used. Computational analysis was performed using Materials Studio 2017, HABIT98, and Mercury software. [30][31][32] The crystal structure was minimized using the Forcite module in Materials Studio 2017, using the same methodology described in previous publications. [22][30] The files were exported as .car files (Cartesian coordinates), converted to fractional coordinates, and then fractional charges were calculated using the AM1 method within MOPAC. [33] The bulk intrinsic synthon analysis was carried out using the HABIT98 software, which takes in structural information to construct a series of unit cells in three dimensions, and calculates the pairwise intermolecular interaction between a molecule in the origin unit cell and all the other molecules within a fixed radius of 30Å from the central molecule. [31][34][35] The calculation of intermolecular interaction energies was performed using the Dreiding II force-field. [36] The ranking of the intermolecular interactions by strength was outputted using the DEBUG-1 function. All visualization of molecular and crystal packing were carried out in Mercury CSD 3.10. [32]

4.4 Results

4.4.1 Quercetin-DMSO solvate (QDMSO) Single Crystal Structure

Cooling of all the saturated solutions of quercetin in the DMSO-Water mixture solvents (from 50% to 80% w/w DMSO) resulted in the formation of colorless plate-like crystals. However, crystals of suitable size for SCXRD were only obtained from the 70%(w/w) DMSO solution at the end of the temperature cycling period. The crystal structure was identified as a quercetin-DMSO solvate that crystallized in a monoclinic cell. SEM images of the crystals are shown in Figure 4.1, QDMSO present a plate-like morphology. The structure was solved in the *I*2/*a* space group, with two molecules of quercetin and three molecules of DMSO in the asymmetric unit. The structure exhibited disorder, where one of the three DMSO molecules was modelled across two positions in an 85:15 ratio. The crystallographic data and structure refinement data for the QDMSO structure are presented in Appendix A Table A.1.

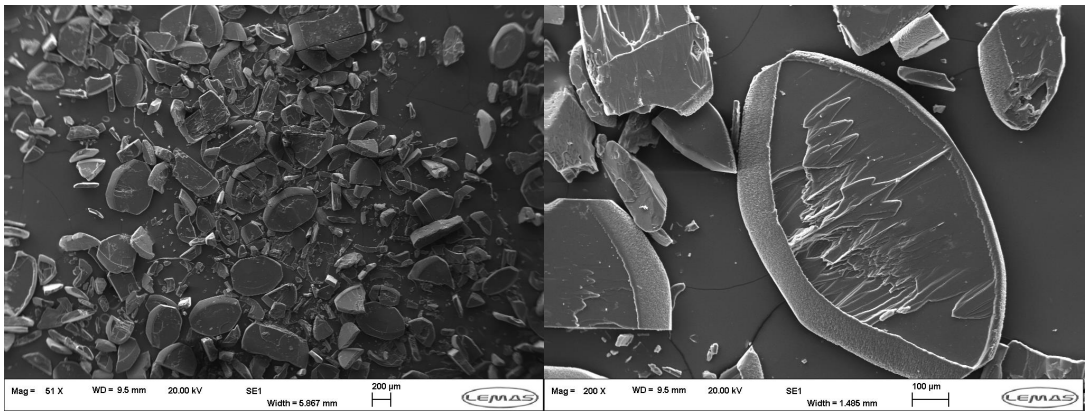

Figure 4.1 SEM images of QDMSO at 51X (left) and 200X (right) magnification.

The PXRD pattern obtained experimentally from the bulk powder samples and the simulated pattern from the cif file in Mercury (calculated based on the QDMSO single crystal structure solved) are shown in Figure 4.2. The two patterns closely matched confirming that the bulk sample is a highly pure phase and the single crystal is representative of the bulk material. A

slight shift in the whole pattern was observed between the experimental and simulated patterns due to the fact that the SCXRD was run at 120K while the PXRD was performed at room temperature (25 °C). The higher temperature at which the PXRD was run resulted in a general expansion of the unit cell of the structure, resulting in the observed shift in the pattern.

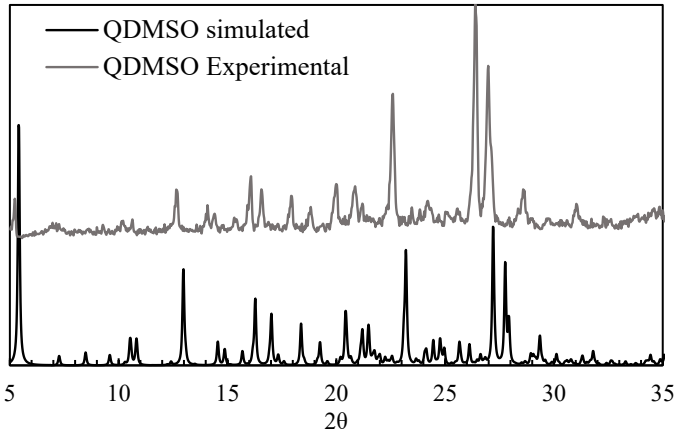

Figure 4.2 PXRD pattern for QDMSO obtained experimentally and simulated from crystal structure.

The DMSO solvate crystallizes with two quercetin molecules (Q1 & Q2) and three DMSO molecules (D1, D2 & D3) in the asymmetric unit (Figure 4.3 a). This arrangement allows all of the carbonyl and hydroxyl groups to form at least one intermolecular hydrogen bond, whereby several of the hydroxyl groups act as both H-bond acceptors and donors. This creates 'cooperative hydrogen bonds', whereby all the hydrogen bonds formed from these groups will be strengthened. [37]

Figure 4.3 shows that the H-bonding provided by the DMSO molecules allows the unbroken chain of close stacking of the quercetin molecules along the b-axis (Figure 4.3 c). These interactions have previously been shown to be important in stabilizing the hydrated structures of quercetin. [22] Most of the hydrogen bonds are aligned in the OC/OA plane (Figure 4.3 b),

since the stacking of the quercetin molecules along the b-axis requires a planar conformation of the quercetin molecules, which in turn arranges the H-bonds to be planar as well. Though there is a limited amount of H-bonding shown in Figure 4.3 d, due to the DMSO molecules filling spaces in the direction of the a-axis, the H-bonds are not all aligned specifically in one direction, forming unbroken chains instead.

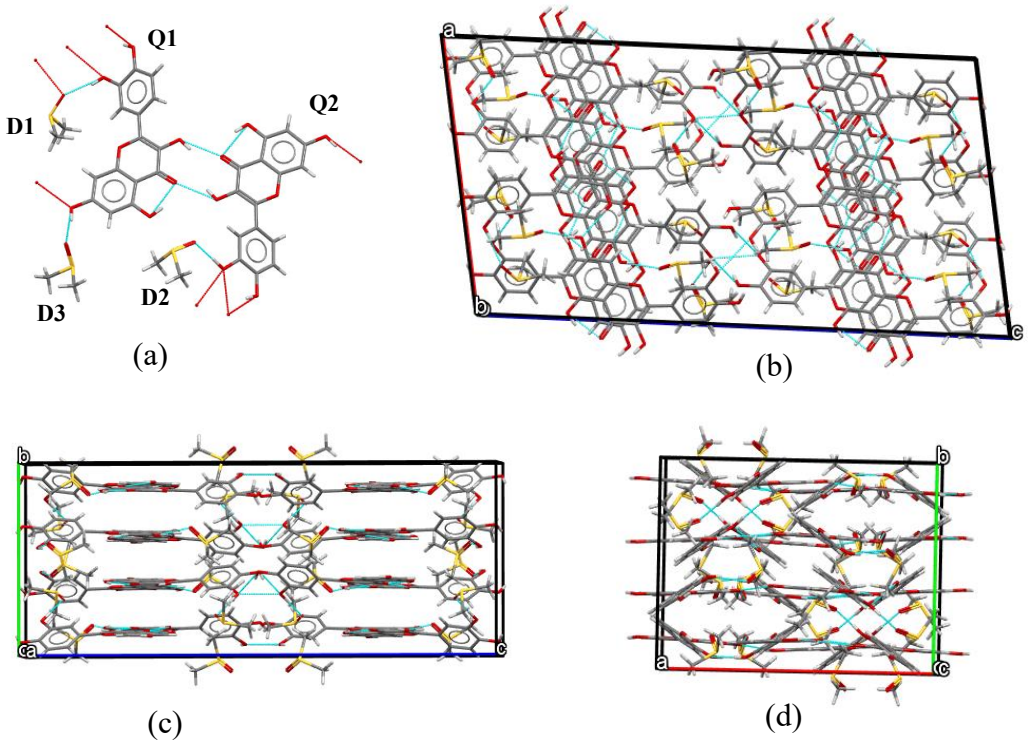

Figure 4.3 The packing diagrams for the QDMSO solvate structure. (a) The asymmetric unit with the H-bonds to neighbouring molecules shown as 'hanging'; (b) the OC/OA view of the unit cell, where the majority of H-bonds are formed; (c) the OB/OC view of the unit cell showing the close stacking of the quercetin molecules; (d) the OA/OB view of the unit cell showing a limited amount of H-bonding in this direction.

The arrangement of the DMSO molecules shows that they are woven tightly into the arrangement of the quercetin molecules, without any obvious channel for de-solvation. The

strong synergistic H-bonding and lack of an obvious de-solvation route may be reason for the superior thermal stability of the DMSO solvate.

When considering the arrangement of this solvate, as compared to the hydrated and non-solvated forms, it seems that the increasing presence of solvent encourages the planar close packing of the quercetin molecules. [22] Indeed, as the solvent/solute ratio increases, the propensity for all the quercetin molecules to align and stack in one direction increases. Such packing characteristics have been linked with crystal forms that are relatively easy to nucleate and grow, in particular showing needle like morphologies. [38][39]

The torsion angle of the pyrone to the phenyl ring for both molecules in the asymmetric unit of QDMSO was measured: τ1 represents the torsion angle for molecule Q1 while τ2 is the torsion angle for Q2. It was found that τ1 and τ2 for the two quercetin molecules of the asymmetric unit have slightly different torsion angles of 30.71° and 31.11°, respectively, as shown in Figure 4.4.

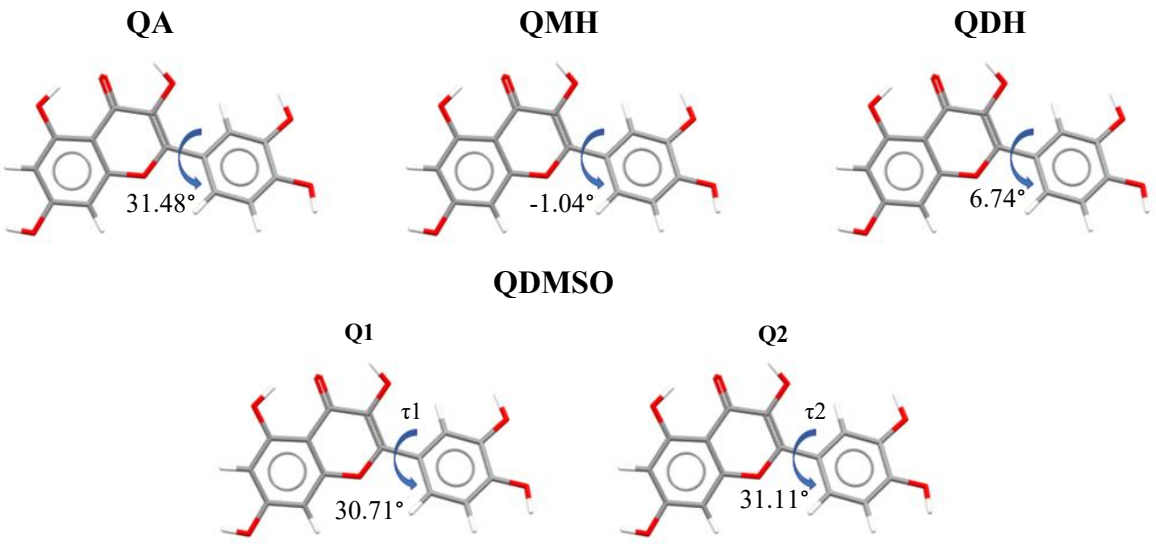

Figure 4.4 Torsion angles of phenyl to pyrone rings for quercetin molecules in quercetin structures (quercetin anhydrous – QA, quercetin monohydrate – QMH, quercetin dihydrate – QDH, quercetin – DMSO solvate – QDMSO). [22]

A previous study identified that the quercetin molecules in the QMH and QDH structures were close to planar, as the water molecules helped in satisfying the hydrogen bonding sites on the quercetin molecule, and the planar conformation facilitated close packing and favourable quercetin-quercetin stacking interactions. [22] In comparison, the quercetin conformation in the QA structure was found to be almost identical to that found in the new QDMSO structure. Since DMSO has no hydrogen bonding hydrogens and only one hydrogen bonding oxygen, in combination with it being bulkier than water, results in it being far less effective at hydrogen bonding. Hence, the quercetin molecule must adopt the twisted conformation to maximise its quercetin-quercetin hydrogen bonds.

4.4.2 Bulk Synthon Analysis for QDMSO

The six strongest intermolecular interactions in the QDMSO structure, those having the lowest energy values which represent interactions of greater strength and stability, are illustrated in Figure 4.5, in order of increasing strength. For each synthon the packing of molecules in the lattice is presented and a closer view on the two interacting molecules for each synthon is also included. The properties of each studied synthon are summarised in Table 4.1. The first two strongest interactions, QDMSO1 and QDMSO2, are both π-π stacking interactions contributing to growth along the b-axis of the unit cell. In QDMSO1 the phenyl rings of the interacting molecules face opposite directions, while in QDMSO2 these rings face the same direction. The centroid-centroid distances of the quercetin molecules in the two interactions are similar (5.998Å in QDMSO1 and 5.034Å in QDMSO2). However, the interplanar angles differ significantly. In QDMSO1 the interplanar angle is 3.64° while in QDMSO2 it is 22.73°, meaning that QDMSO2 does not result in a parallel packing of the quercetin molecules in the lattice as much as QDMSO1 does. Table 4.1 shows that for both interactions the contributions

of the aromatic rings (pyrone and phenyl) to the total energy of each synthons are high, about 55.8% and 74.4% for QDMSO1 and QDMSO2 respectively. Instead, the contribution from the hydroxyl groups are lower, meaning that QDMSO1 and QDMSO2 are mostly non-polar synthons. The 5th strongest interaction, QDMSO5, is another non-polar interaction due to the high contribution of the aromatic rings. The quercetin molecules pack in a parallel orientation (interplanar angle is 0.00°). However, the offset between the molecules is much greater, having a centroid-centroid distance of 9.995Å. The multiplicity of this interaction is 1 since only one of the two quercetin molecules of the asymmetric unit forms this interaction. This means that this specific interaction is encountered half the times compared to others that have a multiplicity of 2; this reflects on the contribution of the specific interaction on the total lattice energy.

The 3rd and 4th strongest interactions, QDMSO3 and QDMSO4, are double hydrogen bonding interactions between a hydroxyl and a carbonyl group (for QDMSO3) and two hydroxyl groups (for QDMSO4) of two adjacent quercetin molecules. For QDMSO3 it was found that the contribution of hydroxyl groups (34.5%) and carbonyl groups (11.1%) to the total synthon energy are relatively high, which indicates that this interaction is mostly polar. For QDMSO4, the contribution of hydroxyl groups to the synthon energy is very high, 83.1%, marking this interaction as the most polar of the key synthons presented here.

The quercetin molecules in the QDMSO structure are found to form hydrogen bonds with the DMSO molecules. QDMSO6, is a hydrogen bond between a hydroxyl hydrogen on the phenyl ring of a quercetin molecule and a sulfinyl oxygen of a DMSO molecule. QDMSO6, which is the strongest quercetin-DMSO hydrogen bond in QDMSO, is found to be much stronger (QDMSO6=-4.14 kcal.mol^{-1}), compared to the strongest quercetin-solvent interaction in QMH (QMH3=-2.55 kcal.mol^{-1}) or QDH (QDH2=-1.71 kcal.mol^{-1}), suggesting that quercetin-DMSO hydrogen bonds are stronger compared to quercetin-water interactions.

A closer look at the hydrogen bonding network in the structure reveals that the first quercetin molecule of the asymmetric unit, Q1, forms 6 hydrogen bonds, of which 3 are with 3 DMSO molecules and 3 with 2 quercetin molecules. The second quercetin molecule of the asymmetric unit, Q2, forms 6 hydrogen bonds, of which 1 is with a DMSO molecule and 5 are with 3 other quercetin molecules. This information is summarised in Appendix A Table A.2.

QDMSO1

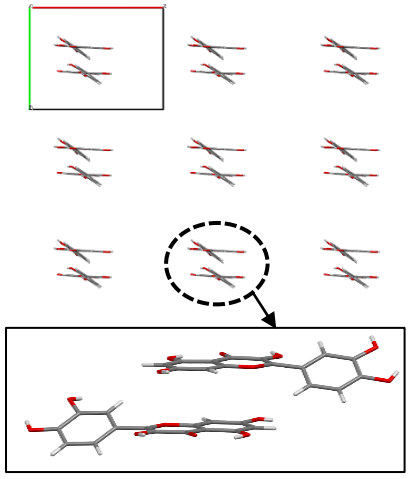

QDMSO2

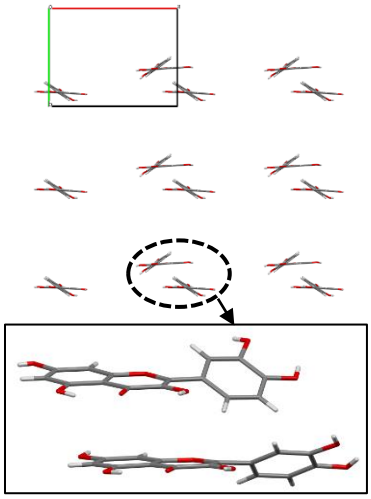

QDMSO3

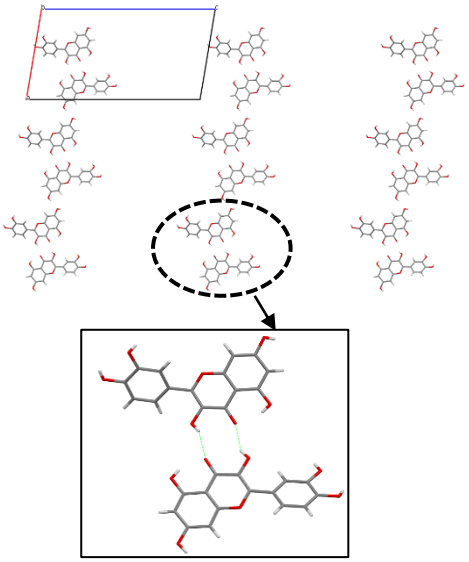

QDMSO4

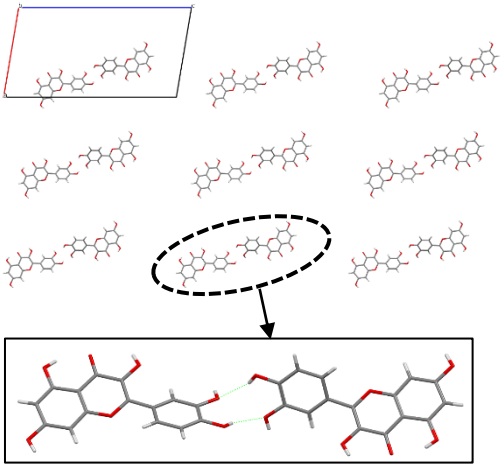

QDMSO5

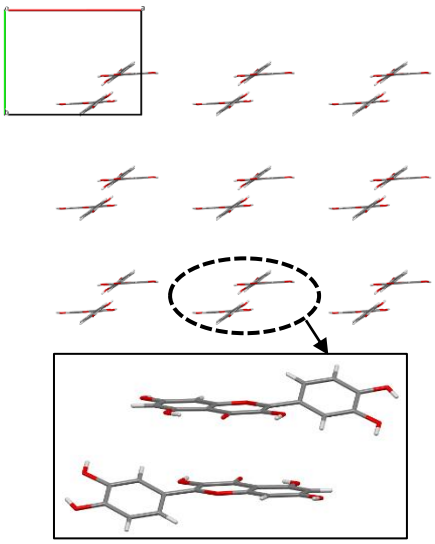

QDMSO6

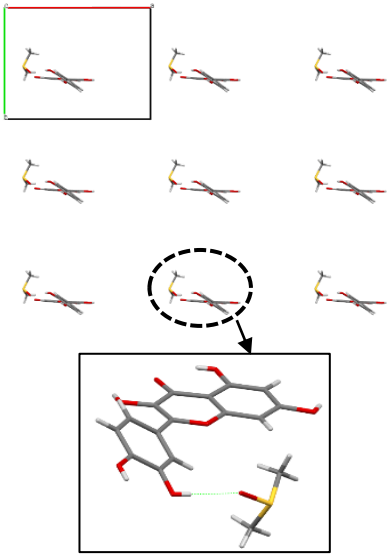

Figure 4.5 Main bulk intrinsic synthons in QDMSO ordered by strength (green dotted lines indicate hydrogen bond).

Table 4.1 Summary of bulk intrinsic synthons in QDMSO.

Synthon name	QDMSO1	QDMSO2	QDMSO3	QDMSO4	QDMSO5	QDMSO6
Molecules involved	Q-Q	Q-Q	Q-Q	Q-Q	Q-Q	Q-D
Synthon type	π-π stacking	π-π stacking	H-bond	H-bond	π-π stacking	H-bond
Intermolecular distance (Å)	5.83	5.05	8.36	13.12	6.69	5.27
Synthon energy (kcal.mol^{-1})	-7.37	-5.74	-5.42	-4.87	-4.24	-4.14
Multiplicity	2	2	2	1	1	2
% contribution of synthon to total lattice energy	6.2%	4.8%	4.5%	2.1%	1.8%	3.5%
% contribution of aromatic rings to synthon	55.8%	74.4%	54.4%	21.3%	63.6%	33.3%
% contribution of hydroxyl groups to synthon	22.2%	15.2%	34.5%	83.1%	34.3%	45.2%
% contribution of carbonyl bond to synthon	22.0%	10.4%	11.1%	-4.4%	2.0%	21.5%

4.4.3 Comparison of quercetin structures

A comparison of the modelling work for the different quercetin structures (QDMSO, QDH, QMH and QA) has been conducted and the main findings are summarised in Table 4.2. A more extensive comparison can be found in Appendix A Table A.3. [22] As discussed earlier, the asymmetric units of the quercetin structures contain: two molecules of quercetin and three molecules of DMSO in QDMSO, one molecule of quercetin and two molecules of water in QDH, one molecule of quercetin and one molecule of water in QMH and one molecule of quercetin in QA. It was found that the unit cell densities for the solvated structures were very similar and higher than that of QA (0.964 u/Å^3 and 1.007 u/Å^3 for QDH and QMH respectively,

while 0.702 u/Å^3 for QA), due to the formation of hydrogen bonds with the solvent molecules that result in a more close-packed structure. The unit cell density of QDMSO was found to be slightly lower than those of QMH and QDH, possibly because of the less planar conformation of the quercetin molecule in QDMSO.

The contribution of the quercetin-solvent interactions to the lattice energy was found to be very high for QDMSO (45.1%) and QDH (45.9%) and considerably lower for QMH (27.2%). This emphasizes that both QDMSO and QDH are structures where the quercetin-solvent interactions are critical for the stabilization of the lattice. The loss of those interactions, due to a heat-induced de-solvation for example, could result in a thermodynamically unstable structure. It should be noted that although the first five strongest synthons for QDMSO are quercetin-quercetin interactions, QDMSO6 and many the following synthons are quercetin-DMSO interactions. Summing the energies of these quercetin-QDMSO interactions the overall contribution is very high (45.1%) and equal to the overall contribution of all the quercetin-quercetin interactions.

Table 4.2 Comparison of quercetin structures [22]

	QDMSO	QDH	QMH	QA
Unit cell Density (u/Å³)	0.900	0.964	1.007	0.702
Interactions' contribution to lattice energy:*				
Quercetin – Quercetin	45.1%	53.8%	72.6%	100%
Quercetin – Solvent	45.1%	45.9%	27.2%	-
Solvent – Solvent	9.7%	0.3%	0.2%	-
Contribution of Van der Waals interactions to lattice energy*	60.8%	91.2%	89.1%	92.1%
Contribution of hydrogen bonds and dipole-dipole interactions to lattice energy*	39.2%	8.8%	10.9%	7.9%
Q-Q H-bonds (per quercetin molecule)	3 for Q1 5 for Q2	0	6	6
Q-solvent H-bonds (per quercetin molecule)	3 for Q1 1 for Q2	6	4	-

* Based on the energy of interactions

Comparing the main bulk synthons, while in QDH and QMH there is only one type of π-π stacking interaction, in QDMSO there are several different π-π stacking interactions (QDMSO1, QDMSO2, QDMSO5). [22] However, in these interactions the quercetin molecules are not found to stack as closely as in QDH or QMH, as seen by comparing the intermolecular distances of QDMSO1 and QDMSO2 to those of QDH1 and QMH1. This is probably due to the less planar conformation of the quercetin molecule in QDMSO compared to QDH and QMH.

The contribution of hydrogen bonds and dipole-dipole interactions to the lattice energy is more significant for QDMSO (39.2%) compared to all the other structures, for which those interactions contribute to less than around 11%. This indicates that quercetin-quercetin and quercetin-DMSO hydrogen bonds and other polar interactions in QDMSO are stronger compared to other quercetin crystal structures. Moreover, in our previous work it was stated that for QA, QMH and QDH, as the number of water molecules in the unit cell increases,

hydrogen bonding is more satisfied by interactions with the incorporated water molecules than by quercetin-quercetin interactions. [22] For QDMSO, hydrogen bonding is partially satisfied between quercetin-quercetin and quercetin-DMSO molecules. Although the quercetin-DMSO hydrogen bonds are favourable and relatively stronger compared to the quercetin-water hydrogen bonds, the much larger size of the DMSO molecule compared to water does not allow these molecule to be positioned close to all the polar groups of the quercetin molecules to completely satisfy all hydrogen bonds. Thus, hydrogen bonds are also formed and satisfied among quercetin molecules, which attain a less planar conformation to facilitate interaction between their polar groups.

4.4.4 Thermal analysis (DSC-TGA)

Experimental characterisation for the quercetin structures was only performed for QDMSO and QDH as it was very difficult to obtain pure forms of QMH and QA, which were stable for long enough to allow any characterization. Furthermore, the pure form of quercetin obtained from the de-solvation of QDMSO and QDH, as discussed below, did not match the deposited PXRD pattern of QA, therefore it could not be related to the modelling work previously performed.

The differential scanning calorimetry coupled with thermogravimetric analysis of QDMSO and QDH was performed to evaluate the thermal stability of the quercetin structures, and results are shown in Figure 4.6. Two endothermic peaks were observed for QDH, which were identified as the dehydration and melting of the solid. The dehydration peak was accompanied with a weight loss of 10.0%, as shown in the TGA curve. This is very close to the calculated theoretical loss in mass (10.7%) that would result from the loss of two water molecules per molecule of quercetin, confirming the 1:2 stoichiometry of QDH. The onset temperature for dehydration was found to be approximately 95°C, in agreement with previously published data.[24],[40] There was only one endothermic peak related to dehydration of the QDH, meaning

that the two water molecules are lost from the crystal lattice in one single dehydration step. The second endotherm, which corresponds to the melting of the dehydrated form, was observed at an onset temperature of 316°C. The melting temperature agrees with previous studies on the thermal stability of quercetin. [24][40] A second loss in mass, corresponding to the decomposition of quercetin was observed at 330°C, together with an exotherm peak in the DSC curve.

Upon heating the QDMSO structure, two weight losses were observed in the TGA data, corresponding to de-solvation and the molecular decomposition. The onset temperature for de-solvation was 136°C, as confirmed by the DSC endotherm at that temperature. The endotherm for de-solvation exhibits a shoulder at around 167°C, and the endset temperature for the de-solvation from the TGA curve was found to be 197°C, which could indicate that the

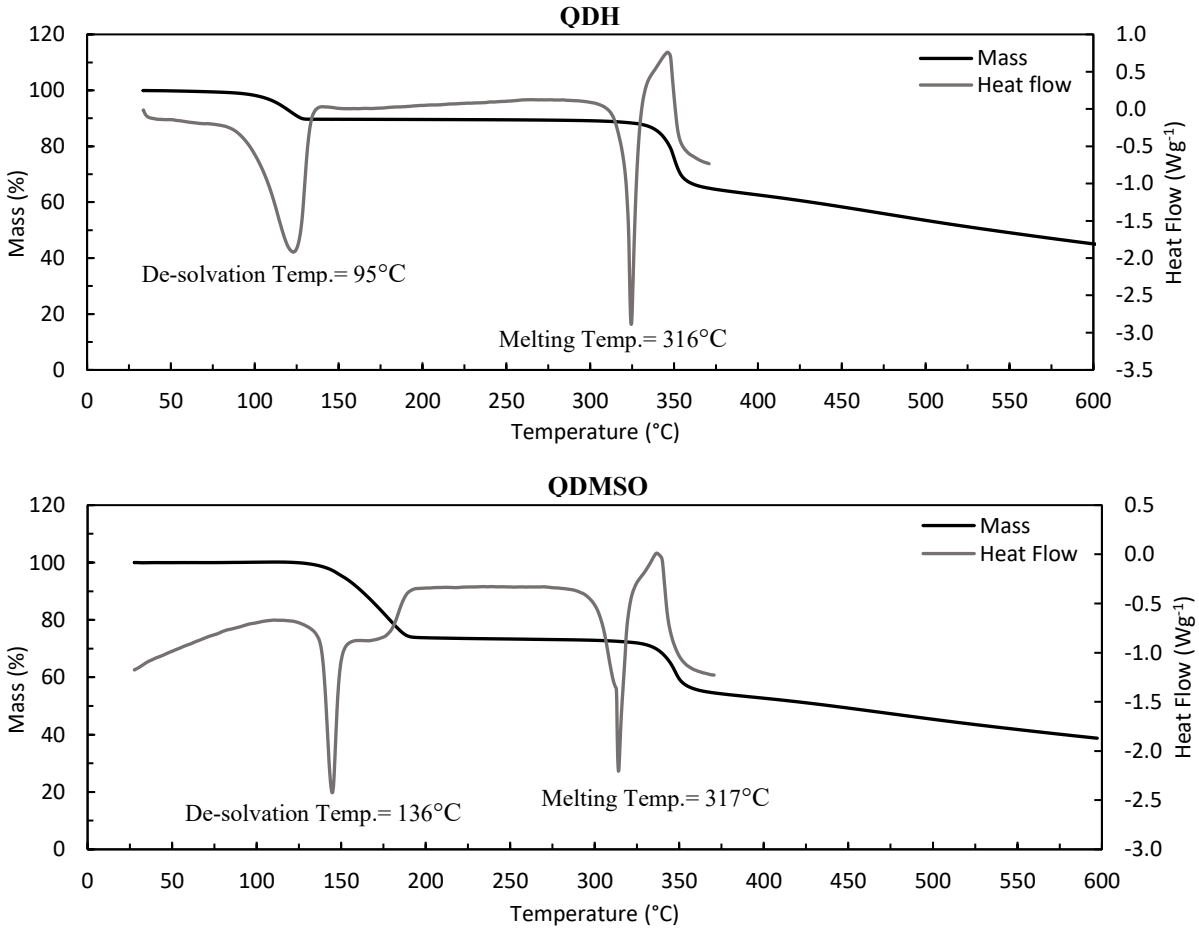

Figure 4.6 DSC and TGA curves for QDH (top) and QDMSO (bottom).

DMSO molecules are lost from the lattice not in one single de-solvation step but in more consecutive steps. This result was observed in all three repeats of the DSC-TGA analysis performed. The observed loss in mass after complete de-solvation, 26.4%, is close to the theoretical value of 27.9% for a stoichiometry of 1:1.5. The endotherm peak onset temperature for melting was obtained at 317°C. A small shoulder appeared just before the melting peak and it was observed only in one of three measurements carried out on QDMSO. The shoulder could be due to the presence of an impurity in the sample, which probably originated from the purchased quercetin (97% w/w purity). The decomposition takes place at 331°C. All information obtained by DSC-TGA is summarized in Appendix A Table A.4.

4.4.5 Hot Stage Microscopy (HSM)

The temperature at which de-solvation of QDMSO was observed using HSM was consistent with the onset de-solvation temperature as calculated by DSC. It was found that the colourless plate-like crystals of QDMSO were transparent at temperatures between 25 °C to 130 °C, after which the crystals appeared to darken and became less transparent due to structural changes related to the loss of solvent. At 140 °C the crystals were completely opaque but maintained the plate-like shape, as shown in Figure 4.7. The HSM onset temperature (130 °C) agrees with the DSC onset temperature for the loss of the DMSO solvent from the structure. The resulting crystals were tested using SCXRD, but it was found that a single crystal of QDMSO did not give a single crystal of the de-solvated form, therefore the structure of these crystals could not be solved.

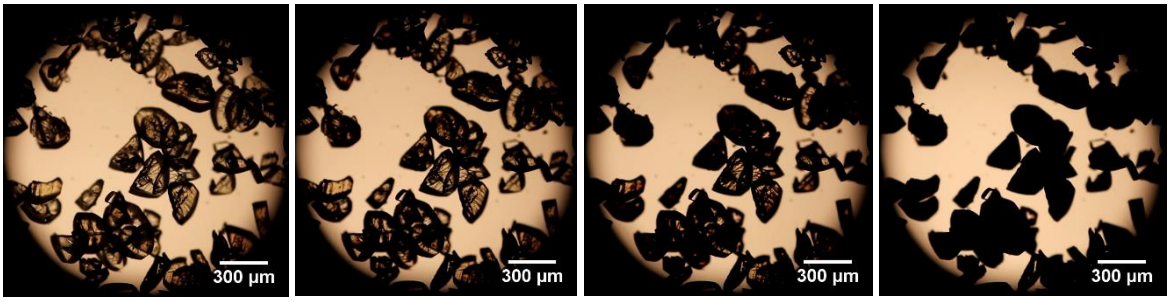

(a) (b) (c) (d)

Figure 4.7 HSM images of QDMSO at (a) 25 °C, (b) 130 °C, (c) 135 °C, (d) 140 °C

4.4.6 Variable Temperature Powder X-Ray Diffraction (VT-PXRD) analysis

The thermal stability of the two solvates was further analysed using VT-PXRD. XRD patterns of QDH were observed in a temperature range between 25°C and 140°C. This is illustrated in Figure 4.8 (top). At room temperature the PXRD pattern of QDH exhibited distinct peaks in agreement with the data obtained by Rossi et al. (CSD Refcode: FEFBEX) and with other PXRD patterns for QDH previously reported in literature. [14][24] The PXRD pattern of QDH remained unchanged between 25°C and 70°C, while at 100°C many of the peaks characteristic for QDH (10.70, 16.02, 23.70, 38.54) decreased in intensity indicating the start of a phase transition. The PXRD pattern stopped changing at 110°C and remained unchanged up to the maximum temperature of 140°C and also upon cooling down to 25°C. This behaviour shows that the resultant quercetin form does not change back to the QDH form after cooling, at least during the time frame of the VT-PXRD experiment. Combining this information with the DSC-TGA analysis, the phase change at 100°C corresponds to the dehydration of QDH. Since no further loss in mass occurred after the first dehydration step, and before decomposition, as indicated by the TGA curve in Figure 4.6, the PXRD pattern obtained at 110°C should correspond to an anhydrous form of quercetin. It should be noted that the PXRD pattern of this

anhydrous polymorph of quercetin does not match with the pattern reported by Vasisht et al. (CSD Refcode: NAFZEC) for the anhydrous structure of quercetin. [18]

The PXRD pattern for QDMSO is illustrated in Figure 4.8 (bottom). The structure appeared to be stable between 35°C and 100°C. At 120°C a phase change started occurring and a new PXRD pattern was exhibited from 140°C up to 180°C, which remained unchanged when the temperature was reduced to 120°C and further down to 25°C. This phase change corresponds to the loss of the DMSO solvent molecules observed in the DSC-TGA data. The PXRD pattern of the de-solvated QDMSO is almost identical to the PXRD pattern obtained from the dehydration of the QDH, both having common reflections at 2θ values of 12.84, 16.58, 25.87, 26.61, 34.64, 37.21 and 42.80. This suggests that both forms lose the solvent and transform to the same de-solvated polymorph of quercetin.

VT-PXRD and DCS-TGA showed that QDH and QDMSO exhibited different thermal stabilities in their heat-induced de-solvation process: QDH appears to de-solvate at a lower temperature of about 100°C (95°C from DSC-TGA) while the de-solvation for QDMSO begins at a higher temperature of about 120°C (136°C from DSC-TGA). It has been reported in literature that the thermal stability of solvate structures in heat-induced de-solvation is dependent on the type and strength of intermolecular interactions of solvent molecules with the main compound as well as on crystal packing. [6][13] Our synthonic modelling work demonstrated that the strongest quercetin-DMSO hydrogen bonds are stronger in energy (lower energy value) compared to the quercetin-water hydrogen bonds in QDH.

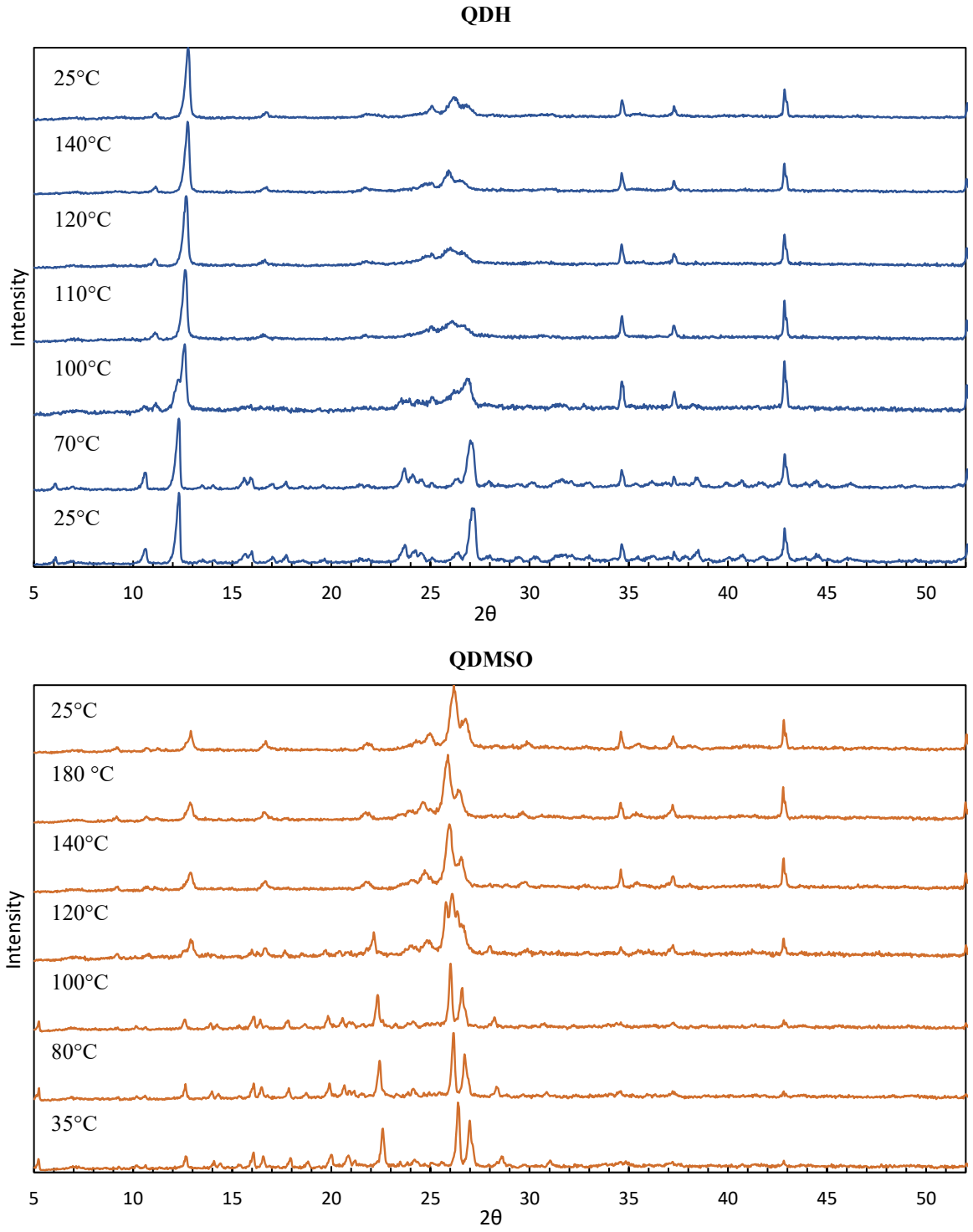

Figure 4.8 The VT-PXRD patterns for QDH (top) and QDMSO (bottom).

This can explain the greater thermal stability of QDMSO compared to QDH. In fact, more energy is required to break the quercetin-DMSO hydrogen bonds to release the solvent, and

this occurs at a higher temperature. The loss of solvent results in a solid-state transformation to a pure quercetin form. It is clear that in both solvates the quercetin-solvent interactions are critical for the stabilization of the crystal lattice. When the solvent molecules are lost during the heat-induced de-solvation, the quercetin molecules rearrange to form new interactions and compensate for the lost quercetin-solvent interactions.

4.4.7 Dynamic Vapour Sorption (DVS) analysis

The moisture-dependent stability of the two solvates was evaluated in a RH range from 0-90%. The mass of QDH appeared to be stable over a wide humidity range from RH=10% to RH=80%, as shown in Figure 4.9 (top). At RH=90%, both during sorption and desorption, a small increase in the mass of QDH was observed (approximately 2%) which could be a result of adsorption of water moisture on the surface of the QDH crystals. Below RH=10% the mass decreased down to 95% of the initial value. This roughly corresponds to the loss of one water molecule from the lattice per molecule of quercetin (theoretical value of 94.6%) and could indicate a moisture dependent transformation from the dihydrate structure to a monohydrate form. Figure 4.9 shows that the mass of QDH was still changing at 604 min, when the humidity was changed from RH=0% to RH=10% (this is because the sample reached the maximum allowed time at constant humidity). This behaviour indicates that the loss of water from QDH is slow. During sorption, at RH=10% there was an increase in mass to 98.6% of the initial value, which indicates a potential rehydration of the dehydrated form back to QDH. This behaviour shows that the QDH structure is the stable form for values of RH=10% and above. Once again, the fact that QDH is only unstable at very low RH (below 10%) highlights the importance of the quercetin-water interactions in the stabilization of the crystal lattice, which were found to contribute to 45.9% of the total lattice energy.

DVS analysis for the QDMSO structure showed that this solvate is stable over a RH range from 0% to 80%, where the sample mass only increased up to 102.2% of the starting mass, most likely because of adsorption of water at the crystal surface. At RH=90% the mass increased significantly to 112% of the initial value. This could be the result of a gain in water molecules and potential transformation of the DMSO solvate into the QDH form. Because of its low volatility the DMSO incorporated in QDMSO will unlikely evaporate during this polymorphic conversion. This explains why the change in mass recorded by DVS corresponds to the water incorporation only.

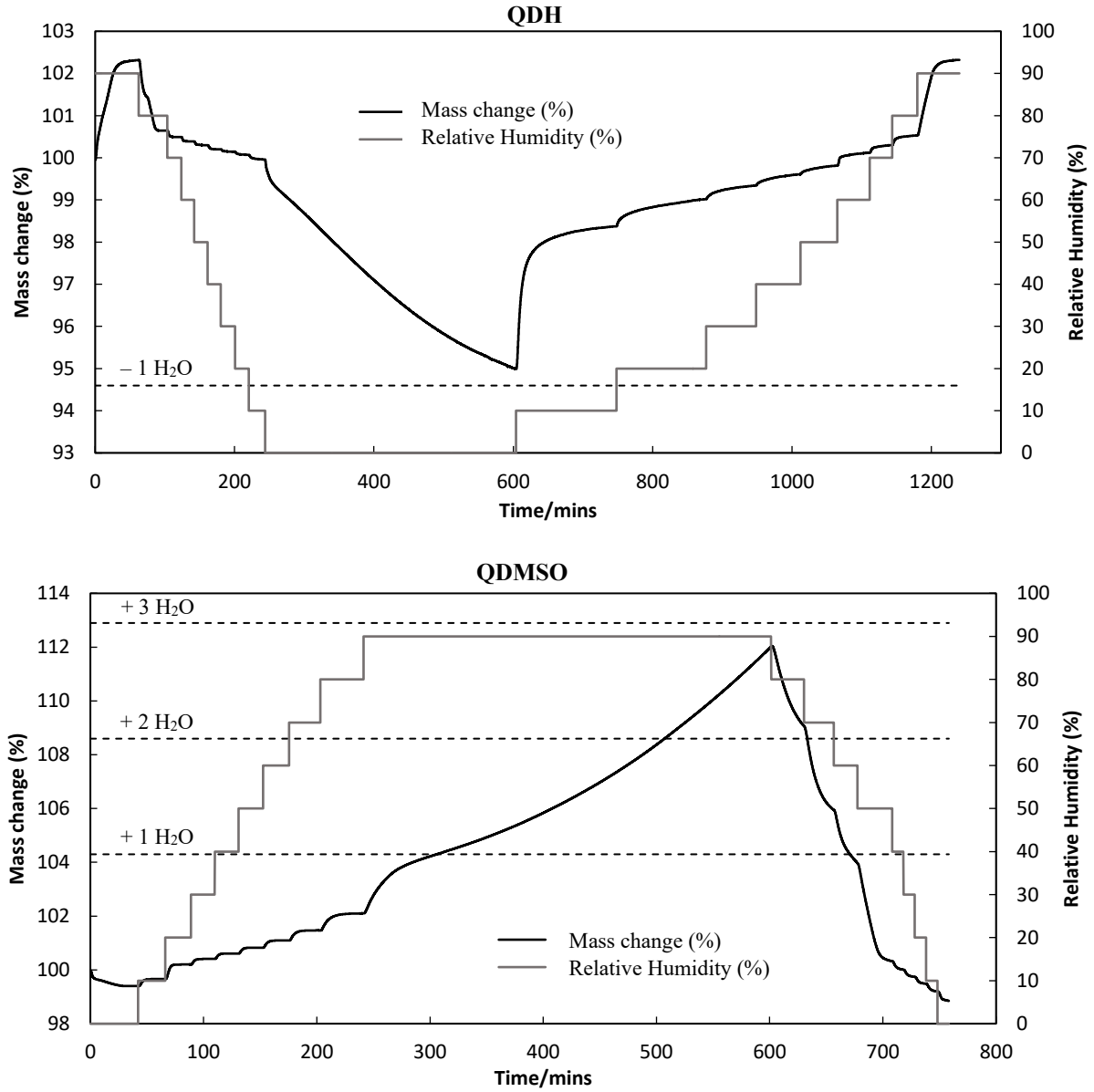

Figure 4.9 DVS diagrams for QDH (top) and QDMSO (bottom), illustrating the mass change at different relative humidity values. The dotted horizontal lines indicate the theoretical mass change for the loss/gain of water molecules per quercetin molecule in the lattice of each structure.

Figure 4.9 shows that the mass was still changing at the end of the RH=90% step as the maximum hold time was exceeded, meaning that any transformation to QDH was possibly still ongoing at that time. During desorption the sample lost all the water gained during the sorption

step, with the final mass at RH=0% was found to be 98.6% of the initial value, perhaps indicating evaporation of part of the DMSO released from the structure at RH=90. The modelling results for QDMSO showed that the overall energy of the quercetin-DMSO hydrogen bonds was higher than the sum of the energies related to the quercetin-water interactions in QDH. This could explain why QDMSO appeared to be stable over such a wide RH range, and why the quercetin molecules would preferentially form hydrogen bonds with water only above a RH of 80%.

In summary, the DVS results show that, at ambient temperature, QDMSO is stable over a RH range from 0% to 80%, while QDH is stable from 10% to 90% RH, showing slow dehydration at RH=0%.

4.5 Conclusion

Crystallization of quercetin from DMSO-water mixtures resulted in a novel crystal structure of quercetin, a quercetin DMSO-solvate. This form was identified via SCXRD and its physiochemical properties and phase transitions were characterised by VT-PXRD, DSC-TGA, HSM and DVS. The crystal structure packing and bulk intermolecular interactions of QDMSO were studied and compared to other quercetin structures (quercetin anhydrous, monohydrate and dihydrate) and experimental solid-state characterisation was performed for QDMSO and QDH.

It was found that quercetin molecules in QDMSO assume a less planar conformation compared to QDH and QMH, which results in slightly higher intermolecular distances between the interacting molecules, and lower unit cell density. This can be attributed to the larger size of the DMSO molecules compared to water. Molecular modelling calculations showed that the

contribution of hydrogen bonds and dipole-dipole interactions to the total lattice energy was much higher for QDMSO compared to all other quercetin structures. Also, the stronger quercetin-DMSO hydrogen bonds can explain the improved thermal stability of QDMSO compared to that of QDH. It was further demonstrated that both QDMSO and QDH transform to the same anhydrous form after heat-induced de-solvation, which was found to generate molecular packing rearrangements in the lattice. DVS showed that the QDH structure was stable above RH=10% while it exhibited dehydration below that. QDMSO was stable from RH=0% to RH=80%, with a possible transformation to QDH above RH=80%. Both the kinetics of dehydration of QDH and the transformation of QDMSO were found to be slow.

In summary, the novel solvated structure of quercetin, QDMSO, exhibits superior thermal stability compared to that of QDH which is the commercial form of quercetin.

The work demonstrates how synthonic modelling can be used to explain many of the physiochemical properties of solvated quercetin crystals via finding strong correlations between experimental findings and type/strength of intermolecular interactions. This multiangle characterization method, which couples computational and experimental techniques can be applied for other systems, and observations regarding the type and strength of interactions and packing can be extended to other solvated crystalline structures. The presented work can also assist in the ongoing effort to design and predict the behaviour of crystallization processes. In fact, the synthonic modelling methodology proposed here can be used during solid form screening of crystalline products such as pharmaceuticals or agrochemicals, to guide the design of crystallization conditions, such as the choice of solvent, and to infer the physiochemical properties of the generated crystal forms without the need of a large number of experiments. This is particularly useful when little amount of crystallizing material is available, for example in early drug development stages, and it can result in faster product and process development.

Acknowledgements

The authors acknowledge the Bragg Centre for Materials Research at the University of Leeds for the technical support in running experiments and analysing data of X-ray diffraction and electron microscopy facilities. Dr Simone would like to acknowledge the Royal Academy of Engineering (grant n IF\192031) for financial support.

References

[1] Healy, A. M.; Worku, Z. A.; Kumar, D.; Madi, A. M. Pharmaceutical Solvates, Hydrates and Amorphous Forms: A Special Emphasis on Cocrystals. *Adv. Drug Deliv. Rev.* **2017**, *117*, 25–46. https://doi.org/10.1016/j.addr.2017.03.002.

[2] Threlfall, T. L. Analysis of Organic Polymorphs. A Review. *Analyst* **1995**, *120* (10), 2435–2460. https://doi.org/10.1039/AN9952002435.

[3] Tilbury, C. J.; Chen, J.; Mattei, A.; Chen, S.; Sheikh, A. Y. Combining Theoretical and Data-Driven Approaches To Predict Drug Substance Hydrate Formation. **2018**. https://doi.org/10.1021/acs.cgd.7b00517.

[4] Vippagunta, S. R.; Brittain, H. G.; Grant, D. J. W. Crystalline Solids. **2001**, *48*, 3–26.

[5] Griesser, U. J. The Importance of Solvates. *Polymorphism*. May 22, 2006. https://doi.org/doi:10.1002/3527607889.ch8.

[6] Zhu, B.; Zhang, Q.; Ren, G.; Mei, X. Solid-State Characterization and Insight into Transformations and Stability of Apatinib Mesylate Solvates. *Cryst. Growth Des.* **2017**, No. 17, 5994–6005. https://doi.org/10.1021/acs.cgd.7b01123.

[7] Reutzel-Edens, S. M.; Bush, J. K.; Magee, P. A.; Stephenson, G. A.; Byrn, S. R. Anhydrates and Hydrates of Olanzapine: Crystallization, Solid-State Characterization, and Structural Relationships. *Cryst. Growth Des.* **2003**, *3* (6), 897–907. https://doi.org/10.1021/cg034055z.

[8] Groenendaal, J. W.; Antonius Maria Leenderts, E. J.; VanvDer Does, T. AMOXCILLIN TRHYDRATE. US 2006/0172987 A1, 2006.

[9] Ahire, V.; Sasane, S.; Deshmukh, A.; Kumbhar, K.; Bhatnagar, A.; Verma, D.; Vyas, R.; Singh, G. P.; Bishe, N. PROCESS FOR PREPARATION OF DARUNAVIR AND DARUNAVIR ETHANOLATE OF FINE PARTICLE SIZE. US 9,062,065 B2, 2015.

[10] Li, J.; Tilbury, C. J.; Kim, S. H.; Doherty, M. F. A Design Aid for Crystal Growth Engineering. *Prog. Mater. Sci.* **2016**, *82*, 1–38. https://doi.org/10.1016/j.pmatsci.2016.03.003.

[11] Sung, H.; Fan, Y.; Yeh, K.; Chen, Y.; Chen, L. Colloids and Surfaces B : Biointerfaces A New Hydrate Form of Diflunisal Precipitated from a Microemulsion System. **2013**, *109*, 68–73.

[12] Bauer, J.; Spanton, S.; Henry, R.; Quick, J.; Dziki, W.; Porter, W.; Morris, J.

Ritonavir: An Extraordinary Example of Conformational Polymorphism. *Pharm. Res.* **2001**, *18* (6), 859–866. https://doi.org/10.1023/a:1011052932607.

[13] Zhu, B.; Fang, X.; Zhang, Q.; Mei, X.; Ren, G. Study of Crystal Structures, Properties, and Form Transformations among a Polymorph, Hydrates, and Solvates of Apatinib. *Cryst. Growth Des.* **2019**, *19*, 3060–3069. https://doi.org/10.1021/acs.cgd.9b00397.

[14] Rossi, M.; Rickles, L. F.; Halpin, W. A. The Crystal and Molecular Structure of Quercetin: A Biologically Active and Naturally Occurring Flavonoid. *Bioorg. Chem.* **1986**, *14* (1), 55–69. https://doi.org/10.1016/0045-2068(86)90018-0.

[15] Srinivas, K.; King, J. W.; Howard, L. R.; Monrad, J. K. Solubility and Solution Thermodynamic Properties of Quercetin and Quercetin Dihydrate in Subcritical Water. *J. Food Eng.* **2010**, *100* (2), 208–218. https://doi.org/10.1016/j.jfoodeng.2010.04.001.

[16] Luo, Z.; Murray, B. S.; Yuso, A.; Morgan, M. R. a; Povey, M. J. W.; Day, A. J. Particle-Stabilizing Effects of Flavonoids at the Oil - Water Interface. *J. Agric. ...* **2011**, *59*, 2636–2645.

[17] Ay, M.; Charli, A.; Jin, H.; Anantharam, V.; Kanthasamy, A.; Kanthasamy, A. G. Quercetin. *Nutraceuticals* **2016**, 447–452. https://doi.org/10.1016/B978-0-12-802147-7.00032-2.

[18] Vasisht, K.; Chadha, K.; Karan, M.; Bhalla, Y.; Jena, A. K.; Chadha, R. Enhancing Biopharmaceutical Parameters of Bioflavonoid Quercetin by Cocrystallization. *CrystEngComm* **2016**, *18* (8), 1403–1415. https://doi.org/10.1039/C5CE01899D.

[19] Domagała, S.; Munshi, P.; Ahmed, M.; Guillot, B.; Jelsch, C. Structural Analysis and Multipole Modelling of Quercetin Monohydrate - A Quantitative and Comparative Study. *Acta Crystallogr. Sect. B Struct. Sci.* **2011**, *67* (1), 63–78. https://doi.org/10.1107/S0108768110041996.

[20] Nifant'ev, E. E.; Koroteev, M. P.; Kaziev, G. Z.; Uminskii, A. A.; Grachev, A. A.; Men'shov, V. M.; Tsvetkov, Y. E.; Nifant'ev, N. E.; Bel'skii, V. K.; Stash, A. I. On the Problem of Identification of the Dihydroquercetin Flavonoid. *Russ. J. Gen. Chem.* **2006**, *76* (1), 161–163. https://doi.org/10.1134/S1070363206010324.

[21] Jin, G. Z.; Yamagata, Y.; Tomita, K. Structure of Quercetin Dihydrate. *Acta Crystallogr. Sect. C Cryst. Struct. Commun.* **1990**, *46* (2), 310–313. https://doi.org/10.1107/S0108270189006682.

[22] Klitou, P.; Rosbottom, I.; Simone, E. Synthonic Modeling of Quercetin and Its

Hydrates: Explaining Crystallization Behavior in Terms of Molecular Conformation and Crystal Packing. *Cryst. Growth Des.* **2019**, *19* (8), 4774–4783. https://doi.org/10.1021/acs.cgd.9b00650.

[23] Olejniczak, S.; Potrzebowski, M. J. Solid State NMR Studies and Density Functional Theory (DFT) Calculations of Conformers of Quercetin†. **2004**, 2315–2322.

[24] Borghetti, G. S.; Carini, J. P.; Honorato, S. B.; Ayala, A. P.; Moreira, J. C. F.; Bassani, V. L. Thermochimica Acta Physicochemical Properties and Thermal Stability of Quercetin Hydrates in the Solid State. *Thermochim. Acta* **2012**, *539*, 109–114. https://doi.org/10.1016/j.tca.2012.04.015.

[25] Spiteri, L.; Baisch, U.; Vella-Zarb, L. Correlations and Statistical Analysis of Solvent Molecule Hydrogen Bonding – a Case Study of Dimethyl Sulfoxide (DMSO). *CrystEngComm* **2018**, *20* (9), 1291–1303. https://doi.org/10.1039/C7CE02206A.

[26] Desiraju, G. R. Supramolecular Synthons in Crystal Engineering—A New Organic Synthesis. *Angew. Chemie Int. Ed. English* **1995**, *34* (21), 2311–2327. https://doi.org/10.1002/anie.199523111.

[27] Desiraju, G. R. Crystal Engineering: Structure, Property and beyond. *IUCrJ* **2017**, *4* (Pt 6), 710–711. https://doi.org/10.1107/S2052252517014853.

[28] Sheldrick, G. M. {\it SHELXT} {--} Integrated Space-Group and Crystal-Structure Determination. *Acta Crystallogr. Sect. A* **2015**, *71* (1), 3–8. https://doi.org/10.1107/S2053273314026370.

[29] Sheldrick, G. M. Crystal Structure Refinement with {\it SHELXL}. *Acta Crystallogr. Sect. C* **2015**, *71* (1), 3–8. https://doi.org/10.1107/S2053229614024218.

[30] AS, I. Discovery Studio Modeling Environment, Release 7.0 [Software Program]. Accelrys Software Inc.: San Diego 2013.

[31] Clydesdale, G.; Roberts, K. J.; Docherty, R. HABIT95 — a Program for Predicting the Morphology of Molecular Crystals as a Function of the Growth Environment. *J. Cryst. Growth* **1996**, *166* (1–4), 78–83. https://doi.org/10.1016/0022-0248(96)00056-5.

[32] Van de Streek, J.; Motherwell, S. New Software for Searching the Cambridge Structural Database for Solvated and Unsolvated Crystal Structures Applied to Hydrates. *CrystEngComm* **2007**, *9* (1), 55–64. https://doi.org/10.1039/B613332K.

[33] Stewart, J. J. P. M. MOPAC for Solid-State Physics. Quant. Chem. Prog. Exchange 1985, p 62.63.

[34] Pickering, J.; Hammond, R. B.; Ramachandran, V.; Soufian, M.; Roberts, K. J.

Synthonic Engineering Modelling Tools for Product and Process Design. In *Engineering Crystallography: From Molecule to Crystal to Functional Form*; Roberts, K. J., Docherty, R., Tamura, R., Eds.; Springer Netherlands: Dordrecht, 2017; pp 155–176. https://doi.org/10.1007/978-94-024-1117-1_10.

[35] Rosbottom, I.; Roberts, K. J.; Docherty, R. The Solid State, Surface and Morphological Properties of *P* -Aminobenzoic Acid in Terms of the Strength and Directionality of Its Intermolecular Synthons. *CrystEngComm* **2015**, *17* (30), 5768–5788. https://doi.org/10.1039/C5CE00302D.

[36] Mayo, S. L.; Olafson, B. D.; Goddard, W. A. DREIDING: A Generic Force Field for Molecular Simulations. *J. Phys. Chem.* **1990**, *94* (26), 8897–8909. https://doi.org/10.1021/j100389a010.

[37] Parker, L. L.; Houk, A. R.; Jensen, J. H. Cooperative Hydrogen Bonding Effects Are Key Determinants of Backbone Amide Proton Chemical Shifts in Proteins. *J. Am. Chem. Soc.* **2006**, *128* (30), 9863–9872. https://doi.org/10.1021/ja0617901.

[38] Walshe, N.; Crushell, M.; Karpinska, J.; Erxleben, A.; McArdle, P. Anisotropic Crystal Growth in Flat and Nonflat Systems: The Important Influence of van Der Waals Contact Molecular Stacking on Crystal Growth and Dissolution. *Cryst. Growth Des.* **2015**, *15* (7), 3235–3248. https://doi.org/10.1021/acs.cgd.5b00348.

[39] Cruz-Cabeza, A. J.; Davey, R. J.; Oswald, I. D. H.; Ward, M. R.; Sugden, I. J. Polymorphism in P-Aminobenzoic Acid. *CrystEngComm* **2019**, *21* (13), 2034–2042. https://doi.org/10.1039/C8CE01890A.

[40] Costa, E. M.; Filho, J. M. B.; do Nascimento, T. G.; Macêdo, R. O. Thermal Characterization of the Quercetin and Rutin Flavonoids. *Thermochim. Acta* **2002**, *392–393*, 79–84. https://doi.org/https://doi.org/10.1016/S0040-6031(02)00087-4.

CHAPTER 5 - QUERCETIN-ETHANOL SOLVATE: AN ELUSIVE STRUCTURE OF THE POPULAR FLAVONOID SUBSTANCE

Abstract

Quercetin, a naturally occurring bioflavonoid substance widely used in the nutraceutical and food industries, exists in various solid forms that can have different physiochemical properties, thus, impacting this compound's performance in various applications. In this work, the solid forms attainable from crystallization in different ethanol-water solvent mixtures were studied, and a novel quercetin-ethanol solvate was prepared and characterized using a range of experimental techniques. The structure was found to be unstable and difficult to isolate in pure form, and to readily de-solvate upon heating at a temperature of just over 28°C, or when treated in vacuum, to form another novel anhydrous quercetin structure. The elusive solvate was found to de-solvate over a period of 16 months at ambient conditions, and to transform into quercetin dihydrate when slurried in pure water. In this work, the full known solid form landscape of quercetin was mapped to provide conditions under which each form is stable as well as information on their kinetics of solid state transformations. Exploring the solid form landscape of quercetin is essential to ensure accurate control of the functional properties of products containing crystals of this substance.

5.1 Introduction

Quercetin, 2-(3,4-Dihydroxyphenyl)-3,5,7-trihydroxy-4H-chromen-4-one, is a major dietary flavonol found in many fruits and vegetables, including onions, tomatoes, apples and berries.

[1][2] It belongs to a group of plant metabolites, named flavonoids, which are thought to provide health benefits through cell signalling pathways and antioxidant effects. [3] Quercetin has stimulated considerable interest in recent years, and it is the most extensively studied flavonoid, due to its significant association between dietary consumption and various health benefits, including antioxidant, anti-inflammatory and antitumor activities. [1][2][4][5][6]

The quercetin molecule consists of a pyrone ring and a phenyl ring, which constitute the hydrophobic part of the molecule and can form hydrophobic interactions such as Van der Waal's forces of attraction. [2][6] The hydrophilic part of the molecule consists of five hydroxyl groups that determine the molecule's biological activity and can act as hydrogen bond acceptors and/or donors, as well as an ether and carbonyl group acting as acceptors for both intramolecular and intermolecular hydrogen bonding. [6][7][8][9] Quercetin can exist as an anhydrous structure, a monohydrate and a dihydrate structure, with one or two water molecules per quercetin molecule respectively, and a DMSO-solvate structure (QDMSO). [1][8][10][11][12][13][14] Solvates of quercetin can present significantly different physical and chemical properties (solubility, density, bioavailability etc.) due to the different intermolecular interactions that the quercetin molecules can form with the solvent molecules in the lattice, thus, these different properties can dramatically affect the quality and efficiency of a particulate product. [13][14][15][16][17]

Because of its wide range of health benefits and biological effects, quercetin finds use in the nutraceutical industry and food supplements. [2] Quercetin dihydrate is marketed as a dietary supplement in capsule form, to help improve anti-inflammatory and immune response. [18] In 2018, Zembyla et. al have used quercetin crystals as a Pickering stabilizer to stabilize water in oil emulsions. They observed that the quercetin crystals absorb at the interface and provide stabilization of water droplets for several days. [19][20] The ability of quercetin to act as a

Pickering stabilizer may lead to various soft matter applications where stabilization using biocompatible particles is necessary. [21] More recently, Ma et al. have studied the oral bioavailability of quercetin encapsulated in zein-based Pickering emulsions using a simulated gastrointestinal track. [22] The quercetin-loaded zein colloid particles were prepared from the simultaneous precipitation of quercetin and zein from an aqueous ethanol solution. [22][23] Quercetin is sparingly soluble in water and this results in difficulties in obtaining quercetin di-hydrate crystals with controlled size distribution from aqueous solvents. To increase the solubility of quercetin, mixtures of alcohols and water are normally used. [2][24][25][26][27]

In food, quercetin mainly exists in a bounded form, with sugars, phenolic acids, alcohols etc. After ingestion, derivatives of quercetin are hydrolysed in the gastrointestinal tract and are then absorbed and metabolized. [6] The content and form of all quercetin derivatives in food is significant for their bioavailability as aglycone. However, due to its poor aqueous solubility and extensive phase-II metabolism, the bioavailability of quercetin is relatively low, and this severely limits its potential health benefits. [28] The challenges faced by poorly water-soluble drugs or nutraceuticals, particularly around re-precipitation in the gastrointestinal track are highlighted in literature. [28][29] Hence, the development of effective formulations for poorly soluble substances heavily relies on a good knowledge of the landscape of all their existing solid forms, as well as on an understanding of the chemical, physiological and biochemical processes that occur between substance administration and absorption. Although quercetin is one of the most exploited flavonoid substances, extensively studied by researchers over the past thirty years, more needs to be understood about the different crystalline solid forms that quercetin can form, as these can influence its performance in the different industrial applications, its digestion dynamics, and its bioavailability. In this work, the crystallization behavior of quercetin at different ethanol-water solvent mixtures was investigated, and two novel forms, a weak quercetin-ethanol solvate, QE, and its de-solvated structure, were found

and are reported here. The two crystal forms were studied and characterized fully using a range of solid-state characterization techniques. Furthermore, the solid form landscape of quercetin, including all the known solid forms of quercetin is summarized.

5.2 Experimental section

Materials. Quercetin dihydrate with a purity of 97% was obtained from Alfa Aesar (Port of Heysham Industrial Park, Lancashire, England). Ethanol solvent, 99.98%, was purchased from VWR chemicals. Water purified by treatment with a Milli-Q apparatus was used for all the experiments.

Slurrying of quercetin dihydrate (QDH) in ethanol-water solvent mixtures. Slurries of quercetin in ethanol-water solvent mixtures were prepared by adding 4.0 g of quercetin dihydrate in 100g of 100%, 90%, 85%, 75%, 60% and 15% (w/w) ethanol in water solvent mixtures. The temperature of the slurry was kept constant at 20 ℃ using a Tamson TLC2 recirculating chiller. The slurry was stirred using magnetic stirring at approximately 300 rpm for 48 hours. The solid samples removed from the slurry were filtered using a buchner flask, funnel and filter paper to remove the solvent. The samples were allowed approximately 24 hours to dry completely.

The slurring behaviour of quercetin in other solvents including acetonitrile, acetone and methanol was also investigated, and the resulting solids were partly characterised, however, it was decided to study the ethanol form further due to the fact that ethanol is more frequently used as a solvent to dissolve quercetin. The methodology followed for the preparation of those solids was identical to that used for the preparation of the ethanol form, by slurrying quercetin dihydrate in 100% acetonitrile, acetone or methanol, respectively.

Growth of QE crystals on petri dish. Approximately 10 mL of supernatant solution of QDH in 100% ethanol solvent was transferred to several petri dishes, and seed crystals from the 100% ethanol slurry were added to the petri dishes at different ratios of seeds to solution. This was done to promote growth of the seeds by evaporation. The petri dishes were covered with parafilm with holes to allow evaporation of the ethanol.

Scanning Electron Microscopy (SEM). The crystal morphology of the QE crystals was determined using SEM. The dry samples were imaged using a Carl Zeiss EVO MA15 scanning electron microscope. Samples were arranged on Leit tabs attached to SEM specimen stubs and an Iridium coating was applied before measurement. Samples from the 100% ethanol slurry and from the growth experiments on the petri dishes were imaged.

Thermogravimetric Analysis coupled with Differential Scanning Calorimetry (DSC/TGA). TGA and DSC experiments were performed on a Mettler Toledo TGA/DSC 3+ Stare System equipment. The samples (around 10−15 mg) were placed in 70 μL aluminum pans, covered with a lid, and heated from 20 to 500 °C at a heating rate of 10 °C min^{-1}. Nitrogen was used as the purge gas at 50 mL min^{-1}. Measurements were repeated three times. The QE samples were filtered the day before the analysis and left to dry overnight.

X-Ray diffraction (SAXS/WAXS, PXRD, VT-PXRD). The small and wide angle X-ray scattering (SAXS/WAXS) data were collected on a SAXSpace instrument (Anton Paar GmbH, Graz, Austria) equipped with a Cu anode that operates at 40 kV and 50mA (λ=0.154nm). The powder X-ray diffraction (PXRD) data were collected on a Panalytical X'Pert PRO which was set up in Bragg -Brentano mode, using Cu Kα radiation (λ = 1.54184 Å), in a scan between 5° to 50° in 2θ with a step size of 0.032° and time per step 25 seconds. The Variable Temperature PXRD (VT-PXRD) data were collected on the Panalytical X'Pert PRO and the temperature was increased from 20 °C to 90 °C at a rate of 10 °C min^{-1}.

QE mass loss over time experiments. *Dynamic Vapour Sorption Experiment*: A 50 mg sample of QE in 100% ethanol slurry was placed on a DVS pan and the mass change over a period of 20 hours was monitored at a constant temperature of 20 °C and relative humidity of 20%. The Dynamic vapour sorption experiments were performed on a Surface Measurement Systems DVS Resolution equipment.

Monitoring sample mass of QE over time: A sample of QE was filtered and the solid was placed on a plastic petri dish and left uncovered at ambient conditions. The mass of the sample was measured for 6 days to observe any mass changes.

Stability studies for the QE form. The stability of QE was determined by measuring the SAXS/WAXS patterns of QE samples treated under different conditions. The samples tested include: 4 week old and 16 month old samples of QE left in room temperature conditions in the laboratory, a sample of QE which was slurried in pure water for 24 hours and magnetically stirred at 300 rpm, and a sample of QE that was treated in a vacuum oven at 0 mbar for 24 hours.

5.3 Results

5.3.1 Slurrying of quercetin dihydrate (QDH) in ethanol-water solvent mixtures

The solid crystals from the various ethanol-water solvent mixtures after slurrying were tested using SAXS/WAXS and PXRD to identify the solid form (Appendix B Figure B.1). The PXRD patterns for the solid samples from 15% to 90% (w/w) ethanol slurries were identical to the PXRD pattern of quercetin dihydrate. This means that the stable solid form of quercetin for those ethanol-water solvent mixtures is the dihydrate. Quercetin dihydrate as purchased was also tested using SAXS/WAXS and shown in Figure B.1 for comparison. The solid taken from

the 100% ethanol slurry exhibits a different PXRD pattern, which is not identical either to the quercetin dihydrate or its de-solvated form, nor to any other deposited quercetin structure. [13][14][10][8] However, the pattern looks identical to a pattern previously reported by Miclaus et al. which is believed to be a weak quercetin-ethanol solvate. [30] This is an example of a solvent-mediated polymorphic transformation, where at the 100% ethanol solvent conditions, the metastable QDH interacts with the solvent and subsequently transforms to a more stable solid form by dissolution and recrystallization. To get better quality PXRD data the sample was also run on the Panalytical X'Pert PRO and the PXRD pattern is shown in Figure 5.1. The pattern exhibits its main peaks at 2θ angles of 8.91°, 9.83°, 13.03°, 22.10°, 26.17° and 28.15°.

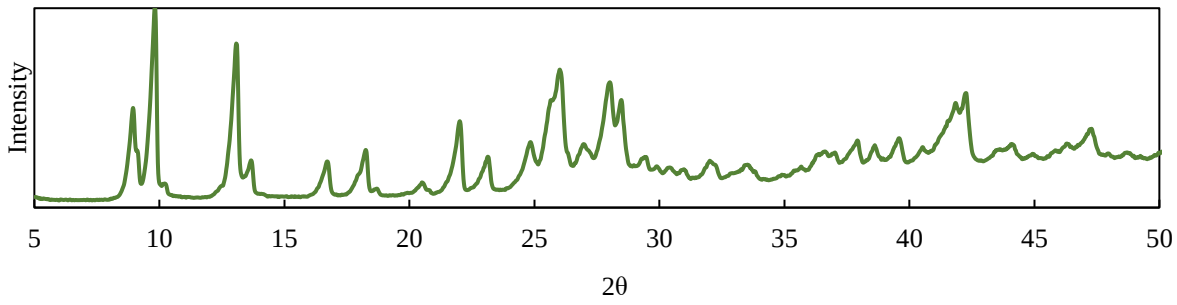

Figure 5.1 PXRD pattern for "QE" – the product of the solvent-mediate transformation QDH in 100% ethanol slurry.

It is interesting to notice that QE is only obtained from slurrying QDH in 100% ethanol solvent, and as little as 10%(w/w) of water in the solvent results in QDH being the most stable form in solution. In our previous publications it was shown how the water molecules in the QDH lattice satisfy the hydrogen bonding interactions, leading to a close-packed structure of higher relative stability compared to the known monohydrate and anhydrous quercetin forms. [13] Therefore, it is not a surprise that even at a lower ratio of water in the solvent, the quercetin dihydrate

structure is the stable form. The existence of a highly unstable quercetin-ethanol solvate was earlier postulated by Miclaus et al. They described that the ethanol molecules are weakly linked by hydrogen bonds to only one neighbouring quercetin molecule, and not incorporated into an extended hydrogen bonding network, therefore they can easily escape to form the anhydrous quercetin. [30] Assuming the QE structure is a quercetin-ethanol solvate, it seems that interaction with the ethanol molecules in solution is not favourable at solvent ratios lower than 100%(w/w) ethanol, and this could possibly be due to the bulkier size of the ethanol molecule compared to the water molecule size, impacting on the strength of the hydrogen bonding interactions with the quercetin molecules, and thus, not being able to offer the same degree of stabilization of the lattice as water molecules. [14]

The slurrying experiments demonstrate that for applications where the quercetin dihydrate crystal form is desired, the use of an aqueous ethanol solvent to increase the solubility of quercetin in solution is safe, as long as the ethanol ratio in solution is 90%(w/w) or lower. A 100% ethanol solvent will result in the formation of a different quercetin structure. The stability and characterisation of this QE form was investigated and discussed in the following sections.

5.3.2 Scanning Electron Microscopy (SEM)

Images of the QE crystals are shown in Figure 5.2.

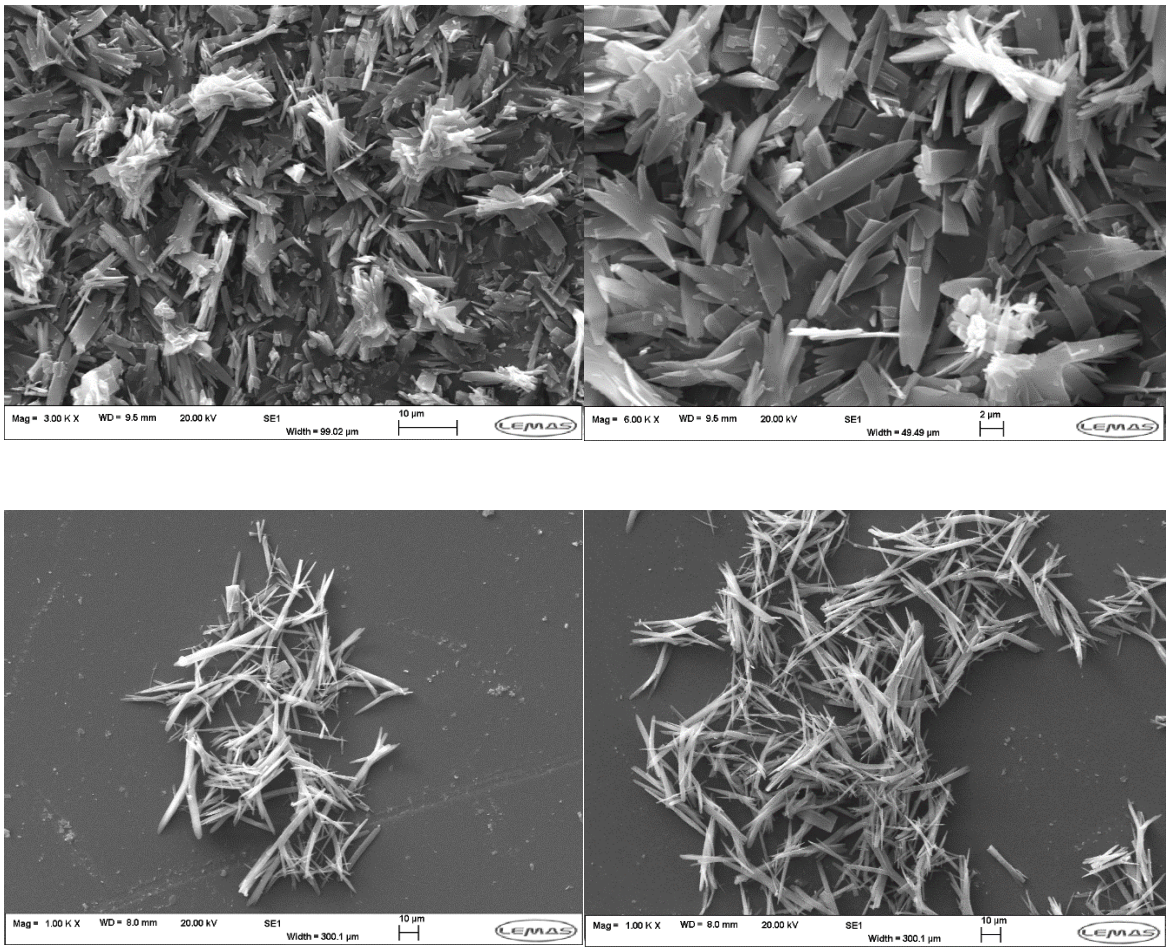

Figure 5.2 SEM images of the QE crystals from the 100% ethanol slurry (top) at 3-6K X magnifications and from the growth experiments on petri dishes (bottom) at 1K X magnifications.

The SEM images show a needle morphology for the QE crystals, although the crystals from the 100% ethanol slurry are more flaky and smaller in size compared to those grown on the petri dishes. The crystals from the petri dish are bigger in size, between 20-40µm, and have a higher aspect ratio compared to those from the slurry. It should be noted that this morphology

is very similar to that of the QDH crystals, which also exhibits a needle shape. For comparison, SEM images of the morphology of the QDH crystals are shown in Appendix B Figure B.2.

5.3.3 Thermal Stability

Thermogravimetric Analysis coupled with Differential Scanning Calorimetry (DSC/TGA). The thermal stability of the QE structure was studied to assess under what temperature conditions the sample undergoes changes in mass or heat flow. The results for the thermogravimetric analysis coupled with differential scanning calorimetry are shown in Figure 5.3.

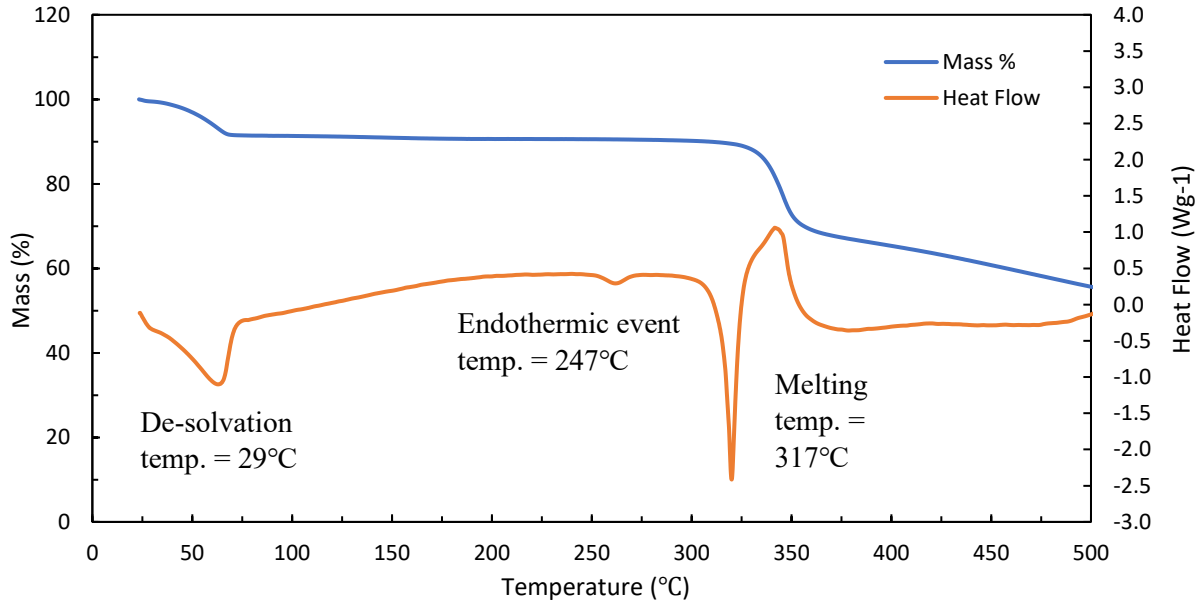

Figure 5.3 DSC and TGA curves for QE.

Observing the TGA curve, there is a loss in mass of about 6.2%, starting at an onset temperature of 28.5°C and finishing at approximately 70 °C. This loss in mass is accompanied by an endotherm as seen on the DSC curve. The loss could be attributed either to free ethanol evaporating from the wet solid (e.g., the sample was not completely dry after being left to dry overnight), or to a de-solvation process, where the ethanol molecules leave the crystal lattice.

To confirm which of the two was the reason for the weight loss, the mass of ethanol was monitored in two different experiments, a DVS experiment where the mass was monitored for 24 hours under controlled relative humidity and temperature conditions, and a mass loss over time experiment, where the mass of a QE sample left in room conditions of approximately 20 °C was monitored for several days. The data for these experiments are shown in Appendix B Figures B.3 and B.4. Both experiments confirmed that the mass of QE does not change considerably after the first day of drying. More specifically, the mass of a sample of QE after one day of drying to the sixth day just decreased by 0.8%. This confirms that during the DSC-TGA experiment, it is very unlikely that the sample lost 6.2% of its mass due to it not being completely dry. Hence, the thermal event observed in the DSC should be associated to a de-solvation event.

The theoretical mass loss for a solvate stoichiometry of one molecule of ethanol to one molecule of quercetin is calculated to be 13.2%. The observed loss was much less than that, almost half, and there was also significant variability between the different repeats. This suggests that the QE sample could be a mixture of a quercetin-ethanol solvate and an anhydrous form of quercetin. Miclaus et al. also emphasized in their paper the difficulty in obtaining a pure form of QE due to its low stability. [30] The possibility of a hemi-solvate, a solvate of one molecule of ethanol per two molecules of quercetin, is ruled out as the theoretical loss for that would be 6.6%, which is lower than the maximum loss obtained from the different repeats of the TGA experiments (8.6%). There is no further loss in mass after the endset temperature of 70°C and before the quercetin chemical decomposition at 335.3 °C.

The melting point of QE occurs at a sharp temperature of 317 °C which agrees with the melting point of quercetin, starting either from the dihydrate or the DMSO-solvate forms. [14] However, it is interesting to note that a small endotherm occurs just before melting at an onset

temperature of 247.3 ℃. This endotherm is not obtained for either the dihydrate or the DMSO-solvate forms, and it is probably due to a structural rearrangement that occurs in the lattice of quercetin before melting. If the ethanol molecules are weakly hydrogen bonded to the quercetin molecules, they could escape the lattice during the thermal de-solvation event, without this process being accompanied by a conformational rearrangement of all the quercetin molecules. In that case, the solvate-specific quercetin molecular conformation would be preserved. Therefore, it is possible that during that small endothermic event, the quercetin molecules rearrange to attain a more stable conformation. The data from the DSC-TGA is summarized in Table 5.1.

Table 5.1 DSC-TGA thermal analysis data for QE.

Assumed stoichiometry	1:1
Theoretical weight loss (%)	13.2%
Observed weight loss TGA (%)	6.2 ± 2.4
Guest loss Temp. (°C)	28.5 ± 5.1
ΔH for guest loss (Jg^{-1})	-102.3 ± 35.5
Structural rearrangement Temp. (°C)	247.3 ± 7.2
ΔH for structural rearrangement (Jg^{-1})	-8.2 ± 1.0
Melting Temp. (°C)	316.5 ± 0.8
ΔH for melting (Jg^{-1})	-125.7 ± 16.0
Decomposition Temp. (°C)	335.3 ± 7.3

Variable Temperature Powder X-ray Diffraction (VT-PXRD). To verify that the QE form loses the ethanol in a de-solvation step between the temperatures of 28 ℃ to 70 ℃, the PXRD pattern of QE was measured up to 90 ℃. The results are shown in Figure 5.4. From the PXRD data it is evident that there is a change in the structure, as the main peaks are different. The two main peaks of QE(20℃), at 8.9° and 9.8° disappear and two new peaks appear for QE(90℃), at 10.2° and 10.9°. Furthermore, the main peak of QE(20℃) at 13.0° disappears and another one at 13.6° appears for QE(90℃).

Combining the data from the TGA curve and the QE(90°C) pattern, it can be confirmed that this pattern belongs to an anhydrous form of quercetin, as no further loss in mass appears to be occurring at any higher temperature before decomposition. Moreover, these data suggest that the initial sample of QE at 20 °C could already contain a small amount of the de-solvated form, as the QE(20°C) pattern contains small peaks at 2θ angles of 10.2° and 13.6°, which increase in intensity in the QE(90°C) pattern. This further highlights the difficulty obtaining a pure sample of QE due to the very low stability of the form, and explains why the mass loss in the de-solvation step from the TGA data does not meet the theoretical loss.

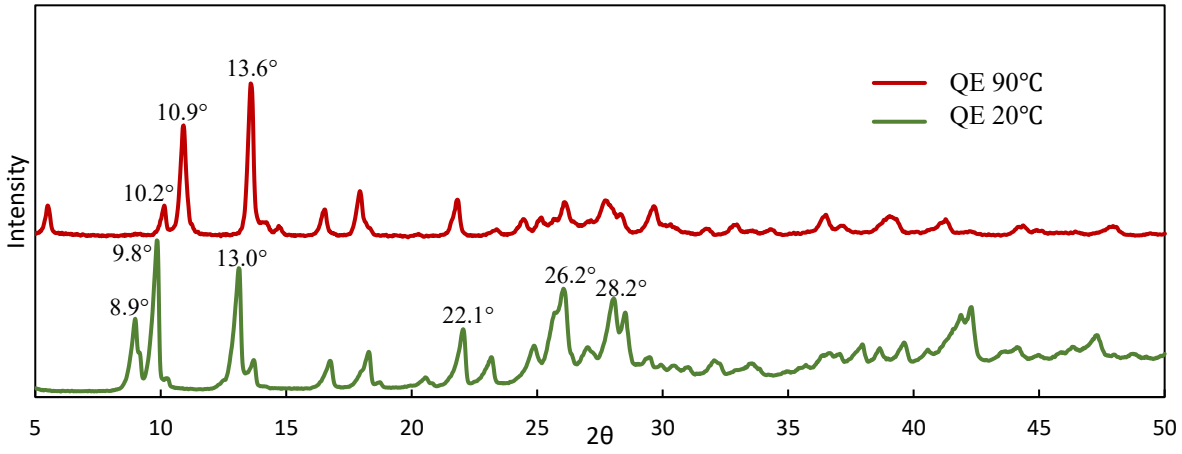

Figure 5.4 VT-PXRD patterns for QE at 20 °C and 90 °C with the important peaks annotated.

It is interesting to note that this anhydrous form of quercetin, obtained from the de-solvation of the quercetin-ethanol solvate, does not match the de-hydrated quercetin dihydrate or de-solvated quercetin-DMSO solvate (QDMSO) patterns obtained previously, nor to the PXRD pattern of the anhydrous quercetin structure (QA) deposited in literature. [8][14] This anhydrous structure could belong to a novel anhydrous quercetin form, which is only seen after de-solvation of the ethanol-solvate. A PXRD pattern comparison between the different anhydrous quercetin structures is shown in Figure 5.5. The different PXRD patterns indicate

that quercetin could have several different polymorphic forms in the anhydrous state. It has been frequently reported in literature that de-solvation of a solvated crystal form can provide an alternative pathway to the formation of polymorphic forms that would otherwise be difficult or impossible to crystallize by conventional crystallization techniques. [31] However, it would be interesting to understand why de-solvation of QDH and QDMSO leads to the formation of the same anhydrous quercetin, while de-solvation of QE, or recrystallization of QDH in a solvent (the QA deposited in CSD), lead to a different anhydrous form. In their work, Garnier et al. postulated that dehydration conditions, whether being mild or hard, will determine the way that the solvent molecules depart from the lattice. [32] A slow thermal de-solvation process would allow the cooperative departure of solvent molecules, followed by a structural reorganization step, leading to the nearest possible crystalline packing. [32] The resulting packing in the anhydrous structure should, at least to a certain extent, be determined by the initial solvated structure.

This is probably what we observe in the de-solvation of QDH and QDMSO. The departure of solvent molecules from QDH and QDMSO leads to some molecular rearrangements, both stabilizing in a new anhydrous polymorph towards the nearest well in energy. In the DSC curve of QDH, a single endotherm is observed for the dehydration event, which leads to the formation of the de-hydrated QDH. In the DSC curve of QDMSO, a second endotherm is observed right after the de-solvation endotherm, probably signalizing the rearrangement of quercetin molecules towards the same anhydrous polymorphic form that is obtained from the de-hydration of QDH. On the contrary, the de-solvation of QE leads to a different anhydrous polymorph, probably a metastable form, which requires further heating to induce polymorphic transformation towards a more stable anhydrous, which probably occurs at 247 °C, and hence an endotherm is observed at that temperature.

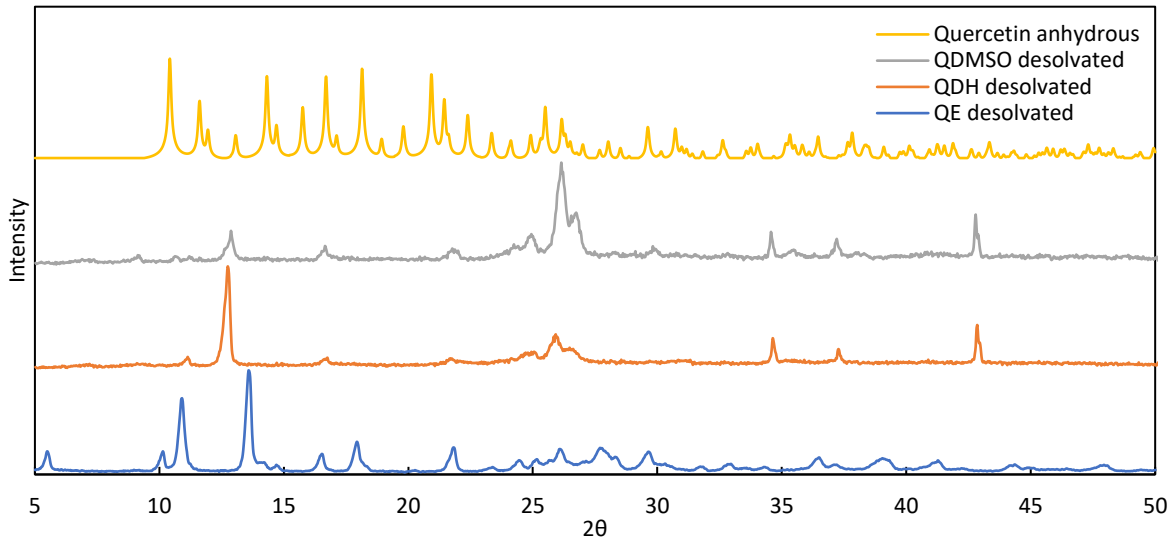

Figure 5.5 Comparison of the PXRD patterns for the different anhydrous quercetin structures, formed by the de-solvation of QE, QDH, QDMSO, and the anhydrous quercetin structure deposited in Cambridge Crystallographic database. [8][14]

The resulting anhydrous structure after de-solvation occurs should in some extent depend on the original solvated forms, their structural arrangements and intermolecular interactions, as well as the arrangement of solvent molecules in the lattice. The structures of QDH and QDMSO could possibly share more common structural characteristics, therefore de-solvation leads to the same anhydrous form, whereas for QE that might not be the case. However, for a more detailed understanding of the dehydration mechanisms of the different forms, further structural information regarding the resulting anhydrous structures would be needed, and a combination of experimental and computational techniques, such as density functional theory (DFT) calculations, would be required.

5.3.4 Stability studies

Samples of QE of different age and processing history were compared to study the stability in atmospheric conditions for this crystal structure. The SAXS/WAXS data of the analysed samples are shown in Figure 5.6.

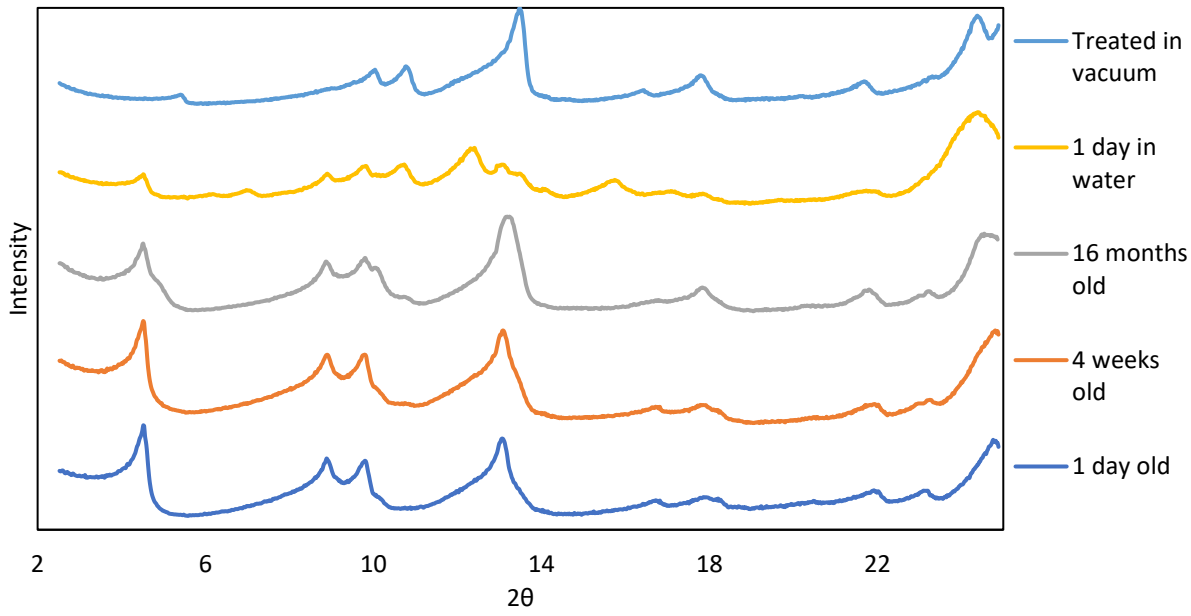

Figure 5.6 SAXS/WAXS patterns of QE samples treated under different conditions.

The QE samples that were 1 day old, 4 weeks old and 16 months old were left in open vials in the laboratory at ambient temperature and pressure. The results show that the patterns for the 1 day old and 4 weeks old samples were identical; therefore, QE is unlikely to transform over such period of time. However, the 16 months old samples exhibited some extra peaks at 10.2° and 10.9°, and the peak around 13.0° appears to be slightly shifted to the right compared to the other patterns. These extra peaks match with the peaks of the de-solvated form of QE shown earlier. As the pattern appears to confirm a mixture of the QE and of its de-solvated form, it shows that over the period of 16 months, QE is likely to slowly de-solvate.

The pattern of a QE sample that was slurried in water for 24 hours contained peaks that are characteristic of QE, but also some extra peaks at 10.8°, 12.9°, 13.9° and 14.2°, which are characteristic peaks of QDH. This indicates that when the QE form is slurried in water it can transform back into the QDH form. However, the pattern suggests that the transformation is incomplete and that the sample is a mixture of both QE and QDH. This shows that for applications of quercetin in water, QE would not be a stable solid form as it would transform to the QDH.

The pattern of the QE sample treated in vacuum for 24 hours exhibits peaks at 5.5°, 10.2°, 10.9° and 13.5° that completely match the peaks of the de-solvated QE obtained by heating the sample to 90 °C. The pattern does not contain any peaks from the original QE pattern; therefore, the de-solvation in vacuum appears to be complete and give a pure de-solvated QE form. Therefore, it can be concluded that the de-solvation of QE can be accelerated either by heating the sample at a temperature above 28°C, as this was the onset of de-solvation from the DSC-TGA experiments, or by treating the solid in vacuum for 24 hours.

When using solid forms of quercetin for various applications in the nutraceutical or food industry, it is of critical importance to have a knowledge of the solid form landscape of the substance. This will guide the choice of crystallization parameters to target a particular form of quercetin and provide information for the conditions under which each structure is stable, to avoid any undesired transformations, and lead to faster product and process development. Figure 5.7 summarizes the solid form landscape of quercetin, showing the different structures of quercetin and transformations between them, based on the work done in this paper and in our previous publications. [13][14]

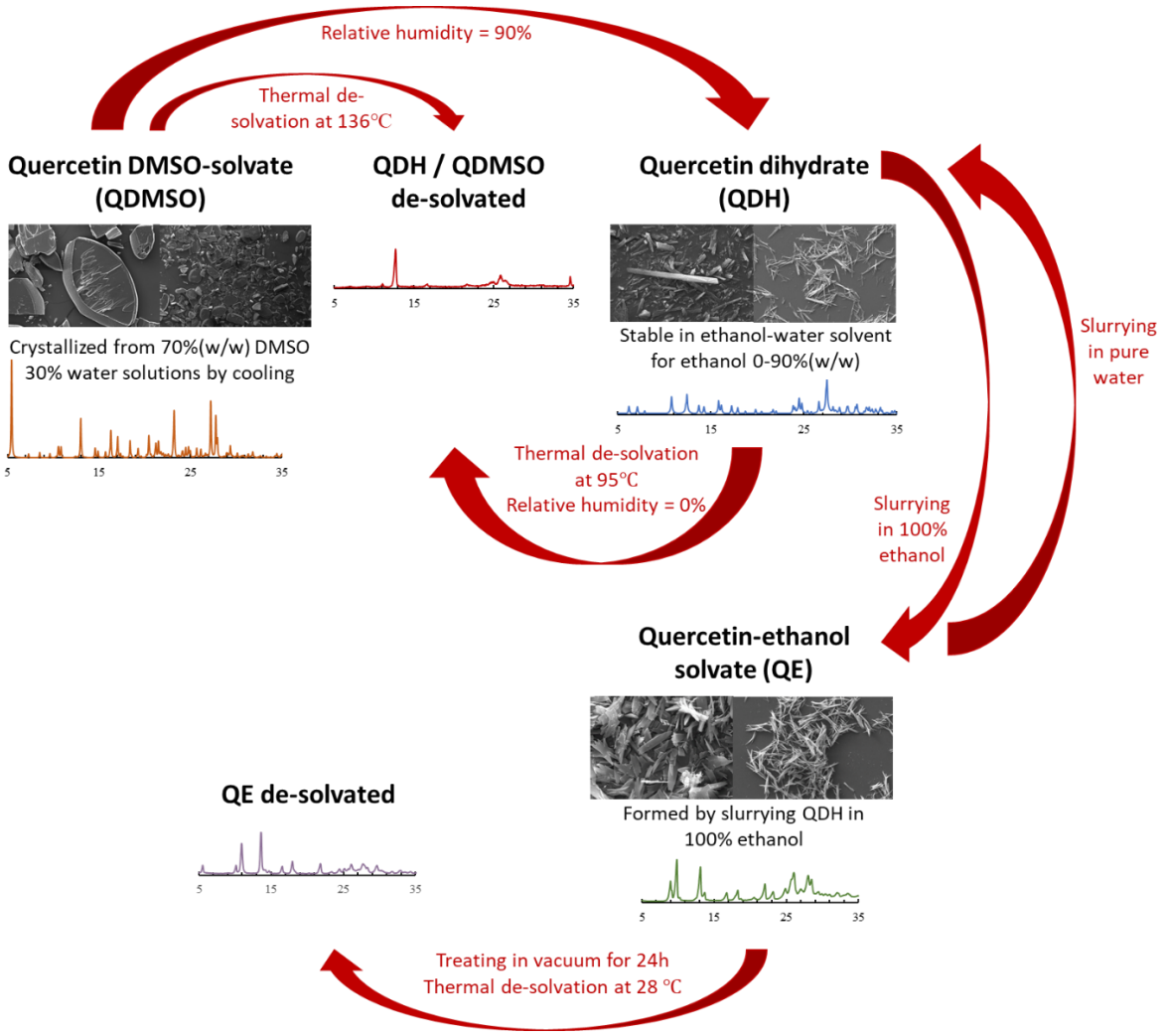

Figure 5.7 The solid form landscape of quercetin, including the dihydrate, DMSO-solvate and ethanol-solvate forms and their de-solvated structures.

5.3.5 Slurrying of quercetin dihydrate (QDH) in methanol, acetone and acetonitrile solvents.

QDH slurried in acetonitrile solvent

The SAXS/WAXS pattern for the acetonitrile slurried sample is illustrated in Figure 5.8. Patterns of QDH and QE are also shown for comparison. It can be observed that the pattern of the acetonitrile slurried sample is not identical to the QDH or QE patterns, neither to any other known quercetin structure. It exhibits characteristic peaks at 2θ angles of 4.71°, 8.53°, and 14.16°, which are not shared with other quercetin structures. The big sharp peak at 4.71° on

the acetonitrile pattern is also exhibited by the QE at a smaller angle of 4.53°, however no other consistent peak shifts were observed for any other peaks of the two structures, which indicates that the two forms are distinct. The acetonitrile slurried pattern is also different to the QDH pattern, however, it exhibits some smaller peaks which are also observed in the QDH pattern, at 10.75° and a smaller one at 12.40°, which could mean that the acetonitrile sample contained some of the QDH form. This could indicate an incomplete transformation from the QDH to the acetonitrile form during the slurrying experiment.

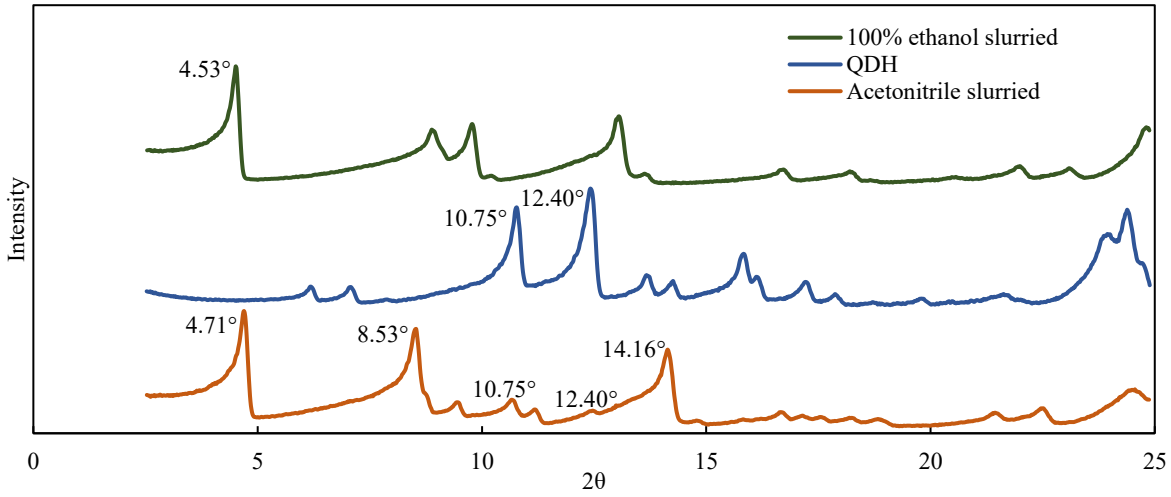

Figure 5.8 SAXS/WAXS patterns for QDH, and for samples obtained by slurrying QDH in acetonitrile and ethanol solvents.

Since no further solid-state characterization was carried out for the acetonitrile form, it is inconclusive whether the form is an acetonitrile solvate of quercetin, or if the pattern belongs to an anhydrous form of quercetin. If the latter is the case, then the form is a novel anhydrous quercetin structure, as its pattern does not match with any other observed anhydrous pattern of quercetin. What can be concluded from the experiment is that quercetin dihydrate is metastable in 100% acetonitrile solvent, which undergoes a solvent-mediated transformation to a novel quercetin form.

QDH slurried in methanol solvent

The XRD pattern for the methanol slurried sample is illustrated in Figure 5.9, together with the QE pattern for comparison. It can be observed that the two patterns are almost identical. The peaks in the methanol pattern are slightly less sharp, possibly indicating a sample of lower crystallinity. The fact that the two forms exhibit almost identical patterns is particularly interesting, as it could indicated that the two quercetin forms are isostructural. Isostructural crystal structures have been previously shown in literature to share very similar XRD patterns resulting from similar crystal structure and packing patterns, but different cell dimensions and chemical composition. [33][34] This type of behaviour would not be a surprise as the methanol and ethanol solvents are very similar, each containing a hydroxyl group of very similar electronegativity, and ethanol only being slightly bigger in size just by a methyl group. It is, therefore, expected that the type and strength of intermolecular interactions that they would form with the quercetin molecules would not differ greatly, and this should result in similar packing arrangements in the lattice.

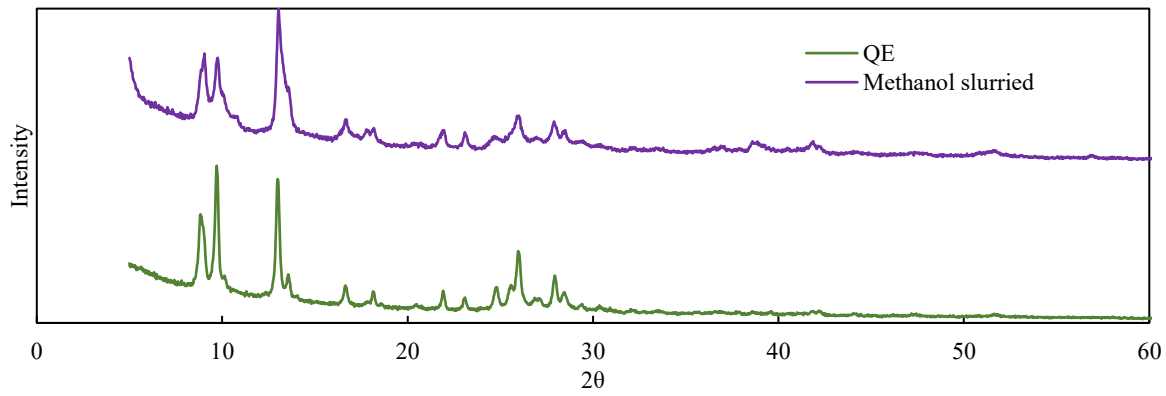

Figure 5.9 XRD patterns for samples obtained by slurrying QDH in methanol and ethanol solvents.

The DSC/TGA curves for the methanol sample are shown in Figure 5.10 (a). A very small loss in mass accompanied with an endotherm is exhibited at an onset temperature of 32 ℃. Also,

at a temperature of 250 °C a small endotherm is observed. The melting temperature of the sample is at 317 °C agreeing with the melting temperature of quercetin. Overall, the thermal events for the methanol sample are similar to those of the QE sample. Both samples show a very similar thermal stability, where they de-solvate at a low temperature, and exhibit an endotherm, possibly due to a structural rearrangement, just before the melting. The actual loss in mass in the de-solvation event was measured to be only 2.1%, whereas the theoretical loss for a 1:1 stoichiometry should be 9.6%, possibly because the sample lost part of the solvent before the thermal analysis, which was also the case with the QE sample.

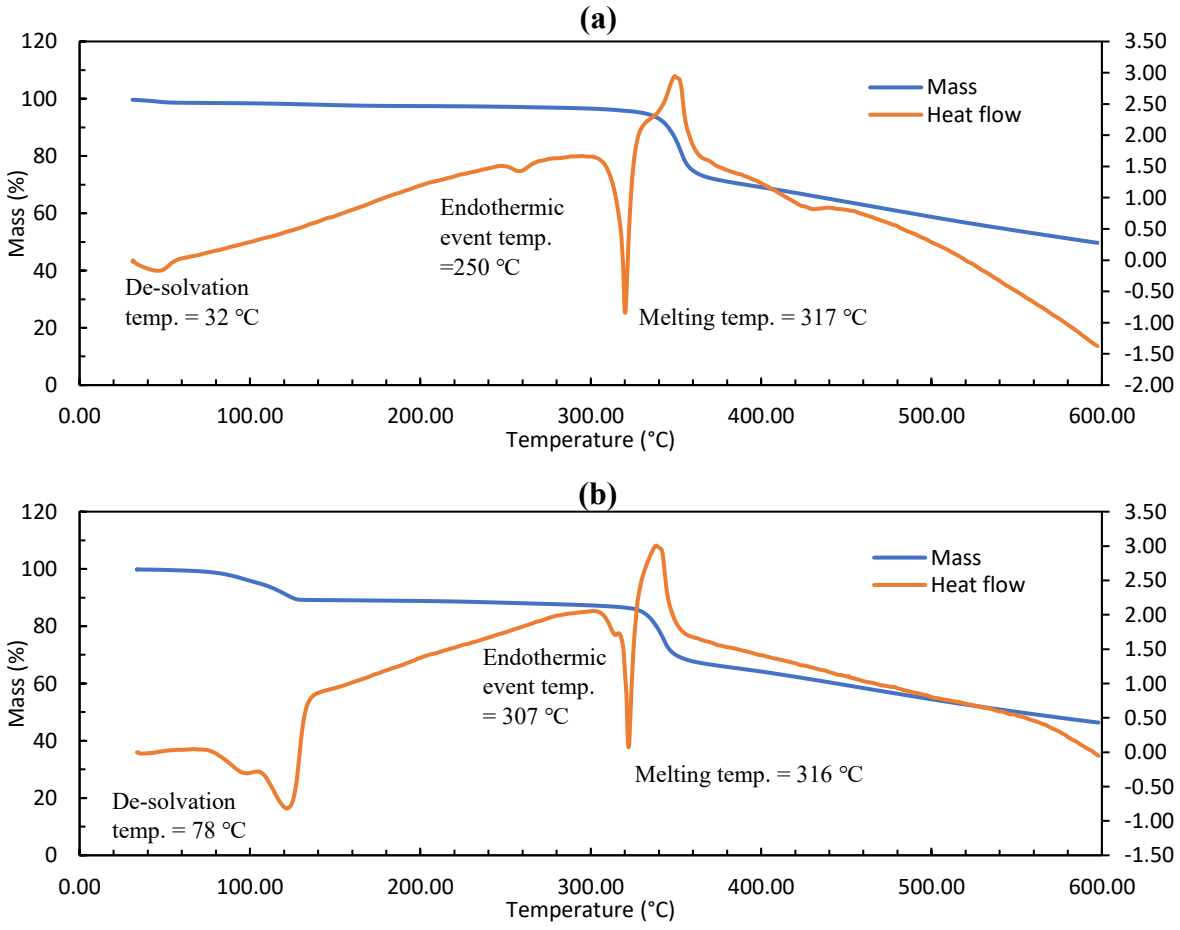

Figure 5.10 DSC and TGA curves for (a) methanol slurried sample (b) acetone slurried sample

QDH slurried in acetone solvent

The XRD pattern of the sample slurried in acetone has not been measured, however, a thermal analysis has been conducted on the sample and the DSC/TGA curves are shown in Figure 5.10 (b). A loss in mass of 10.7% is observed at an onset temperature of 78 °C. Although the loss in mass matches with the theoretical loss that would have been observed from the dehydration of QDH, the event occurs at a much lower temperature of 78 °C, compared to that of QDH which would occur at 95 °C. Further to that, the endotherm appears to form a shoulder at around 108 °C, before a second endotherm is observed. The de-solvation endset temperature is around 131 °C. This thermal behaviour is different to QDH and indicates that the sample is not QDH, and it is probably a solvate of acetone. The two consecutive endotherms suggest that the de-solvation of the sample could be a two-step process similar to that of QDMSO which was discussed in the previous chapter. The sample melts at a sharp temperature of 317 °C, characteristic of all quercetin samples. Before melting, another small endotherm is observed, which could be due to an impurity in the sample, or another structural rearrangement similar to those that were obtained before melting of the QE and the methanol samples. Although the thermal analysis results suggest that the structure could be an acetone solvate, further tests, such as XRD analysis, are required to confirm this.

5.4 Conclusion

In this work, the crystallization behaviour of quercetin in different ethanol-water solvent mixtures was studied. It was found that quercetin dihydrate is always obtained for ethanol in water contents lower than 90%(w/w). In 100% ethanol a different form of quercetin was obtained, which is likely to be an ethanol solvate. The structure is characterised by a low stability at ambient conditions. Slurrying QE in pure water can reverse the transformation and form the dihydrate structure. The thermal analysis showed that the QE structure de-solvates at

an onset temperature of 28.5℃ to form its de-solvated structure that is a novel anhydrous structure of quercetin, different to the de-solvated quercetin structures that are obtained by de-solvation of quercetin dihydrate or its DMSO-solvate. De-solvation of QE can also be achieved by treating the QE form in vacuum for 24 hours. The structure does not appear to de-solvate at room temperature conditions over a period of 4 weeks but it seems to be losing part of the ethanol over 16 months.

These experimental findings enhance the knowledge around the different solid forms of this important bioflavonoid substance. The comprehensive understanding of the physiochemical properties, crystallization conditions and transformation between the various forms is essential when designing processes and optimal solid forms for specific applications using quercetin.

References

[1] M. Rossi, L. F. Rickles, and W. A. Halpin, “The crystal and molecular structure of quercetin: A biologically active and naturally occurring flavonoid,” *Bioorg. Chem.*, vol. 14, no. 1, pp. 55–69, 1986, doi: 10.1016/0045-2068(86)90018-0.

[2] K. Srinivas, J. W. King, L. R. Howard, and J. K. Monrad, “Solubility and solution thermodynamic properties of quercetin and quercetin dihydrate in subcritical water,” *J. Food Eng.*, vol. 100, no. 2, pp. 208–218, 2010, doi: 10.1016/j.jfoodeng.2010.04.001.

[3] P. M. Shah, V. Vishnu Priya, and R. Gayathri, “Quercetin – A flavonoid:A systematic review,” *J. Pharm. Sci. Res.*, vol. 8, no. 8, pp. 878–880, 2016.

[4] Z. Luo, B. S. Murray, A. Yuso, M. R. a Morgan, M. J. W. Povey, and A. J. Day, “Particle-Stabilizing Effects of Flavonoids at the Oil - Water Interface,” *J. Agric. …*, vol. 59, pp. 2636–2645, 2011.

[5] M. Ay, A. Charli, H. Jin, V. Anantharam, A. Kanthasamy, and A. G. Kanthasamy, “Quercetin,” *Nutraceuticals*, pp. 447–452, Jan. 2016, doi: 10.1016/B978-0-12-802147-7.00032-2.

[6] M. MATERSKA, “Quercetin and Its Derivatives : Chemical Structure and Bioactivity -a Review,” *Polish J. food Nutr. Sci.*, vol. 58, no. 4, pp. 407–413, 2008.

[7] E. Grotewold, *The science of flavonoids*. 2006.

[8] K. Vasisht, K. Chadha, M. Karan, Y. Bhalla, A. K. Jena, and R. Chadha, “Enhancing biopharmaceutical parameters of bioflavonoid quercetin by cocrystallization,” *CrystEngComm*, vol. 18, no. 8, pp. 1403–1415, 2016, doi: 10.1039/C5CE01899D.

[9] J. Hanuza *et al.*, “Vibrational Spectroscopy Molecular structure and vibrational spectra of quercetin and quercetin-5 ’ -sulfonic acid,” vol. 88, pp. 94–105, 2017, doi: 10.1016/j.vibspec.2016.11.007.

[10] S. Domagała, P. Munshi, M. Ahmed, B. Guillot, and C. Jelsch, “Structural analysis and multipole modelling of quercetin monohydrate - A quantitative and comparative study,” *Acta Crystallogr. Sect. B Struct. Sci.*, vol. 67, no. 1, pp. 63–78, 2011, doi: 10.1107/S0108768110041996.

[11] E. E. Nifant'ev *et al.*, "On the problem of identification of the dihydroquercetin flavonoid," *Russ. J. Gen. Chem.*, vol. 76, no. 1, pp. 161–163, Jan. 2006, doi: 10.1134/S1070363206010324.

[12] G. Z. Jin, Y. Yamagata, and K. Tomita, "Structure of quercetin dihydrate," *Acta Crystallogr. Sect. C Cryst. Struct. Commun.*, vol. 46, no. 2, pp. 310–313, 1990, doi: 10.1107/S0108270189006682.

[13] P. Klitou, I. Rosbottom, and E. Simone, "Synthonic Modeling of Quercetin and Its Hydrates: Explaining Crystallization Behavior in Terms of Molecular Conformation and Crystal Packing," *Cryst. Growth Des.*, vol. 19, no. 8, pp. 4774–4783, Aug. 2019, doi: 10.1021/acs.cgd.9b00650.

[14] P. Klitou, C. M. Pask, L. Onoufriadi, I. Rosbottom, and E. Simone, "Solid-State Characterization and Role of Solvent Molecules on the Crystal Structure, Packing, and Physiochemical Properties of Different Quercetin Solvates," *Cryst. Growth Des.*, vol. 20, no. 10, pp. 6573–6584, Oct. 2020, doi: 10.1021/acs.cgd.0c00751.

[15] C. J. Tilbury, J. Chen, A. Mattei, S. Chen, and A. Y. Sheikh, "Combining Theoretical and Data-Driven Approaches To Predict Drug Substance Hydrate Formation," 2018, doi: 10.1021/acs.cgd.7b00517.

[16] A. M. Healy, Z. A. Worku, D. Kumar, and A. M. Madi, "Pharmaceutical solvates, hydrates and amorphous forms: A special emphasis on cocrystals," *Adv. Drug Deliv. Rev.*, vol. 117, pp. 25–46, 2017, doi: 10.1016/j.addr.2017.03.002.

[17] S. R. Vippagunta, H. G. Brittain, and D. J. W. Grant, "Crystalline solids," vol. 48, pp. 3–26, 2001.

[18] Y. Li *et al.*, "Quercetin, inflammation and immunity," *Nutrients*, vol. 8, no. 3, pp. 1–14, 2016, doi: 10.3390/nu8030167.

[19] M. Zembyla, B. S. Murray, and A. Sarkar, "Water-in-Oil Pickering Emulsions Stabilized by Water-Insoluble Polyphenol Crystals," *Langmuir*, vol. 34, no. August, pp. 1–7, 2018, doi: 10.1021/acs.langmuir.8b01438.

[20] M. Zembyla, A. Lazidis, B. S. Murray, and A. Sarkar, "Water-in-Oil Pickering

Emulsions Stabilized by Synergistic Particle − Particle Interactions," 2019, doi: 10.1021/acs.langmuir.9b02026.

[21] M. Zembyla, B. S. Murray, and A. Sarkar, "Water-in-oil emulsions stabilized by surfactants , biopolymers and / or particles : a review," *Trends Food Sci. Technol.*, vol. 104, no. July, pp. 49–59, 2020, doi: 10.1016/j.tifs.2020.07.028.

[22] J. Ma, X. Huang, S. Yin, Y. Yu, and X. Yang, "Bioavailability of quercetin in zein-based colloidal particles-stabilized Pickering emulsions investigated by the in vitro digestion coupled with Caco-2 cell monolayer model," *Food Chem.*, vol. 360, no. April, p. 130152, 2021, doi: 10.1016/j.foodchem.2021.130152.

[23] A. R. Patel, P. C. M. Heussen, J. Hazekamp, E. Drost, and K. P. Velikov, "Quercetin loaded biopolymeric colloidal particles prepared by simultaneous precipitation of quercetin with hydrophobic protein in aqueous medium," *Food Chem.*, vol. 133, no. 2, pp. 423–429, 2012, doi: 10.1016/j.foodchem.2012.01.054.

[24] M. H. Abraham and W. E. Acree, "On the solubility of quercetin," *J. Mol. Liq.*, vol. 197, pp. 157–159, 2014, doi: 10.1016/j.molliq.2014.05.006.

[25] R. S. Razmara, A. Daneshfar, and R. Sahraei, "Solubility of Quercetin in Water + Methanol and Water + Ethanol from (292.8 to 333.8) K," vol. 2, no. 2, pp. 3934–3936, 2010.

[26] L. Chebil, C. Humeau, J. Anthony, F. Dehez, J. M. Engasser, and M. Ghoul, "Solubility of flavonoids in organic solvents," *J. Chem. Eng. Data*, vol. 52, no. 5, pp. 1552–1556, 2007, doi: 10.1021/je7001094.

[27] J. L. Dias, M. Lanza, and S. R. S. Ferreira, "Cocrystallization: A tool to modulate physicochemical and biological properties of food-relevant polyphenols," *Trends Food Sci. Technol.*, vol. 110, no. December 2020, pp. 13–27, 2021, doi: 10.1016/j.tifs.2021.01.035.

[28] A. D. Gilley *et al.*, "Novel cellulose-based amorphous solid dispersions enhance quercetin solution concentrations in vitro," *Carbohydr. Polym.*, vol. 157, pp. 86–93, 2017, doi: https://doi.org/10.1016/j.carbpol.2016.09.067.

[29] B. J. Boyd *et al.*, “Successful oral delivery of poorly water-soluble drugs both depends on the intraluminal behavior of drugs and of appropriate advanced drug delivery systems.,” *Eur. J. Pharm. Sci. Off. J. Eur. Fed. Pharm. Sci.*, vol. 137, p. 104967, Sep. 2019, doi: 10.1016/j.ejps.2019.104967.

[30] M. O. Miclaus, X. Filip, C. Filip, F. A. Martin, and I. G. Grosu, “Highly sensitive solid forms discrimination on the whole tablet of the active ingredients in quercetin dietary supplements by NMR crystallography approaches,” *J. Pharm. Biomed. Anal.*, vol. 124, pp. 274–280, 2016, doi: 10.1016/j.jpba.2016.03.006.

[31] D. E. Braun *et al.*, “Unraveling Complexity in the Solid Form Screening of a Pharmaceutical Salt: Why so Many Forms? Why so Few?,” *Cryst. Growth Des.*, vol. 17, no. 10, pp. 5349–5365, Oct. 2017, doi: 10.1021/acs.cgd.7b00842.

[32] Garnier, S.; Petit, S.; Coquerel, G. Dehydration Mechanism and Crystallisation Behaviour of Lactose. *J. Therm. Anal. Calorim.* 2002, 68 (2), 489–502. https://doi.org/10.1023/A:1016087702409.

[33] M. C. Pfrunder, A. S. Micallef, L. Rintoul, D. P. Arnold, K. J. P. Davy, and J. McMurtrie, “Isostructural Co-crystals Derived from Molecules with Different Supramolecular Topologies,” *Cryst. Growth Des.*, vol. 14, no. 11, pp. 6041–6047, Nov. 2014, doi: 10.1021/cg501210t.

[34] J. Fang, Q. Zhang, M. Li, J.-R. Wang, and X. Mei, “Isostructural Solvates of Naturally Occurring Allocryptopine Exhibit Both Mechanochromic and Hydrochromic Luminescent Properties,” *ACS Omega*, vol. 3, no. 8, pp. 9220–9226, Aug. 2018, doi: 10.1021/acsomega.8b01267.

CHAPTER 6 - DESIGNING PARTICLES WITH TAILOR-MADE SURFACE PROPERTIES: A STUDY ON QUERCETIN SOLID FORMS

Abstract

The surface energy heterogeneity and surface chemistry anisotropy of a crystal are of great importance when designing particles for a specific application, as these will impact both downstream manufacturing processes as well as final product quality. In this work, the surface properties of different solid forms of quercetin, including solvates, are studied using molecular modelling and experimental techniques, including Inverse Gas Chromatography (IGC). The aim of this study was to investigate the relationship between crystallographic structure and surface properties of quercetin particles. The surface chemistry and hydrophobicity of the different facets of several quercetin structures were evaluated through the study of their extrinsic synthons. The modelling results showed that the most dominant facet of quercetin dihydrate is mostly hydrophobic as it grows by non-polar stacking interactions, while for quercetin-DMSO solvate, the most dominant surface grows by polar hydrogen bonds, granting it a hydrophilic nature. Water contact angle measurements and IGC confirmed the modelling results, and showed the anisotropic nature of the different forms studied. When designing particles with tailored surface properties, knowledge of the surface chemistry is vital; the results presented here can guide the choice of crystallization conditions which will determine the optimal crystal form and final morphology for optimal surface properties.

6.1 Introduction

The anisotropic nature of crystalline solids has been a subject of considerable interest for researchers for many years, and results from differences in physical, thermodynamic, kinetic, surface, spectroscopic, optical, or electrical properties along different index crystal planes. [1][2][3] Surface energy heterogeneity in crystalline substances is perhaps the most significant manifestation of thermodynamic anisotropy, and involves variations in surface energy, adsorption energy and type of favorable chemical interactions (e.g. hydrophobic/hydrophilic) of the different facets of a crystal. [4][5] This heterogeneity is due to the different molecular arrangements relative to each crystal surface (e.g. different functional groups of the crystal molecules being exposed). [4][5][6]

In the pharmaceutical industry, where crystalline powders are widely used, the surface energy and its distribution along the different facets of a crystal play an important role in both downstream processing and product performance. For example, these properties have been found to significantly influence the performance of dry powder inhalers, powder mixing and the cohesion of compressed tablets. [4][5][7] Crystal surface energy can also influence particle agglomeration phenomena, wetting phenomena and behavior of particle dispersions in liquids. [7] Furthermore, unfavorable crystal morphologies can disturb the operating conditions of downstream operations and affect product stability during storage. [8][9] It is, therefore, vital to have a good knowledge of the surface properties of crystalline powders, and to understand how such properties are affected by crystal structure (e.g., polymorphs or solvates) as well as morphology. Such knowledge can enable the design of particles with optimal surface properties and surface energy distribution along the different surfaces.

Predictive computational techniques and molecular modelling can be used to predict crystal morphologies, and to provide a vital insight into the facet specific properties of crystalline

materials. [10][11][12][13][14] This can aid in the design of a crystal morphology with optimal surface properties. Synthonic engineering tools, such as the HABIT software, allow morphological and surface chemistry predictions through the calculation of the 'extrinsic synthons', the synthons that are unsaturated (broken) at the crystal facets due its termination. [15][16][17][18][19][20] These extrinsic synthons are important as they impact the physical and chemical properties of the crystals, for example crystal growth rate of specific facets, particle shape and aspect ratio, tendency to agglomerate etc. [21] Rosbottom et al. have used synthonic modelling to examine the crystal morphology and analyze the surface chemistry of the α and β polymorphs of p-aminobenzoic acid, by establishing the key intermolecular interactions that contribute to the attachment energies of the morphologically important surfaces. [22] Nguyen et al. have characterized the extrinsic synthons of RS-ibuprofen to assess how the crystal might interact with the surrounding solution and understand its interfacial stability. [21] In parallel with modelling it is also important to estimate experimentally facet specific surface properties of crystalline solids. The experimental determination of the surface properties of powders includes contact angle measurements, probe force microscopy and atomic force microscopy and inverse gas chromatography (IGC). [4] Finite dilution inverse gas chromatography (FD-IGC) has been demonstrated as a practical technique for measuring surface energy in a range of probe molecule surface coverages. [3][7][5][23][24] [25][26][27]

In our previous publications it was demonstrated that quercetin, a bioflavonoid substance widely used in the food and nutraceutical industries, can exist as an anhydrous pure form or as different solvated structures, including two types of hydrates and a DMSO solvate, which possess different physiochemical properties. [28][29][30][31][32] As different solid forms of quercetin can have different surface properties, choosing the optimal one can offer improved materials handling, flowability, compaction, tabletting and dissolution properties. [5][33][34][35][36]. Although the use of solvates in formulations is becoming more common,

understanding of the surface anisotropic properties of a solid form, and more specifically between different solvates of the same substance, is yet under-researched and more needs to be invested into exploiting these structures.

In this paper, a holistic study of the morphologies and surface chemistry of different quercetin forms is presented. The extrinsic synthons and surface energies of the forms are calculated and related to the facet specific polarity. The role of the solvent molecules on the facet growth and facet characteristics is discussed. The modelling calculations are compared to experimental surface properties measurements, including inverse gas chromatography and water contact angle measurements. Experimental characterization was performed on quercetin dihydrate and quercetin-DMSO solvate, the two forms that could be obtained experimentally in the laboratory. The work aims to provide a complete and comprehensive study of the surface properties of different solvates of quercetin. Understanding and controlling the morphology and surface chemistry of crystalline solids of a material, whether this is a polymorph or a solvate, enables the manipulation of its surface properties, therefore engineering a particle with the most desirable characteristic and interfacial behavior. Ultimately, this will lead to a rational and quicker product design.

6.2 Experimental section

Materials. Quercetin dihydrate with a purity of 97% was obtained from Alfa Aesar (Port of Heysham Industrial Park, Lancashire, England). Dimethyl sulfoxide (DMSO) solvent was purchased from Fisher Scientific (Bishop Meadow Road, Loughborough, England) and ethanol solvent, 99.98%, was purchased from VWR chemicals. Water purified by treatment with a Milli-Q apparatus was used.

Crystallization of quercetin dihydrate (QDH). A 200g solution of 90%(w/w) ethanol and 10% water solvent with quercetin concentration of 0.01g/g was prepared at 20°C. The quercetin dihydrate was recrystallized by adding water as the antisolvent until the final solvent mixture was 45%(w/w) ethanol 55% water. The first 100g of water was added at a rate of 400 mL/hr, using a Cole-Parmer syringe infusion pump. At the end of the first addition, 0.3g of QDH seeds (from the bottle) was added to the solution and a further 100g of water was added to the solution at a rate of 50 mL/hr. The temperature was controlled using a Huber Ministat 230 thermoregulator and a PT100 temperature probe, connected to a 500mL jacketed vessel. The crystals were then vacuum filtered using disposable paper filters.

Crystallization of quercetin-DMSO solvate (QDMSO). A 100g solution of 60% (w/w) DMSO and 40% water solvent with quercetin concentration of 0.05g/g was prepared via heating to 50 °C to ensure complete dissolution of the solid material. Such solution was then subjected to cooling at a rate of -0.3 °C/min to a temperature of 10 °C. The temperature was then cycled from 10 °C to 14 °C at a cooling/heating rate of $\pm$0.5 °C/min for 24 hours, to promote growth of the crystals and Ostwald ripening. The temperature was controlled using a Huber Ministat 230 thermoregulator and a PT100 probe connected to a 100 mL jacketed vessel. The crystals were then vacuum filtered using disposable paper filters.

Inverse Gas Chromatography. The QDMSO and QDH crystals obtained as previously described were studied for their surface energy heterogeneity using Inverse Gas Chromatography, IGC surface energy analyzer (IGC SEA, SMS, UK). Due to the difference in the specific surface areas of the two samples different amounts of samples were used for the analysis. About 25 mg of the QDH and 115 mg of QDMSO sample was packed into a silanized glass column (internal diameter = 4 mm) and plugged with silanized glass wool on both the ends. A jolting voltameter (Surface Measurement Systems, London, UK) was used to provide

mechanical tapping to the sample in order to remove the voids in the packed sample bed. The packed sample column was placed into the column oven and conditioned at the analysis temperature of 30°C and 10% relative humidity (RH) for 2 hours under 10 mL/min carrier gas (Helium) flow rate prior to each measurement. Helium was used as a carrier gas at a flow rate of 10 mL/min and methane was used as a reference gas to determine the dead volume. The RH was kept at 10% to avoid the dehydration of the QDH sample, which would occur at a lower RH. The analysis was carried out in the finite dilution range using a series of n-alkane probes like nonane, octane, heptane and hexane to determine the dispersive interactions.

Contact Angle measurements and Wettability. The water contact angle measurements were carried out at 25 °C using a OCA25 drop-shape tensiometer (DataPhysics Instruments, Germany) fitted with a microsyringe and a high-speed camera. Compressed discs of the QDH and QDMSO samples were prepared by placing 0.3 g of QDH or 0.6 g of QDMSO between the plates of a hydraulic bench press (Clarke, UK) using a 1.54 cm diameter die under a weight of 6 tonnes for 30 s. Static contact angles were measured using the sessile drop method. Water droplets (3 μL) were produced using a straight needle of 0.52 mm outer diameter, to form a sessile drop onto the compressed particle disc surfaces. A video camera was used to record the droplet behavior. The droplet contour was fitted using the SCA V.20 software, and the contact angles between the compressed disk and the water droplet were measured. All measurements were repeated at least 6 times to ensure consistency of measurements, using three different disks for each material.

Powder X-ray Diffraction (PXRD). PXRD was used to confirm the quercetin solid form and identify the morphologically dominant crystals facets. This was estimated by a comparison of the experimental and a predicted diffractogram from the crystal structure, where the reflection that was significantly enhanced in the experiment as compared to the theoretical was assumed

to be the dominant plane. PXRD patterns were collected on a Panalytical X'Pert PRO which was set up in Bragg -Brentano mode, using Cu Kα radiation (λ = 1.54184 Å), in a scan between 5° to 50° in 2θ with a step size of 0.032° and time per step 25 seconds.

Scanning Electron Microscopy (SEM). The crystal morphologies of the quercetin forms were imaged using SEM. The dry samples were imaged using a Carl Zeiss EVO MA15 scanning electron microscope. Samples were arranged on Leit tabs attached to SEM specimen stubs and an Iridium coating was applied before measurement.

6.3 Computational procedures

The crystallographic information files (.cif) for the four quercetin structures used in the analysis were obtained from the Cambridge Structural Database (CDS): quercetin anhydrous (REFCODE: NAFZEC), quercetin monohydrate (REFCODE: AKIJEK), quercetin dihydrate (REFCODE: FEFBEX), quercetin-DMSO solvate (REFCODE: VUVHOM). [29][32][37][38] Computational analysis was performed using Materials Studio 2017, HABIT98, and Mercury CSD 2020.3. [15][39][40] The structures were minimized using the Forcite module in Materials Studio 2017, using methodologies described in previous publications. [22][31][39] The files were exported as .car files (Cartesian coordinates), converted to fractional coordinates, and then fractional charges were calculated using the AM1 method within MOPAC. [41] The synthonic analysis was carried out using the HABIT98 software, which takes in structural information to construct a series of unit cells in three dimensions, and calculates the pairwise intermolecular interaction between a molecule in the origin unit cell and all the other molecules within a fixed radius of 30Å from the central molecule. [15][22][42] The calculation of intermolecular interaction energies were performed using the Momany and Dreiding II force-fields. [17][19] The ranking of the intermolecular interactions by strength

was outputted using the DEBUG-1 function. All visualization of molecular and crystal packing were carried out in Mercury CSD 2020.3. [40]

Morphology and Surface Chemistry calculations. The most likely growth slices and BFDH morphologies were calculated using the BFDH morphology calculation feature in Mercury CSD 2020.3, based on the fact that the facets with the largest interplanar spacing (dhkl) are likely to be morphologically important. [32][40][42][43] For the slices with the largest interplanar spacing, the lattice energy, E_{latt}, was partitioned into a slice energy, E_{sl}, and attachment energy, E_{att}, according to Equation 6.1. [42][44][45]

$$E_{latt} = E_{sl} + E_{att} \quad (6.1)$$

Where the slice energy, E_{sl}, is the summation of all the interactions between a central molecule and all other molecules within a growth slice of thickness dhkl, and the attachment energy, E_{att}, is the summation of all the interactions between the central molecule and molecules outside the growth slice. The attachment energy can be taken to be proportional to the growth rate of that facet, according to Equation 6.2.

$$R \propto E_{att} \quad (6.2)$$

The relative attachment energies of each surface were expressed as centre to facet distances, then used to determine the external morphology based on the "attachment energy rule". Furthermore, the surface anisotropy factor, ε_{hkl}, was calculated to provide a measure as to how satisfied the possible intermolecular interactions of a molecule at a growing surface are when compared to those of a molecule within the bulk, according to Equation 6.3.

$$\varepsilon_{hkl} = \frac{E_{hkl}^{sl}}{E_{latt}} \quad (6.3)$$

6.4 Results

6.4.1 Attachment energy and morphological simulations analysis

The calculated slice energies and attachment energies for the specific surfaces of the four quercetin structures, as well as the anisotropy factors, are shown in Table 6.1. It should be noted that the faces that are grouped together have the same surface properties due to the symmetry of the structures. The surface anisotropy factor, ε_{hkl}, provides the degree of satisfaction of the intermolecular interactions of a molecule at a facet, compared to a molecule in the bulk and can be related to how labile a surface is to accepting molecules from solution, and thus how fast a given facet will grow. For example, for QDH the surface anisotropy factors for the different facets are significantly different. The (010),(0-10) facets are calculated to have 93.1% of the interactions satisfied, compared to the capping surfaces (001),(00-1) and (01-1),(0-11) that both have 35.2% of the interactions satisfied, meaning that those facets are likely to grow significantly faster than the (010) and (0-10) surfaces that grow at a much slower rate and hence become the dominant facets. Figure 6.1 shows the predicted morphologies based on the attachment energy model.

Table 6.1 Slice, attachment and surface energies and anisotropy factor of the important faces predicted by the attachment energy rule for the quercetin structures.

Quercetin anhydrous (QA)

Facet (hkl)	Slice Energy (Kcal/mol)	Attachment Energy (Kcal/mol)	Surface Energy (mJ/m^2)	ε_{hkl}
(101),(10-1),(-101),(-10-1)	-16.6	-6.7	48.6	71.2%
(200),(-200)	-13.9	-9.4	55.6	59.8%
(011),(01-1),(0-11),(0-1-1)	-12.2	-11.1	69.5	52.5%
(111),(11-1),(-111),(-11-1),(1-11),(1-1-1),(-1-11),(-1-1-1)	-9.5	-13.8	76.4	40.9%
(210),(-210),(2-10),(-2-10)	-6.9	-16.5	83.4	29.4%
(020),(0-20)	-5.8	-17.5	76.4	24.9%

Quercetin monohydrate (QMH)

Facet (hkl)	Slice Energy (Kcal/mol)	Attachment Energy (Kcal/mol)	Surface Energy (mJ/m^2)	ε_{hkl}
(002),(00-2)	-23.1	-3.9	62.5	85.6%
(100),(-100)	-18.8	-8.2	76.4	69.6%
(10-2),(-102)	-15.7	-11.3	97.3	58.2%
(11-1),(1-1-1),(-111),(-1-11)	-8.9	-18.2	83.4	32.7%
(110),(1-10),(-110),(-1-10)	-8.4	-18.6	83.4	31.2%
(011),(0-11),(01-1),(0-1-1)	-7.4	-19.6	104.2	27.5%

Quercetin dihydrate (QDH)

Facet (hkl)	Slice Energy (Kcal/mol)	Attachment Energy (Kcal/mol)	Surface Energy (mJ/m^2)	ε_{hkl}
(010),(0-10)	-13.1	-1.0	13.9	93.1%
(100),(-100)	-11.9	-2.2	27.8	84.5%
(-110),(1-10)	-11.3	-2.8	34.7	80.3%
(001),(00-1)	-5.0	-9.1	34.7	35.2%
(01-1),(0-11)	-5.0	-9.2	34.7	35.2%

Quercetin DMSO Solvate (QDMSO)

Face (hkl)	Slice Energy (Kcal/mol)	Attachment Energy (Kcal/mol)	Surface Energy (mJ/m^2)	ε_{hkl}
(011),(01-1),(0-1-1),(0-11)	-26.7	-4.00	20.8	92.0%
(002),(00-2)	-25.1	-2.3	13.9	86.3%
(110),(-110),(1-10),(-1-10)	-24.7	-4.3	13.9	85.1%

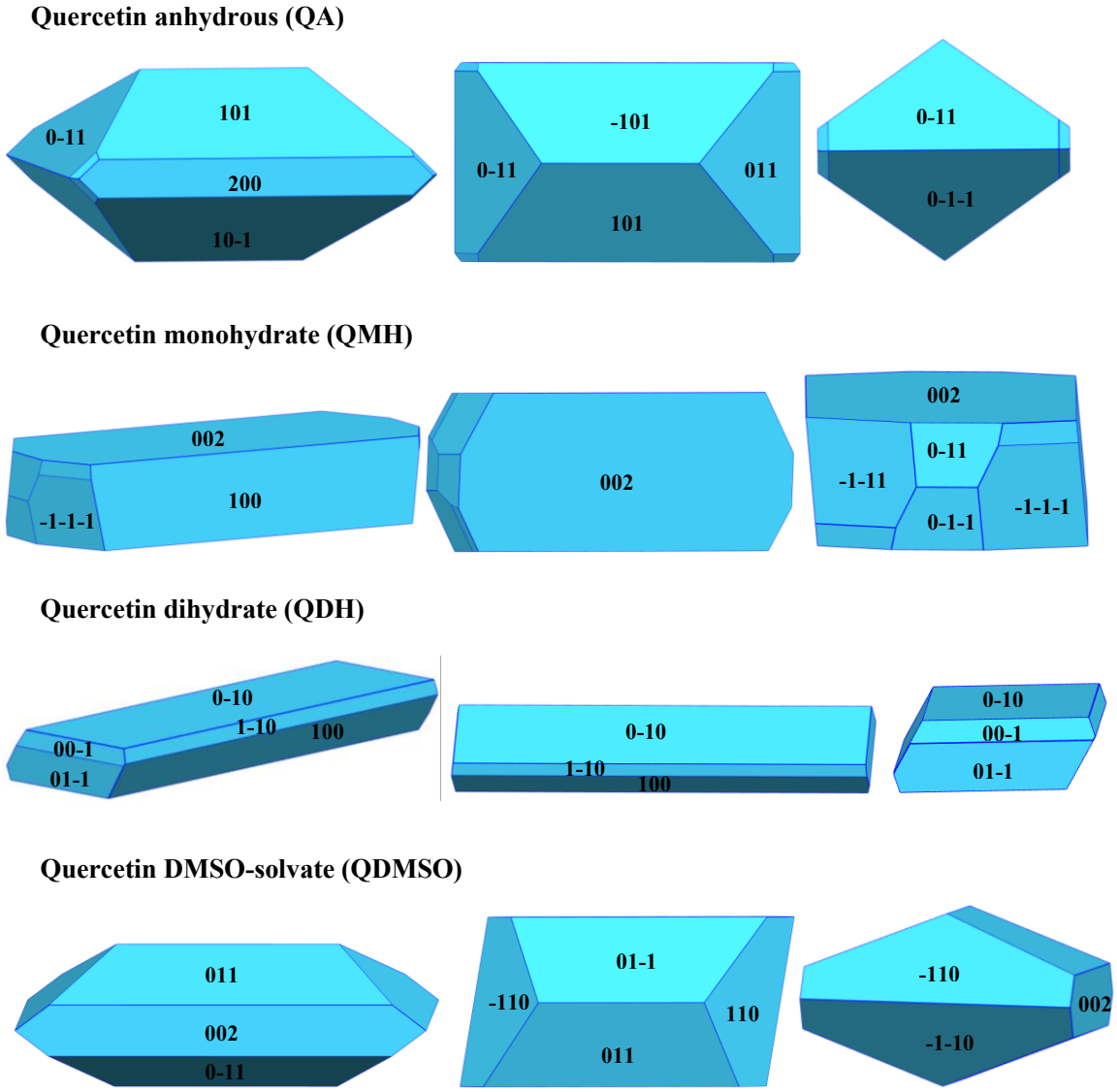

Figure 6.1 Attachment energy morphological predictions for the four different quercetin structures, showing the major faces that are predicted in the final morphology.

The experimental morphologies of QDH and QDMSO, grown from an ethanol-water solvent and a DMSO-water solvent respectively, are shown in Figure 6.2. It should be noted that only these two quercetin forms could be obtained in the laboratory, therefore comparison of modelling to experimental findings will be conducted only for these two crystal structures.

For QDH, SEM images show a needle morphology. The experimental morphology is in a reasonably good agreement with the predicted morphology, showing a large dominant facet that runs along the length of the crystal and a high aspect ratio. The QDH crystal are very small in size comparatively to the QDMSO crystals, approximately 30 microns in length instead of 100 of microns for QDMSO, as shown from the SEM image analysis. The crystals do not seem to have a well-defined shape, and the different faces of the needle crystals, especially the capping faces are not clearly seen from the SEM images. This might impact the experimental surface energy measurements for the QDH crystals. Due to the slow growth kinetic and low water solubility suitable size crystals of QDH for single crystal indexing could not be obtained. Figure 6.3 (a) shows the simulated XRD pattern of QDH as obtained from Mercury software (REFCODE: FEFBEX), and the experimental PXRD pattern from the crystallized sample. Comparing the two, it can be seen that the intensity of certain peaks is enhanced in the experimental pattern. It has been reported in literature that crystalline materials with largely exposed facets tend to orient in a particular direction during XRD analysis, thus the diffraction peaks corresponding to the lattice planes perpendicular to the direction are intensified. [46][47] For QDH, the planes corresponding to the peaks that exhibited considerably higher intensity than the simulated pattern were identified from Mercury, and were found to be planes (020) and (300). The (020) plane is part of the $(0k0)$ indices family, therefore it confirms the presence of a dominant (010) facet on the crystals measured, agreeing with the morphological predictions which give that facet as the most dominant one. Moreover, the (300) plane belongs to the $(h00)$ indices family and confirms the presence of a large exposed (100) facet as was also predicted from the attachment energy model.

For QDMSO, SEM images show a thin, plate-like morphology. From the SEM images, three different facets can be distinguished. One is the large flat surface, and two different side facets of much smaller relative surface area. Comparing the experimental to the simulated PXRD

pattern for QDMSO, Figure 6.3 (b), it is obvious that some peaks have a greatly enhanced intensity compared to some other peaks for QDMSO, which were found to be for the (002), (004), (006) and (008) planes, all belonging to the (00l) indices family. This indicates a large exposure of the (002) facet. Thus, it can be assumed that the large dominant facets of the plate-like crystals shown in the SEM images are the (002),(00-2) facets. This result does not seem to agree with the attachment energy morphological predictions, which give the (011),(01-1),(0-1-1),(0-11) to be the most dominant facets, with an anisotropy factor of $\varepsilon_{hkl} = 92.0\%$, followed by the (002),(00-2) facets, having an $\varepsilon_{hkl} = 86.3\%$. However, it should be considered that the attachment energy model prediction assumes the growth of the crystal to take place in vacuum, and does not account for the external growth conditions, such as the crystallization temperature, supersaturation or interactions of the crystal surfaces with the solvent or solution impurities, which have been shown to significantly affect the crystal habit. [44][48][49][50]

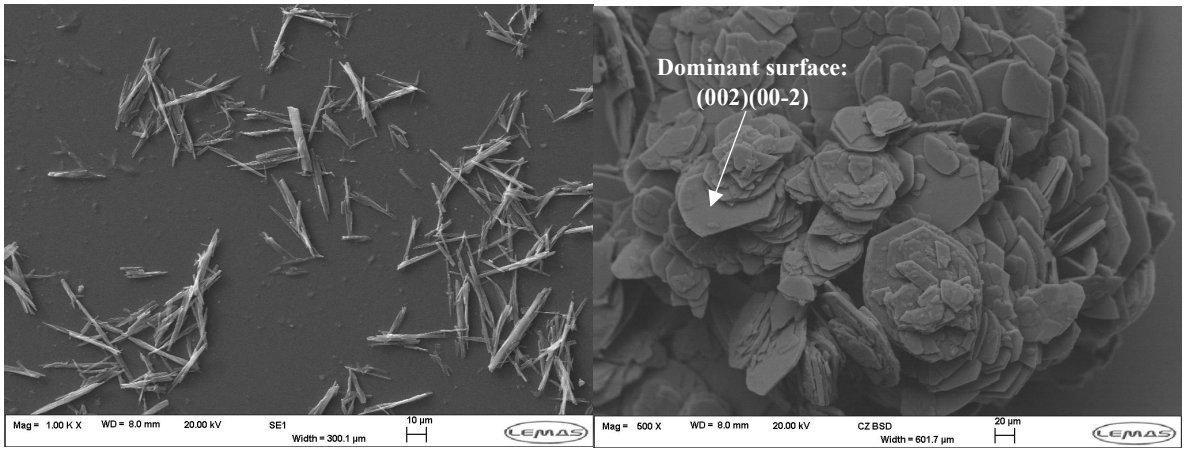

(a) (b)

Figure 6.2 SEM images for (a) QDH grown from an ethanol-water solvent and (b) QDMSO grown from a DMSO-water solvent.

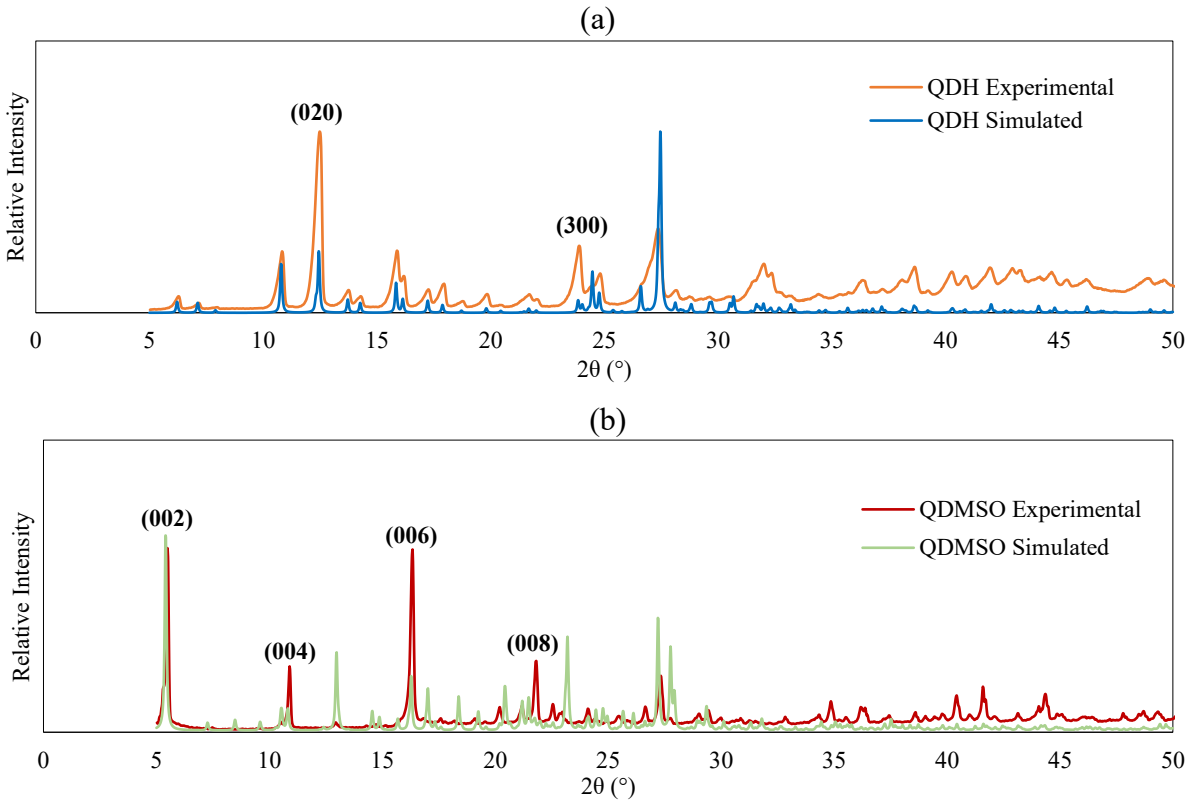

Figure 6.3 PXRD patterns for simulated and experimental crystal structures of (a) QDH and (b) QDMSO.

6.4.2 Surface Chemistry Analysis

The extrinsic synthons and the specific unsaturated interactions that contribute to the attachment energy and growth for the different facets of the QDH and QDMSO structures were calculated and characterised. The six strongest intermolecular synthons found in the lattice of QDH and QDMSO, which contribute to the growth of some of their facets, were calculated in previous publications, and their properties are summarised in Appendix C Table C.1. [31][32]

Quercetin dihydrate (QDH). For the most dominant facet pair (010),(0-10), it was found that none of the first five strongest synthons contribute to the attachment energy, instead synthon QDH6 which is an offset stacking interaction between two quercetin molecules is the main way that the facet pair grows. The strength of that synthon was predicted to be seven times smaller than the strongest synthon in the lattice of QDH, which is consistent with the low attachment

energy and growth rate of the facet. As shown in Table 6.2, the contribution to the growth of this facet pair comes mainly from the exposed -OH groups at the surface termination, which participate in this offset stacking of quercetin molecules. The aromatic hydrogens on the phenyl and pyrone rings that participate in the stacking interaction also show a significant contribution to the growth of the facet. No hydrogen bonding was found to contribute to the growth. The fact that the facet (010),(0-10) terminates with -OH groups but it does not grow via hydrogen bonds is a particularly interesting observation. This behavior could be due to the orientation of the quercetin molecules on the facet that prevents the –OH groups from forming hydrogen bonds with other incoming molecules. Instead, stronger stacking interactions could be preferentially formed to grow this pair of facets. This behavior could indicate that this facet has a non-polar nature.

On the contrary, the facet pair (100),(-100) grows mainly through synthon QDH5, which is a quercetin-water hydrogen bond. The surface termination shows the exposed oxygens on the hydroxyl groups of the pyrone ring of the quercetin molecule which are available to participate in a hydrogen bonding with the water molecules from solution. This justifies the high hydroxyl groups contribution, 72%, to the growth of the facet. It is therefore expected that this facet pair would present a strong polar character.

The needle capping facets (001),(00-1) and (01-1),(1-11) that were predicted to have the highest attachment energy and growth rate, were found to have very similar surface chemistries. The growth direction of these facets is almost parallel to the π-π stacking of the quercetin molecules, the strongest synthon in the structure (QDH1), and it was found to contribute to their growth. This is reflected by the high contribution of the phenyl and pyrone rings to the growth of these facets, shown in Table 6.2. At the same time, hydrogen bonding between hydroxyl groups of the quercetin molecules and water molecules were also found to contribute to the growth (synthons QDH2, QDH4). The quercetin molecules were found to

pack more closely along those facets, which favours the faster growth. Since both π-π stacking interaction and hydrogen bonds contribute to the growth of those facets, it is predicted that these are highly energetic facets with a capability of forming both polar and non-polar interactions.

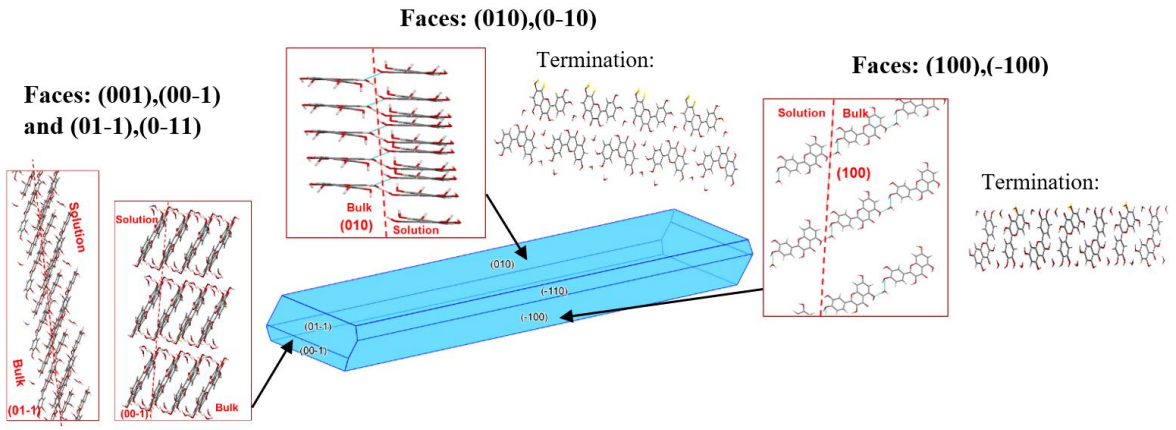

Figure 6.4 Surface chemistry analysis schematic for the habit planes of QDH.

Table 6.2 Functional group contribution to the growth of the habit planes of QDH.

	(010),(0-10)	(100),(-100)	(01-1),(0-11)	(10-1),(-101)
Phenyl & Pyrone rings	32.9%	17.2%	64.3%	64.0%
C=O	18.1%	11.0%	10.4%	10.3%
OH	49.0%	71.8%	25.3%	25.7%

Quercetin DMSO-solvate (QDMSO). For QDMSO the attachment energy model predicted the facet group (011),(01-1),(0-1-1),(0-11) to be of highest morphological importance, followed by the facet pair (002),(00-2) which was in fact shown earlier to be the dominant facet pair for the QDMSO sample prepared experimentally. The facet group (011),(01-1),(0-1-1),(0-11) was found to grow mainly by synthon QDMSO5, which is a non-polar π-π stacking interaction between two quercetin molecules, to which the aromatic rings mainly contribute to the overall interaction, and thus to the growth of those facets. The facet termination prediction confirms

this by showing the phenyl and pyrone rings exposed at the surface. It is, hence, predicted that the (011),(01-1),(0-1-1),(0-11) facets should have a non-polar nature.

On the other hand, the facet pair (002),(00-2) grows mainly from synthon QDMSO4, a double hydrogen bonding interaction between the hydroxyl groups of two quercetin molecules. As seen in Figure 6.5, the hydroxyl groups are exposed at the facet termination. Since the exposed groups can form hydrophilic interactions with polar molecules like DMSO or water, it is suggested that (002),(00-2) should have a polar nature.

As a final comment, it is again demonstrated how the two most morphologically important family of facets in a structure could have so different chemical nature, stemming from the different synthons that contribute to their growth and different functional groups exposed.

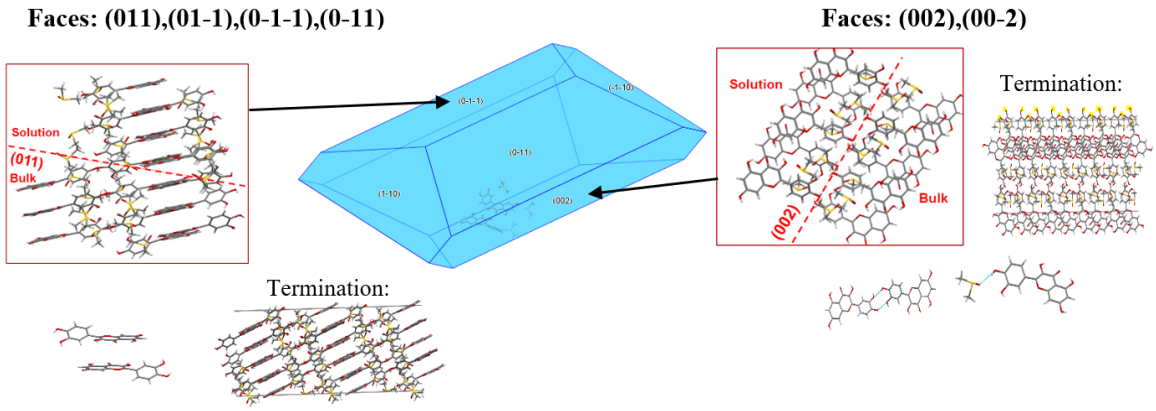

Figure 6.5 Surface chemistry analysis schematic for the habit planes of QDMSO.

6.4.3 Contact Angle measurements and Wettability

The wettability of compressed disks of QDH and QDMSO was assessed by measuring the contact angle of water droplets on their surface, in order to evaluate how these crystals interact with polar solvent, and to assess their overall surface polarity. Facet specific water contact angle measurements were not possible due to the fact that crystals of suitable size for QDH or

QDMSO could not be obtained. This technique measures a single parameter over all sites of a compressed powder surface, and the angle measured is an average depending on the relative area of the different facets present on the surface of the compressed disk. Thus, it does not give a complete picture of the surface anisotropy of a crystal. However, the average hydrophobicity of the two crystal structures tested can be compared and can be related to the surface chemistry of the most dominant facets in each form. The results are shown in Table 6.3.

Table 6.3 Water contact angle measurements for QDH and QDMSO.

QDH water contact angle measurement	48.0 ± 3.2°
QDMSO water contact angle measurement	38.8 ± 1.1°

The lower the water contact angle is, the more hydrophilic the surface. These results show that QDH is relatively more hydrophobic compared to QDMSO. It was earlier shown that the most dominant facets in QDH were (010),(0-10). In the surface modelling section it was demonstrated that the (010),(0-10) facets grow by quercetin-quercetin interactions, and although -OH groups are present at the termination, no hydrogen bonds were observed to form on those facets. It can then be assumed that attachment of water molecules on that facet is not favorable. On the contrary, for QDMSO the most dominant facet pair was shown to be (002),(00-2) and it was predicted to be polar as it grows by quercetin-quercetin hydrogen bonding due to the exposed -OH groups on the quercetin molecules, hence it is reasonable to think that this facet could easily form hydrogen bonds also with different, smaller molecules such as water. These results come in agreement with the contact angle measurements. If it is assumed that the relative area contribution of the most dominant facets is greatest for each form, and the polarity of that facet will contribute more to the overall polarity, then it is well

predicted that the more polar facets (002),(00-2) will interact more strongly with water, thus exhibit a smaller contact angle compared to the QDH.

6.4.4 Inverse Gas Chromatography (IGC)

The contact angle measurements give a quantitative measurement for the bulk polarity of the two solvates studied, but it is not facet specific. IGC goes one step ahead because it can be used to evaluate the surface energy heterogeneity profile of the substances under study, and assess their surface chemistry anisotropy. IGC data give the relationship of the dispersive component of the surface energy at different surface coverages of alkane probe molecules. Since different crystal facets have different adsorption energies, it is expected that for a heterogeneous material, the surface energy will decrease with increasing surface coverage, as at a lower surface coverage the more energetic sites will interact with the alkane probes first. As the surface coverage increases the interaction strength between the probe molecules and the less energetic sites will be weaker. All measurements shown here were carried out at 35°C and 10% RH. To confirm that the two solvates were stable at these conditions, the specific surface area (SSA) of the crystals was measured at different RH, using an octane isotherm Brunauer-Emmett-Teller (BET) method. As de-solvation processes are often associated to changes in shape of a crystal, SSA measurements at different RH values can give an indication of the presence of solid phase transition. To validate the BET SSA measurements, the crystal size distribution for QDH and QDMSO was also measured using image analysis (Morphologi G3). The methodology and results for these are shown in SI. The IGC data for the two quercetin solvates are shown in Figure 6.6, for the dispersive component of the surface energy.

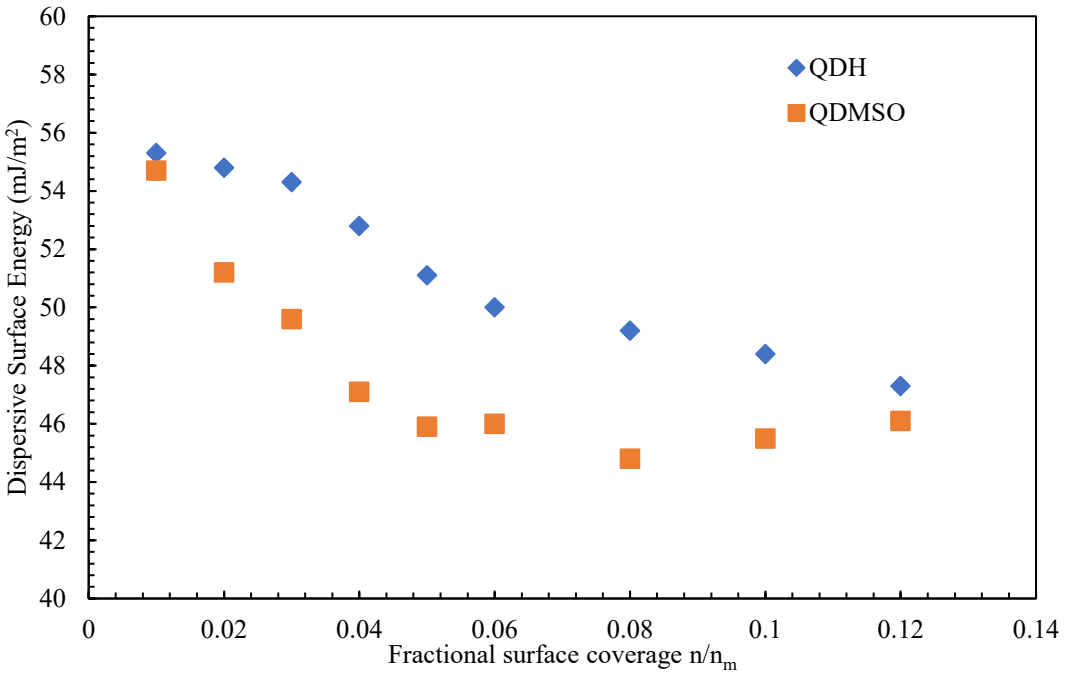

Figure 6.6 Dispersive surface energy as a function of surface coverage for QDH and QDMSO.

The first observation to be made from the IGC data is that both QDH and QDMSO show surface energy heterogeneity, as the surface energy changes as a function of the surface coverage. This goes in line with the modelling calculations that predict facets of both solvates to have different surface chemistries and polarities. The dispersive surface energy changes as the energy of adsorption of the alkane probe molecules changes when it interacts with a different facet. At low fractional surface coverages, the probe molecules will interact with the most energetic sites that can form the strongest non-polar interactions with. At higher fractional surface coverages, the facets that can form weaker interactions with the probe molecules will also start interacting, and this is the reason that the dispersive surface energy component decreases at higher fractional surface coverages. [4][7][23]

When comparing the two solvates, the energy range for QDMSO is higher, from 54.7 mJm^{-2} at a surface coverage of 0.01 to 44.8 mJm^{-2} at a surface coverage of 0.08; whereas QDH only changes from 55.3 mJm^{-2} to 47.3 mJm^{-2} at surface coverages of 0.01 and 0.12 respectively.

This suggests that the anisotropy in surface chemistry and polar nature for the surfaces is greater for QDMSO, as the surface energy span for QDMSO is greater. Surfaces of similar polarity would form interactions of similar strength with the alkane probe molecules. Thus, a higher variance in the energy of interactions of the QDMSO shows a greater heterogeneity in the polar nature of the different facets. Furthermore, the smaller variability in the dispersive surface energy for QDH could be attributed to the fact that these crystals have poorly-defined facets, which might be contributing less to the energies measured by the IGC, as compared to the much more well-defined facets of the QDMSO.

Although the surface energy range for QDMSO is greater, the surface energy seems to reach a plateau after a surface coverage of 0.06, while the surface energy for QDH keeps decreasing even at higher surface coverages. The reason for this could be that the relative surface area of the (002)(00-2) facets in QDMSO is much greater than that of the side facets. In fact, SEM image analysis revealed that the (002)(00-2) facets account for approximately 95% of the total surface area of the QDMSO crystal. This could explain why the dispersive surface energy remains constant above a fractional surface coverage of 0.06, at about 46 mJ/m^2. This could be the energy of interaction of the probe alkane molecules with the (002)(00-2) surface. Since the (002)(00-2) facets were predicted to have a polar surface chemistry, it is expected that they would have a lower interaction energy with the alkane probe molecules than the (011),(01-1),(0-1-1),(0-11) facets. The (011),(01-1),(0-1-1),(0-11) facets were predicted to have a non-polar nature, thus they would form interactions of higher energy and interact with the probe molecules at lower fractional surface coverages, which is probably what is observed in the IGC data.

When the magnitude of the dispersive surface energy is compared for the two structures, it can be seen that at any surface coverage the energy for QDH is higher compared to that of QDMSO. Since the dispersive component of surface energy is a measure of the van der Waal's

interactions, it is suggested that overall the facets of QDH are more non-polar compared to QDMSO. In fact, this was demonstrated in the modelling section where it was shown that the most dominant facet pair of QDH (010),(0-10) is non-polar as it grows mainly by offset π-π stacking interactions, while the largest facet pair for QDMSO (002),(00-2) is polar because it grows by quercetin-quercetin hydrogen bonds.

Overall, the IGC experiments show a good agreement with the surface chemistry prediction from the modelling work, and they demonstrate that both solvates are anisotropic, exhibiting a surface energy heterogeneity for the dispersive component that is greater for QDH, and that QDH is more non-polar compared to QDMSO. Therefore, due to the vast difference that the surface properties of solvates can have, the most desirable surface characteristics, those that will result in the optimal behaviour in a specific application, can be obtained from the synthonic modelling.

6.5 Conclusion

A molecular modelling analysis has been conducted on several solid forms of quercetin, to rationalize the surface properties of this material through the study of the extrinsic synthons and morphologies. The modelling calculations were then compared to experimental work including IGC and contact angle measurements.

Via synthonic modelling the attachment energies and surface anisotropy factor for the different quercetin solid forms were calculated, along with the predicted morphologies. These were compared to SEM images of the crystals and PXRD data. The surface chemistry analysis confirmed the anisotropy of the different solid forms and helped in the characterization of the hydrophobicity of their surfaces.

For QDH the (010),(0-10) faces were predicted to be hydrophobic as they grow mainly by a non-polar offset quercetin-quercetin stacking interactions, while the (100),(-100) faces are

expected to be hydrophilic as the main growth interaction is a polar quercetin-water hydrogen bond. For QDMSO, the dominant face pair (002),(00-2) grows by a strong polar quercetin-quercetin hydrogen bonding interaction, while the second most dominant face group (011),(01-1),(0-1-1),(0-11) grow by non-polar π-π stacking interactions.

The contact angle measurements showed that the QDMSO form has a greater overall surface hydrophilicity compared to QDH. The IGC data demonstrated surface energy heterogeneity for both structures, as the surface energy changed as a function of surface coverage. The data showed a greater heterogeneity in the polar nature of the facets of QDMSO, as it spanned a greater range of surface energies. The dispersive component of the surface energy for QDH was found to be greater than QDMSO at all surface coverages, which indicated a greater overall hydrophobicity for QDH.

In general, the modelling results combined with the experimental findings demonstrated facet-specific anisotropy in the surface properties of the different quercetin solid forms studied. This includes heterogeneous surface energy along the different facets, and different hydrophobicity and polar nature of facets. This information is vital to know when designing solid forms for a particular application. The approach used in this work can be applied to design particles with optimal crystal structure and morphology and to guide the choice of crystallization solvent and other crystallization parameters such as solvent composition and supersaturation that will affect crystal properties.

References

[1] S. R. Byrn, R. R. Pfeiffer, and J. G. Stowell, *Solid-state chemistry of drugs*. West Lafayette, Ind.: SSCI, Inc., 1999.

[2] E. Hadjittofis, M. A. Isbell, V. Karde, S. Varghese, C. Ghoroi, and J. Y. Y. Heng, "Influences of Crystal Anisotropy in Pharmaceutical Process Development," 2018.

[3] R. Ho and J. Y. Y. Heng, "A Review of Inverse Gas Chromatography and its Development as a Tool to Characterize Anisotropic Surface Properties of Pharmaceutical Solids," vol. 30, no. 30, pp. 164–180, 2013.

[4] A. E. Jefferson, D. R. Williams, and J. Y. Y. Heng, "Computing the Surface Energy Distributions of Heterogeneous Crystalline Powders," vol. 25, pp. 339–355, 2011, doi: 10.1163/016942410X525506.

[5] R. R. Smith, U. V Shah, J. V Parambil, D. J. Burnett, F. Thielmann, and J. Y. Y. Heng, "The Effect of Polymorphism on Surface Energetics of D-Mannitol Polymorphs," vol. 19, no. 1, 2017, doi: 10.1208/s12248-016-9978-y.

[6] U. V Shah *et al.*, "Decoupling the Contribution of Surface Energy and Surface Area on the Cohesion of Pharmaceutical Powders," 2014, doi: 10.1007/s11095-014-1459-3.

[7] P. P. Yla, J. Y. Y. Heng, F. Thielmann, and D. R. Williams, "Inverse Gas Chromatographic Method for Measuring the Dispersive Surface Energy Distribution for Particulates," 2008.

[8] Z. Lukman, N. Anuar, N. F. A. Bakar, and N. A. Rahman, "Alpha lactose monohydrate morphology: Molecular modelling and experimental approach," *Int. J. Eng. Technol.*, vol. 7, no. 4, pp. 107–112, 2018.

[9] I. Rosbottom, "Examination of inequivalent wetting on the crystal habit surfaces of RS-ibuprofen using grid-based molecular modelling," pp. 11622–11633, 2018, doi: 10.1039/c7cp08354h.

[10] C. Schmidt and J. Ulrich, "Morphology prediction of crystals grown in the presence of impurities and solvents - An evaluation of the state of the art," *J. Cryst. Growth*, vol. 353, no. 1, pp. 168–173, 2012, doi: 10.1016/j.jcrysgro.2012.05.001.

[11] P. York, "Solid-state properties of powders in the formulation and processing of solid dosage forms," *Int. J. Pharm.*, vol. 14, no. 1, pp. 1–28, 1983, doi: https://doi.org/10.1016/0378-5173(83)90111-4.

[12] R. B. Hammond, K. Pencheva, and K. J. Roberts, "A structural-kinetic approach to

model face-specific solution/crystal surface energy associated with the crystallization of acetyl salicylic acid from supersaturated aqueous/ethanol solution," *Cryst. Growth Des.*, vol. 6, no. 6, pp. 1324–1334, 2006, doi: 10.1021/cg0505618.

[13] R. B. Hammond, S. Jeck, C. Y. Ma, K. Pencheva, K. J. Roberts, and T. Auffret, "An examination of binding motifs associated with inter-particle interactions between facetted nano-crystals of acetylsalicylic acid and ascorbic acid through the application of molecular grid-based search methods," *J. Pharm. Sci.*, vol. 98, no. 12, pp. 4589–4602, Dec. 2009, doi: https://doi.org/10.1002/jps.21758.

[14] V. Ramachandran *et al.*, "Formulation pre-screening of inhalation powders using computational atom-atom systematic search method," *Mol. Pharm.*, vol. 12, no. 1, pp. 18–33, 2015, doi: 10.1021/mp500335w.

[15] G. Clydesdale, K. J. Roberts, and R. Docherty, "HABIT95 — a program for predicting the morphology of molecular crystals as a function of the growth environment," *J. Cryst. Growth*, vol. 166, no. 1–4, pp. 78–83, Sep. 1996, doi: 10.1016/0022-0248(96)00056-5.

[16] G. Clydesdale, K. J. Roberts, G. B. Telfer, and D. J. W. Grant, "Modeling the Crystal Morphology of α-Lactose Monohydrate," *J. Pharm. Sci.*, vol. 86, no. 1, pp. 135–141, 1997, doi: 10.1021/js950496w.

[17] F. A. Momany, L. M. Carruthers, R. F. Mcguire, and H. A. Scheraga, "Intermolecular Potentials from Crystal Data . III . Determination of Empirical Potentials and Application to the Packing Configurations and Lattice Energies in Crystals of Hydrocarbons , Carboxylic Acids , Amines , and Amides1," vol. 78, no. 16, pp. 1595–1620, 1974, doi: 10.1021/j100609a005.

[18] G. Nemethy, M. S. Pottle, and H. A. Scheraga, "Energy parameters in polypeptides. 9. Updating of geometrical parameters, nonbonded interactions, and hydrogen bond interactions for the naturally occurring amino acids," *J. Phys. Chem.*, vol. 87, no. 11, pp. 1883–1887, May 1983, doi: 10.1021/j100234a011.

[19] S. L. Mayo, B. D. Olafson, and W. A. Goddard, "DREIDING: a generic force field for molecular simulations," *J. Phys. Chem.*, vol. 94, no. 26, pp. 8897–8909, Dec. 1990, doi: 10.1021/j100389a010.

[20] A. T. Hagler, S. Lifson, and P. Dauber, "Consistent force field studies of intermolecular forces in hydrogen-bonded crystals. 2. A benchmark for the objective comparison of alternative force fields," *J. Am. Chem. Soc.*, vol. 101, no. 18, pp. 5122–5130, Aug. 1979, doi: 10.1021/ja00512a002.

[21] T. T. H. Nguyen, I. Rosbottom, I. Marziano, R. B. Hammond, and K. J. Roberts, “Crystal Morphology and Interfacial Stability of RS -Ibuprofen in Relation to Its Molecular and Synthonic Structure,” 2017, doi: 10.1021/acs.cgd.6b01878.

[22] I. Rosbottom, K. J. Roberts, and R. Docherty, “The solid state, surface and morphological properties of *p* -aminobenzoic acid in terms of the strength and directionality of its intermolecular synthons,” *CrystEngComm*, vol. 17, no. 30, pp. 5768–5788, 2015, doi: 10.1039/C5CE00302D.

[23] J. Y. Y. Heng, F. Thielmann, and D. R. Williams, “The Effects of Milling on the Surface Properties of Form I Paracetamol Crystals,” vol. 23, no. 8, pp. 1918–1927, 2006, doi: 10.1007/s11095-006-9042-1.

[24] J. Y. Y. Heng, K. Campus, and U. Kingdom, “Determining Surface Energetics of Solid Surfaces,” pp. 1–14.

[25] R. Ho and J. Y. Y. Heng, “A review of inverse gas chromatography and its development as a tool to characterize anisotropic surface properties of pharmaceutical solids,” *KONA Powder Part. J.*, vol. 30, no. 30, pp. 164–180, 2012, doi: 10.14356/kona.2013016.

[26] J. Schultz, L. Lavielle, and C. Martin, “The Role of the Interface in Carbon Fibre-Epoxy Composites,” *J. Adhes.*, vol. 23, no. 1, pp. 45–60, Sep. 1987, doi: 10.1080/00218468708080469.

[27] G. M. Dorris and D. G. Gray, “Adsorption of n-alkanes at zero surface coverage on cellulose paper and wood fibers,” *J. Colloid Interface Sci.*, vol. 77, no. 2, pp. 353–362, 1980, doi: https://doi.org/10.1016/0021-9797(80)90304-5.

[28] G. Z. Jin, Y. Yamagata, and K. Tomita, “Structure of quercetin dihydrate,” *Acta Crystallogr. Sect. C Cryst. Struct. Commun.*, vol. 46, no. 2, pp. 310–313, 1990, doi: 10.1107/S0108270189006682.

[29] S. Domagała, P. Munshi, M. Ahmed, B. Guillot, and C. Jelsch, “Structural analysis and multipole modelling of quercetin monohydrate - A quantitative and comparative study,” *Acta Crystallogr. Sect. B Struct. Sci.*, vol. 67, no. 1, pp. 63–78, 2011, doi: 10.1107/S0108768110041996.

[30] K. Srinivas, J. W. King, L. R. Howard, and J. K. Monrad, “Solubility and solution thermodynamic properties of quercetin and quercetin dihydrate in subcritical water,” *J. Food Eng.*, vol. 100, no. 2, pp. 208–218, 2010, doi: 10.1016/j.jfoodeng.2010.04.001.

[31] P. Klitou, I. Rosbottom, and E. Simone, “Synthonic Modeling of Quercetin and Its Hydrates: Explaining Crystallization Behavior in Terms of Molecular Conformation

and Crystal Packing," *Cryst. Growth Des.*, vol. 19, no. 8, pp. 4774–4783, Aug. 2019, doi: 10.1021/acs.cgd.9b00650.

[32] P. Klitou, C. M. Pask, L. Onoufriadi, I. Rosbottom, and E. Simone, "Solid-State Characterization and Role of Solvent Molecules on the Crystal Structure, Packing, and Physiochemical Properties of Different Quercetin Solvates," *Cryst. Growth Des.*, vol. 20, no. 10, pp. 6573–6584, Oct. 2020, doi: 10.1021/acs.cgd.0c00751.

[33] V. Stanek and J. Szekely, "The effect of surface driven flows on the dissolution of a partially immersed solid in a liquid-analysis," *Chem. Eng. Sci.*, vol. 25, no. 4, pp. 699–715, 1970, doi: https://doi.org/10.1016/0009-2509(70)85099-0.

[34] Q. Li, V. Rudolph, B. Weigl, and A. Earl, "Interparticle van der Waals force in powder flowability and compactibility," *Int. J. Pharm.*, vol. 280, no. 1–2, p. 77—93, Aug. 2004, doi: 10.1016/j.ijpharm.2004.05.001.

[35] J. Shi, S. Das, D. Morton, and P. Stewart, "The Kinetics of De-agglomeration of Magnesium Stearate Dry-Coated Salbutamol Sulphate Powders," *KONA Powder Part. J.*, vol. 32, pp. 131–142, 2015, doi: 10.14356/kona.2015001.

[36] F. Fichtner, D. Mahlin, K. Welch, S. Gaisford, and G. Alderborn, "Effect of Surface Energy on Powder Compactibility," *Pharm. Res.*, vol. 25, no. 12, pp. 2750–2759, 2008, doi: 10.1007/s11095-008-9639-7.

[37] M. Rossi, L. F. Rickles, and W. A. Halpin, "The crystal and molecular structure of quercetin: A biologically active and naturally occurring flavonoid," *Bioorg. Chem.*, vol. 14, no. 1, pp. 55–69, 1986, doi: 10.1016/0045-2068(86)90018-0.

[38] K. Vasisht, K. Chadha, M. Karan, Y. Bhalla, A. K. Jena, and R. Chadha, "Enhancing biopharmaceutical parameters of bioflavonoid quercetin by cocrystallization," *CrystEngComm*, vol. 18, no. 8, pp. 1403–1415, 2016, doi: 10.1039/C5CE01899D.

[39] I. AS, "Discovery Studio Modeling Environment, Release 7.0 [software program]." Accelrys Software Inc., San Diego, 2013.

[40] J. van de Streek and S. Motherwell, "New software for searching the Cambridge Structural Database for solvated and unsolvated crystal structures applied to hydrates," *CrystEngComm*, vol. 9, no. 1, pp. 55–64, 2007, doi: 10.1039/B613332K.

[41] J. J. P. M. Stewart, "MOPAC for Solid-State Physics." Quant. Chem. Prog. Exchange, p. 62.63, 1985.

[42] J. Pickering, R. B. Hammond, V. Ramachandran, M. Soufian, and K. J. Roberts, "Synthonic Engineering Modelling Tools for Product and Process Design," in *Engineering Crystallography: From Molecule to Crystal to Functional Form*, K. J.

Roberts, R. Docherty, and R. Tamura, Eds. Dordrecht: Springer Netherlands, 2017, pp. 155–176.

[43] R. Docherty, G. Clydesdale, K. J. Roberts, and P. Bennema, “Application of Bravais-Friedel-Donnay-Harker, attachment energy and Ising models to predicting and understanding the morphology of molecular crystals,” *J. Phys. D. Appl. Phys.*, vol. 24, no. 2, pp. 89–99, 1991, doi: 10.1088/0022-3727/24/2/001.

[44] P. Hartman, “The attachment energy as a habit controlling factor. III. Application to corundum,” *J. Cryst. Growth*, vol. 49, no. 1, pp. 166–170, 1980, doi: 10.1016/0022-0248(80)90077-9.

[45] “Attachment Energy Model, R.” .

[46] L. Zhang, A. A. S. Gonçalves, and M. Jaroniec, “Identification of preferentially exposed crystal facets by X-ray diffraction,” *RSC Adv.*, vol. 10, no. 10, pp. 5585–5589, 2020, doi: 10.1039/D0RA00769B.

[47] A. Lynch, V. Verma, J. Zeglinski, P. Bannigan, and Å. Rasmuson, “Face indexing and shape analysis of salicylamide crystals grown in different solvents,” *CrystEngComm*, vol. 21, no. 16, pp. 2648–2659, 2019, doi: 10.1039/C9CE00049F.

[48] E. Simone, G. Steele, and Z. K. Nagy, “Tailoring crystal shape and polymorphism using combinations of solvents and a structurally related additive,” *CrystEngComm*, vol. 17, no. 48, pp. 9370–9379, 2015, doi: 10.1039/C5CE01878A.

[49] C. T. Ó’Ciardhá, N. A. Mitchell, K. W. Hutton, and P. J. Frawley, “Determination of the Crystal Growth Rate of Paracetamol As a Function of Solvent Composition,” *Ind. Eng. Chem. Res.*, vol. 51, no. 12, pp. 4731–4740, Mar. 2012, doi: 10.1021/ie2020262.

[50] I. Rosbottom *et al.*, “Influence of Solvent Composition on the Crystal Morphology and Structure of p - Aminobenzoic Acid Crystallized from Mixed Ethanol and Nitromethane Solutions,” pp. 4151–4161, 2017, doi: 10.1021/acs.cgd.7b00425.

CHAPTER 7 - CONCLUSION AND FUTURE DEVELOPMENTS

Relating crystallographic information to the macroscopic properties of crystalline particles is a challenging task. The comprehensive understanding of the synthons that are important in the self-assembly and growth of a crystalline material can help in the prediction of those physiochemical properties, and it can also guide the choice of crystallization conditions that provide a better control and design of crystals with tailored characteristics.

In this doctoral project, the research goals were motivated by the fact that the model substance, quercetin, is a molecule that readily forms solvates with distinct physiochemical properties, which can undergo solid-state transformations under certain conditions. These research questions aimed to provide a link between the synthonic structure of the quercetin solvates to their physiochemical properties and provide an insight into the crystallization behaviour of this molecule.

The main findings from the modelling and experimental work are summarized to provide an answer to those research questions outlined in Chapter 1 of the thesis:

- *What is the solid-form landscape of this important flavonoid substance, and what are the physiochemical properties and transformation conditions of the different solid forms?*

Quercetin was crystallized from a range of solvents, including water, ethanol and DMSO, and solvent mixtures, to explore the solid-form landscape of this molecule. Further to the quercetin forms already known from literature (QA, QMH and QDH), two novel solvate structures of quercetin, QDMSO and QE, and their de-solvated forms were discovered. [1][2][3] QDMSO

was found to crystallize by cooling from aqueous-DMSO solutions ranging from 50%(w/w) to 80%(w/w) DMSO, to give colourless plate-like crystals. Thermal analysis of the structure revealed that at 136°C it de-solvates to give an anhydrous form of quercetin, which is not the same as the anhydrous quercetin (QA) form reported in literature. The same form is also obtained from the dehydration of QDH at 95 °C.

The QE solvate was obtained by slurrying QDH in 100% ethanol at 20 °C. This form is characterized by low stability at ambient conditions, as it can de-solvate at a temperature of 28.5°C to form a novel anhydrous quercetin structure, which is not the same as the de-solvated form obtained thermally starting from either QDH or QDMSO. De-solvation of QE can be also brought about by treating QE in vacuum for 24 hours, or leaving it at ambient conditions for longer periods of time, approximately 16 months.

These new findings add to the knowledge of the solid-form landscape, physiochemical properties and transformation conditions for quercetin, which are extremely useful when designing processes and optimal solid forms for specific applications using this important bioflavonoid substance.

- Rationalize how the level of hydration/solvation of a solid form affects the crystal structure, packing and conformation energetics, in particular: how do the type and strength of the synthons in the lattice change and how does this affect the conformation and packing of the host molecules?

The QA, QMH, QDH system follows Desiraju's d/a ratio rule for the formation of hydrates which says that a structure with a d/a ratio of less than 0.5 is vulnerable to hydrate formation. [4] Quercetin forms hydrates to reduce the imbalance in the d/a ratio from 0.357 towards unity. It was shown that as the degree of hydration and the number of water molecules increases,

hydrogen bonding is more satisfied by interaction with the incorporated water molecules. This is because the water molecules, being much smaller in size compared to quercetin molecules, can be positioned close to the polar groups of the quercetin molecule forming hydrogen bonds. Once hydrogen bonding is satisfied, the quercetin molecules, having a more planar conformation, can pack more closely and efficiently via strong π-π stacking interactions, thus the contribution of π-π stacking interactions increases with hydration level. The more twisted conformation of the quercetin molecules in QA, 31.5°, probably due to the lack of water molecules and the need to satisfy hydrogen bonding interaction between the quercetin molecules, prevents it from forming strong π-π interactions, thus being a structure of lower unit cell density.

The results highlighted the importance of the water molecules in the stabilization of the hydrated crystal structures, and the influence on the hydrogen bonding pattern and the strength and nature of intermolecular interactions.

- Elucidate the role of solvent molecules on the molecular packing and type of synthons in different solvated structures: do different solvent molecules in the lattice form interactions of different strength and polarity? how do these affect the crystal structure and molecular packing?

The comparison of QDMSO to QMH and QDH revealed that the quercetin molecules in QDMSO were less planar, with a torsion angle of around 31° as compared to the much more planar conformation of the two hydrates. This was explained by the bulkier size of the DMSO molecule compared to the water molecules, and the fact that it has no hydrogen bonding hydrogens but only one hydrogen bonding oxygen atom. Due to this, the quercetin molecules in QDMSO must adopt a more twisted conformation to maximize interaction and facilitate the

quercetin-quercetin and quercetin-DMSO hydrogen bonds. Hydrogen bonding in QDMSO is not exclusively satisfied between host-solvent interactions as in QDH, but also between host molecules. This was again justified due to the bulker size of the DMSO molecule, which was unable to be positioned next to all the hydroxyl groups of the quercetin molecule and form the hydrogen bonding interactions. The less planar conformation of quercetin also resulted in QDMSO having a slightly lower unit cell density compared to QMH and QDH. Several and different π-π stacking interactions were obtained in the lattice of QDMSO; however, the intermolecular distances for those interactions were longer compared to the π-π stacking interactions of QMH and QDH, probably for the same reason of the more twisted molecular conformation.

Although the QDMSO structure was less closely packed, and with generally longer intermolecular distances, the energy of the hydrogen bonding interactions in the lattice, both between host and host-solvent molecules, was found to be stronger than that of QMH or QDH. Furthermore, the arrangement of the DMSO molecules in QDMSO showed that these were woven tightly into the arrangement of the quercetin molecules, without any obvious channel for de-solvation. The stronger synergistic hydrogen bonding and lack of an obvious de-solvation route was used to explain the superior thermal stability of QDMSO compared to QDH.

The study of the intermolecular interactions and the lattice were used to explain some of the physiochemical properties of the structures of quercetin.

- How do the solvent molecules relate to the crystallization behaviour and the physiochemical properties of different solvates?

Relating the modelling work to the experimental study of the quercetin structures was limited to only QDH and QDMSO, due to the fact that pure forms of QA and QMH could not be obtained experimentally. Quite often in literature QDH is reported as the most thermodynamically stable form between the three (QA, QMH and QDH), and the difficulty in obtaining pure QA and QMH is emphasized. [5][6][7][8] This goes in line with the modelling work on the quercetin hydrates. The favourable packing arrangements in QDH, particularly the very strong π-π stacking interaction contributing to 38% of the total lattice energy, and the smaller amount of de-solvation and conformational rearrangement needed during crystallization, probably result in the easier crystallization of this form from an aqueous solution. On the contrary, the unfavourable conformation of the quercetin molecules in QA and less efficient packing, play a role in making this structure especially challenging to crystallize. [5][6][7][8]

The thermal study on the stability of QDH and QDMSO revealed that QDH de-solvates at an onset temperature of 95 °C while QDMSO loses the solvent at 136 °C. Synthonic modelling showed that the quercetin-DMSO hydrogen bonds in QDMSO are stronger compared to the quercetin-water hydrogen bonds in QDH. This can explain the higher energy required to break the stronger quercetin-DMSO hydrogen bonds to release the solvent, occurring at a higher temperature.

The moisture-dependent stability study for QDH and QDMSO revealed that both forms are stable over a wide RH range: 10-90% RH for QDH, and 0-80% RH for QDMSO, showing dehydration or possible solid-state transformation at extreme RH (at 0% RH for QDH and 90% RH for QDMSO). Once again, this highlights the importance of the host-solvent interactions and hydrogen bonding in the two structures. It was shown that the host-solvent interactions account for 45.1% and 45.9% of the total lattice energy, for QDMSO and QDH respectively, thus emphasizing how important these interactions are for the formation of stable structures.

- How does surface chemistry vary for the different facets and between different solvates of the same substance? How does the predicted surface chemistry compare to the experimental one?

A study of the morphologies and surface chemistry of the quercetin structures was conducted through the analysis of their facet-specific extrinsic synthons and exposed functional groups at the surface termination. All quercetin structures exhibited surface anisotropy, with varying surface chemistry and surface energy for each facet.

For QDH, the dominant facet pair (010),(0-10) was found to grow mainly by non-polar offset quercetin-quercetin stacking interactions, thus it was considered to have a hydrophobic nature, while the second most dominant face pair (100),(-100) was expected to be hydrophilic as the main growth interaction is a polar quercetin-water hydrogen bond. For QDMSO, the facets (002),(00-2), which almost completely dominate the surface area of this form, were found to grow by strong polar quercetin-quercetin hydrogen bonding interactions, thus expected to have a hydrophilic nature.

Experimental studies on the two crystal structures (water contact angle measurements and IGC studies) confirmed the surface energy heterogeneity and varying surface chemistry for both solvate forms. It was further shown that all facets on QDMSO were more polar compared to those of QDH, as they could not form as strong dispersive surface energy interactions with a non-polar molecule such as with QDH. The results demonstrated how solvates of the same substance could exhibit substantial differences in their surface chemistry and how a study of the extrinsic growth synthons can enable the understanding and design of particles with desired surface characteristics.

In general, the work presented in this doctoral project has demonstrated a strong correlation between the crystallographic characteristics, and more specifically the synthons' type and strength, to experimental observations regarding the physiochemical properties and the crystallization behaviour of quercetin solvates. This multiangle characterization method, which couples computational and experimental techniques, can be extended to other solvated crystalline structures and can be used to better understand the relationship between crystal structure and product properties.

The presented work can assist in the ongoing effort to design crystallization processes, and the methodology proposed can be used as a tool to guide crystallization conditions in order to engineer crystals with optimal physiochemical characteristics, including morphology and surface chemistry. This will ultimately lead to more efficient product formulations and faster development.

Future developments

- The work in this doctoral thesis has looked at the effect of two different solvent molecules, water and DMSO, on the intermolecular interactions and packing of quercetin molecules in solvated structures, and subsequently the impact on the physiochemical properties of each structure. It would be interesting to look at the effect of other different solvent molecules, to further evaluate how the solvent molecule's size, polarity, abundancy of donors and acceptors and their electronegativity affect the synthons and packing and what effect that would have on the particle properties. A molecule like quercetin would be ideal for this study as it has been shown to be prone to solvate formation.

- While synthonic modelling can be used to predict some physiochemical properties of structures by linking the synthonic structure to macroscopic properties, more needs to be understood about the self-assembly of molecules during nucleation. Experimental techniques, such as Near-edge X-ray absorption fine structure spectroscopy (NEXAFS), have been used to provide molecular-level information about the supersaturated state from which nucleation occurs. It would be extremely useful if modelling tools were developed to provide information about the solute-solute and solute-solvent interactions during that prenucleation state. Such knowledge would allow the prediction of crystallization environments, for example the solvent, which would drive the formation of specific structures with desired properties. That could help direct the choice of crystallization conditions for many processes.
- The facet-specific surface characterization of quercetin was not possible due to the fact that crystals of quercetin large enough for facet-specific measurements could not be obtained. Experimental facet-specific surface characterization could be performed on the crystals of a different compound that can grow to a suitable size, using techniques such as atomic force microscopy (AFM), chemical force microscopy (CFM) or facet-specific wettability measurements, such as water contact angle measurements. That would permit a direct comparison with the modelling calculations and allow a model improvement for more accurate surface chemistry calculations.
- In the work it was shown that quercetin is a molecule that can form a range of solvated structures which, upon de-solvation, give rise to different anhydrous forms of the molecule. The use of Gaussian modelling and Density Functional Theory (DFT) could be employed to further investigate into the de-solvation behaviour, predict the anhydrous quercetin PXRD patterns and elucidate structural differences between them. The solvated forms could be relaxed to remove the solvent molecules and be optimized

to a lower energy to generate the de-solvated structures of quercetin. This could explain why certain solvated forms de-solvate to the same or to different anhydrous polymorphs, and gain a deeper understanding regarding the re-arrangement of quercetin molecules after the loss of the solvent from the lattice.

References

[1] K. Vasisht, K. Chadha, M. Karan, Y. Bhalla, A. K. Jena, and R. Chadha, "Enhancing biopharmaceutical parameters of bioflavonoid quercetin by cocrystallization," *CrystEngComm*, vol. 18, no. 8, pp. 1403–1415, 2016, doi: 10.1039/C5CE01899D.

[2] S. Domagała, P. Munshi, M. Ahmed, B. Guillot, and C. Jelsch, "Structural analysis and multipole modelling of quercetin monohydrate - A quantitative and comparative study," *Acta Crystallogr. Sect. B Struct. Sci.*, vol. 67, no. 1, pp. 63–78, 2011, doi: 10.1107/S0108768110041996.

[3] M. Rossi, L. F. Rickles, and W. A. Halpin, "The crystal and molecular structure of quercetin: A biologically active and naturally occurring flavonoid," *Bioorg. Chem.*, vol. 14, no. 1, pp. 55–69, 1986, doi: 10.1016/0045-2068(86)90018-0.

[4] G. R. Desiraju, "Hydration in organic crystals: prediction from molecular structure," *J. Chem. Soc.{,} Chem. Commun.*, no. 6, pp. 426–428, 1991, doi: 10.1039/C39910000426.

[5] K. Srinivas, J. W. King, L. R. Howard, and J. K. Monrad, "Solubility and solution thermodynamic properties of quercetin and quercetin dihydrate in subcritical water," *J. Food Eng.*, vol. 100, no. 2, pp. 208–218, 2010, doi: 10.1016/j.jfoodeng.2010.04.001.

[6] J. Hanuza *et al.*, "Vibrational Spectroscopy Molecular structure and vibrational spectra of quercetin and quercetin-5 ' -sulfonic acid," vol. 88, pp. 94–105, 2017, doi: 10.1016/j.vibspec.2016.11.007.

[7] X. Filip, I. Grosu, and M. Micla, "NMR crystallography methods to probe complex hydrogen bonding networks : application to structure elucidation of anhydrous quercetin 3," pp. 4131–4142, 2013, doi: 10.1039/c3ce40299a.

[8] G. S. Borghetti, J. P. Carini, S. B. Honorato, A. P. Ayala, J. C. F. Moreira, and V. L. Bassani, "Thermochimica Acta Physicochemical properties and thermal stability of quercetin hydrates in the solid state," *Thermochim. Acta*, vol. 539, pp. 109–114, 2012, doi: 10.1016/j.tca.2012.04.015.

APPENDIX A – SUPPORTING INFORMATION FOR CHAPTER 4

Table A.1 Crystal Data and Structure Refinement for QDMSO.

Empirical formula	$C_{18}H_{19}O_{8.5}S_{1.5}$
Formula weight	419.42
Temperature/K	119.99(10)
Crystal system	Monoclinic
Space group	I2/a
a/Å	17.42258(8)
b/Å	13.09931(7)
c/Å	33.11034(16)
α/°	90
β/°	99.5873(4)
γ/°	90
Volume/Å^3	7451.02(6)
Z	16
ρ_{calc}g/cm^3	1.496
μ/mm^{-1}	2.506
F(000)	3504.0
Crystal size/mm^3	0.55 × 0.36 × 0.06
Radiation	CuKα (λ = 1.54184)
2Θ range for data collection/°	7.272 to 147.678
Index ranges	$-21 \leq h \leq 21$, $-15 \leq k \leq 16$, $-41 \leq l \leq 40$
Reflections collected	74992
Independent reflections	7487 [R_{int} = 0.0427, R_{sigma} = 0.0165]
Data/restraints/parameters	7487/25/569
Goodness-of-fit on F^2	1.039
Final R indexes [I>=2σ (I)]	R_1 = 0.0351, wR_2 = 0.0981
Final R indexes [all data]	R_1 = 0.0370, wR_2 = 0.0998
Largest diff. peak/hole / e Å^{-3}	0.39/-0.50

Table A.2 Hydrogen bond parameters in QDMSO.

Molecules involved	Atoms involved	Bond distance (Å)	Atom-atom interaction Energy (kcal.mol^{-1})
Q1 & Q2	H19-O13	2.11	-7.125
Q1 & Q2	O6-H29	2.02	-6.970
Q1 & D3	H21-O3	1.98	-13.404
Q1 & D1	H22-O1	2.05	-14.207
Q1 & D1	H23-O1	2.02	-14.910
Q2 & Q1	H31-O8	1.96	-4.622

Q2 & Q2	H33-O16	2.19	-5.531
Q2 & Q2	O16-H33	2.19	-5.531
Q2 & D2	H32-O2	1.79	-0.750

Table A.3 Comparison of quercetin structures.

	QDMSO			**QDH**			**QMH**			**QA**		
Unit cell Density (u/Å^3)	0.900			0.964			1.007			0.702		
Quercetin molecule torsion angle (phenyl to pyrone ring)	30.71° for Q1 31.11° for Q2			6.74°			-1.04°			31.48°		
Interactions' contribution to lattice energy:*												
Quercetin – Quercetin	45.1%			53.8%			72.6%			100%		
Quercetin – Solvent	45.1%			45.9%			27.2%			-		
Solvent – Solvent	9.7%			0.3%			0.2%			-		
Contribution of Van der Waals interactions to lattice energy*	60.8%			91.2%			89.1%			92.1%		
Contribution of hydrogen bonds and dipole-dipole interactions to lattice energy*	39.2%			8.8%			10.9%			7.9%		
Q-Q H-bonds (per quercetin molecule)	3 for Q1 5 for Q2			0			6			6		
Number of quercetin-solvent H-bonds (per quercetin molecule)	3 for Q1 1 for Q2			6			4			-		
Main synthons	**QDMSO1**	**QDMSO2**	**QDMSO3**	**QDH1**	**QDH2**	**QDH3**	**QMH1**	**QMH2**	**QMH3**	**QA1**	**QA2**	**QA3**
Type	π-π stacking	π-π stacking	H-bond (Q-Q)	π-π stacking	H-bond (Q-W)	Permanent dipole-dipole	π-π stacking	H-bond (Q-Q)	H-bond (Q-W)	H-bond	H-bond	H-bond
Intermolecular distance (Å)	5.83	5.05	8.36	3.67	5.64	9.14	4.85	7.99	5.93	6.93	7.57	11.24
Synthon Energy (kcal/mol)	-7.37	-5.74	-5.42	-7.66	-1.61	-1.43	-6.39	-5.33	-2.55	-4.26	-2.86	-1.57
% contr. to lattice energy	6.2%	4.8%	4.5%	37.8%	7.9%	3.5%	24.5%	10.2%	9.8%	38.4%	25.8%	14.1%

* Based on the energy of the interactions

Table A.4 DSC-TGA thermal analysis data for QDH and QDMSO.

Guest molecule	H_2O	DMSO
Mw	18.02	78.13
Stoichiometry	1:2	1:1.5
Calculated weight loss (%)	10.7	27.9
Observed weight loss TGA (%)	10.0 ± 0.5	26.4 ± 0.3
Guest loss Temp. (°C)	94.9 ± 2.7	135.9 ± 2.8
ΔH for guest loss (Jg^{-1})	-300.3 ± 70.6	-165.2 ± 23.4
Melting Temp. (°C)	315.8 ± 4.7	317.1 ± 4.0
ΔH for melting (Jg^{-1})	-95.8 ± 32.1	-53.1 ± 2.9
Decomposition Temp. (°C)	330.0 ± 2.9	331.1 ± 2.0

APPENDIX B - SUPPORTING INFORMATION FOR CHAPTER 5

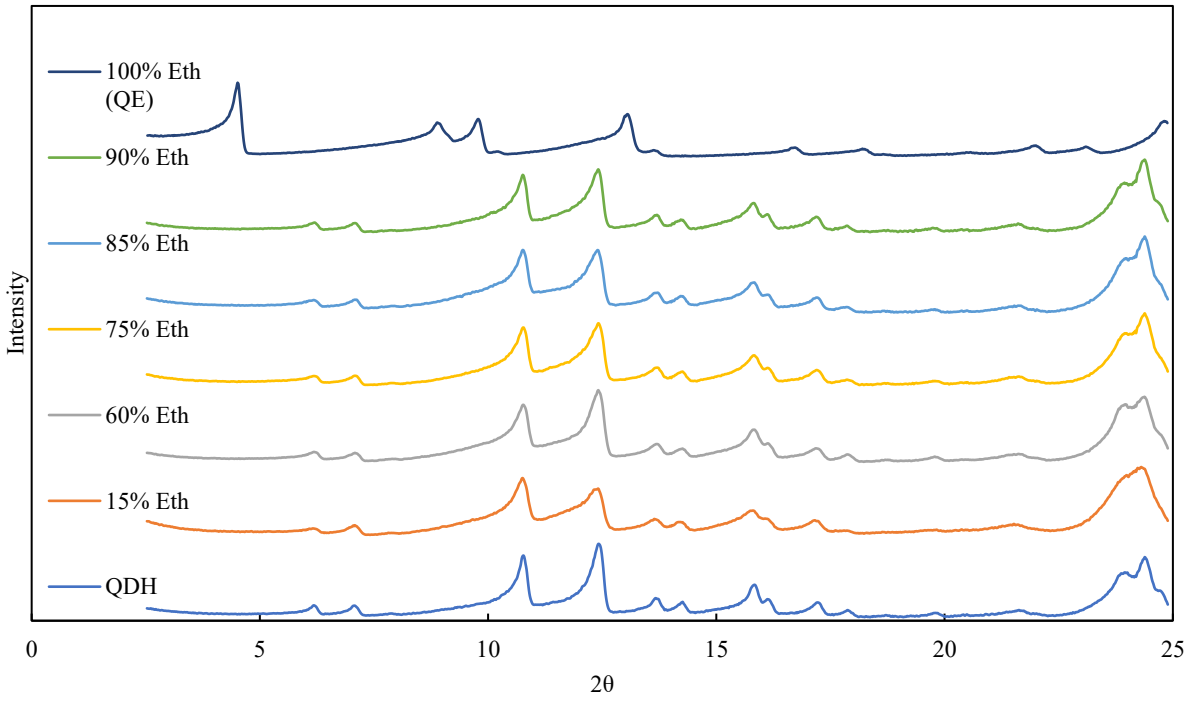

Figure B.1 SAXS/WAXS patterns for samples from slurrying experiments for solvent ratios from 15%(w/w) ethanol to 100% ethanol.

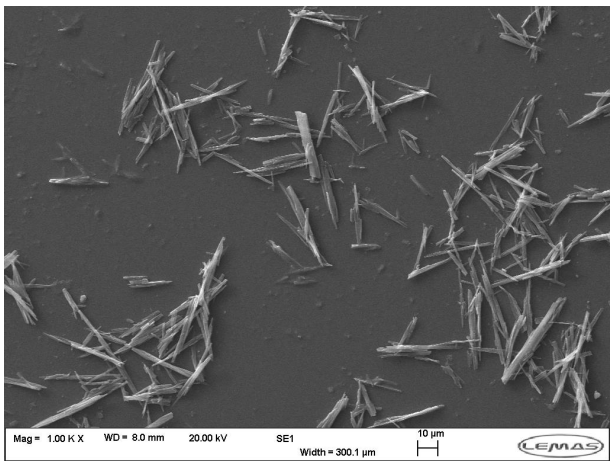

Figure B.2 SEM image of QDH crystals from 70% ethanol (w/w) 30% water solvent.

QE mass loss over time experiments

Dynamic Vapour Sorption Experiment: The results from the DVS experiment are shown in Figure B.3. The data shows that there is a decrease in the mass of the sample for approximately the first 30 minutes, which should be due to the evaporation of the liquid ethanol from the slurry. After that, the mass of the sample appears to be constant. At time t=100 min, the recorded rate of mass change is -0.004 %/min, and after t=288 min the rate becomes 0 %/min. This shows that a time of approximately 300 minutes was enough to dry the specific sample completely and after that no further loss of mass was recorded.

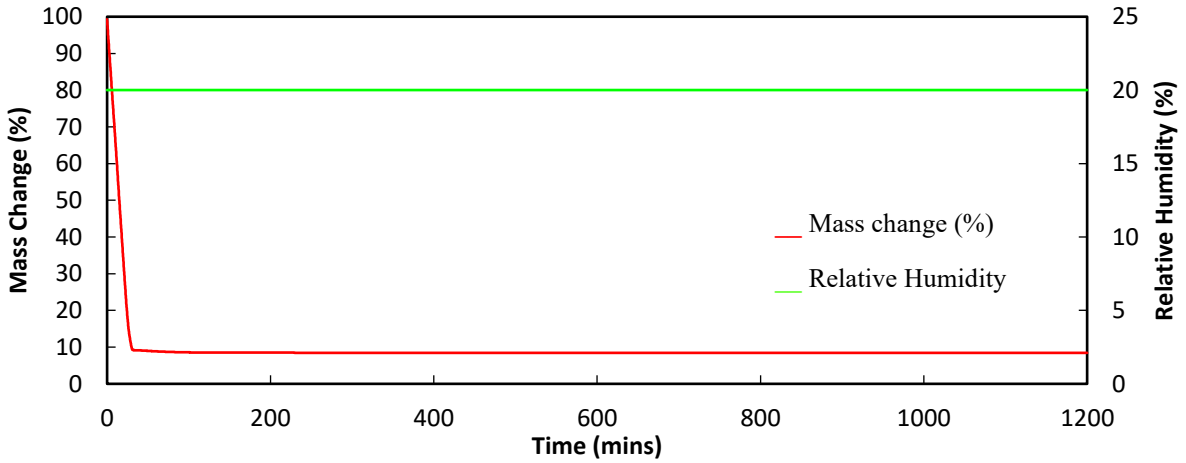

Figure B.3 DVS data for QE slurry at constant temperature of 20°C and relative humidity of 20%.

Monitoring mass sample of QE over time: The results of this experiment, illustrated in Figure B.4, show that the mass of the sample decreases considerably from day 0, which is the day the sample is filtered, to day 1. This initial loss is due to the sample still being wet with ethanol after filtration and the mass loss is due to the evaporation of ethanol. It is assumed that the loss is only due to drying, as suggested by the X-ray data which show that the structure does not change within a time of 4 weeks (See Stability Studies Section). However, after day 1 the mass appears to be fairly stable. Assuming that the sample is dry on day 1, and that being 100% of

the mass, the mass change from day 1 to day 6 is found to be 0.8%. The change in mass is not considerable to be associated with any de-solvation event of the sample during the specific timeframe.

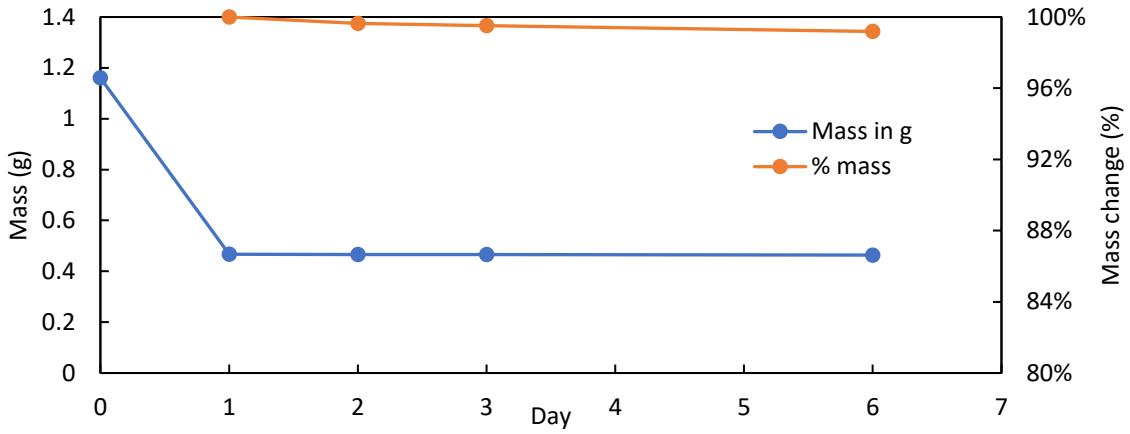

Figure B.4 QE mass loss over time in laboratory conditions

APPENDIX C – SUPPORTING INFORMATION FOR CHAPTER 6

Table C.1 Summary of the six strongest bulk intermolecular synthons for QDMSO and QDH and their properties. [1]

	QDMSO Intermolecular Interactions						QDH Intermolecular Interactions					
Main synthons	**QDMSO1**	**QDMSO2**	**QDMSO3**	**QDMSO4**	**QDMSO5**	**QDMSO6**	**QDH1**	**QDH2**	**QDH3**	**QDH4**	**QDH5**	**QDH6**
Type	π-π stacking	π-π stacking	H-bond (Q-Q)	H-bond (Q-Q)	π-π stacking	H-bond (Q-D)	π-π stacking	H-bond (Q-W)	Permanent dipole-dipole	H-bond (Q-W)	H-bond (Q-W)	Offset stacking
Intermolecular distance (Å)	5.83	5.05	8.36	13.12	6.69	5.27	3.67	5.64	9.14	6.60	6.69	8.12
Synthon Energy (kcal/mol)	-7.37	-5.74	-5.42	-4.87	-4.24	-4.14	-7.66	-1.61	-1.43	-1.40	-1.15	-1.07
% contribution of aromatic rings to synthon	55.8	74.4	54.4	21.3	63.6	33.3	66.7	11.3	56.0	5.4	17.2	33.0
% contribution of hydroxyl groups to synthon	22.2	15.2	34.5	83.1	34.3	45.2	23.0	72.7	27.1	91.8	71.8	49.0
% contribution of carbonyl bond to synthon	22.0	10.4	11.1	−4.4	2.0	21.5	10.3	15.7	16.9	2.8	11.0	18.1

BET analysis of Quercetin dihydrate and Quercetin DMSO crystals using Inverse Gas Chromatography at different RH

Method

BET using IGC

The Quercetin crystals were studied for their BET using Inverse Gas Chromatography, IGC surface energy analyser (IGC *SEA*, SMS, UK). Due to the difference in the specific surface areas of the 2 samples different amounts of samples were used for the analysis. About 25 mg of the Quercetin dihydrate and 115 mg of Quercetin DMSO sample was packed into a silanised glass column (internal diameter = 4 mm) and plugged with silanised glass wool on both the ends. A jolting voltameter (Surface Measurement Systems, London, UK) was used to provide mechanical tapping to the sample in order to remove the voids in the packed sample bed. The packed sample column was analysed using Octane as a solvent at 10% RH , 30% RH and 50% RH conditions at a temperature of 35°C. Prior to BET measurement, the sample column was conditioned at the same RH and temperature conditions for a period of 2 h with Helium as a carrier gas at 10 ml · min^{-1} carrier gas flow. Methane was used as a reference gas to determine the dead volume.

Results

Table C.2 Specific surface area using octane isotherm in IGC

Quercetin dihydrate

RH (%)	BET SSA (m^2/g)
10	31.4
30	31.1
50	31.4

Table C.3 Specific surface area using octane isotherm in IGC

Quercetin DMSO

RH (%)	BET SSA (m^2/g)
10	6.3
30	6.2
50	6.4

The BET SSA values for both QDH and QDMSO do not change considerably as a function of the RH. As de-solvation processes are often associated to changes in shape of a crystal, the constant SSA values indicate that the two structures do not undergo any de-solvation process within the RH range tested.

Morphologi G3 size measurements

Morphologi G3 is a particle characterization technique using imaging and data analysis, which can measure the particle size and shape distribution of extremely large number of crystals. The technique measures the area of a 2D image of the particle which can be used to calculate a circle equivalent diameter distribution.

The Circle Equivalent (CE) diameters for QDH and QDMSO are shown in the figures below.

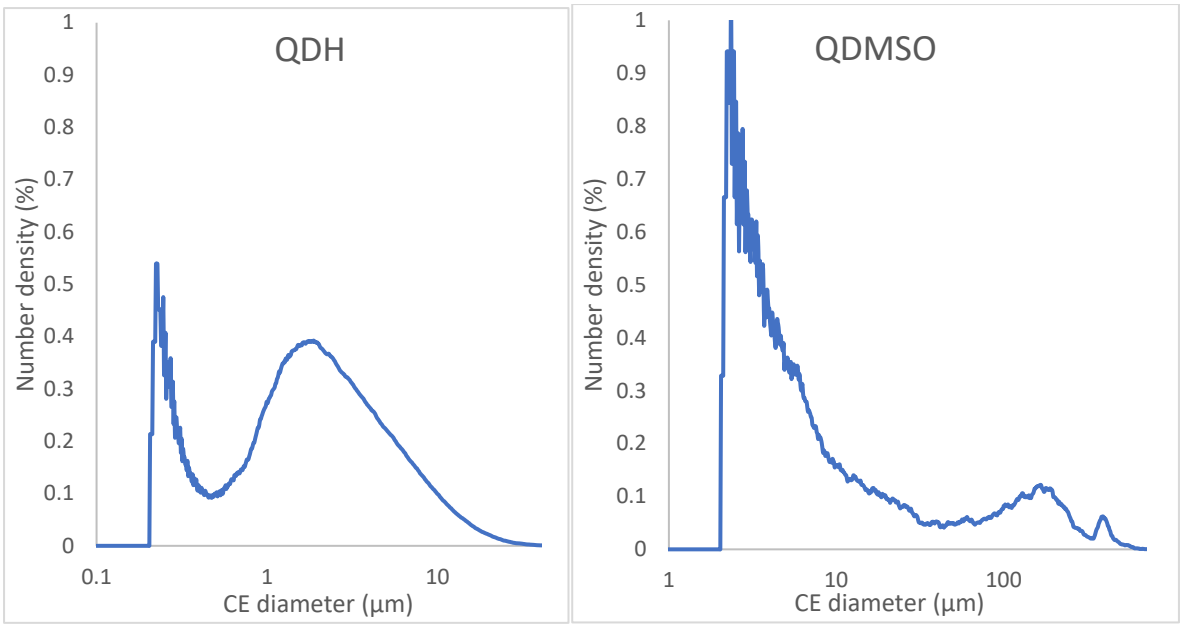

Figure C.1 Circle Equivalent (CE) diameters for QDH and QDMSO

For the QDH crystal specific surface area (SSA) approximation from the Morphologi G3 measurements, certain assumptions had to be made:

1. The QDH crystals have rectangular cuboid shape.
2. The aspect ratio of the crystals (width/length) was 0.56 for the whole population. This was the peak aspect ratio measured by the technique.
3. The thickness of the crystals is 1/3 of the width. This assumption was made based on measurements taken from SEM images of QDH which showed that usually the thickness was 1/3 of the width.

The density of QDH (1600.24 kg/m^3) was used to calculate the mass based on the predicted volume.

The predicted SSA for QDH was 10.18 m^2/g. This is approximately 3 times smaller than the SSA measured from the BET octane isotherm method before the IGC. However, it is expected

that the prediction from the Morphologi G3 data is greatly underestimated due to the significant degree of agglomeration of the QDH crystals which the software recognizes as a single particle. This means that the agglomerated sides of the crystals would not contribute to the predicted SSA. An example of agglomerated QDH crystals is shown below.

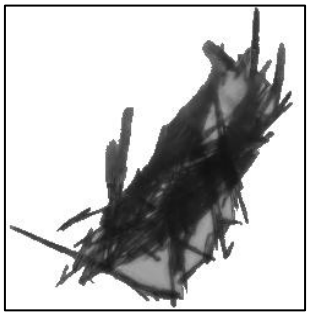

Figure C.2 Agglomerated QDH crystals shown on Morphologi G3 size measurement tool.

For the QDMSO SSA prediction, different assumptions were made:

1. The shape of the QDMSO crystals are circular plates.
2. The thickness of the plates is 0.026 times the circle equivalent diameter of the circular surface.

The SSA was calculated to be 11.39 m2/g, where as the BET measured one was 6.3 m2/g. This overestimation is likely to be due to the overlapping agglomeration of the QDMSO crystals as seen from the software imaging. Example image is shown below.

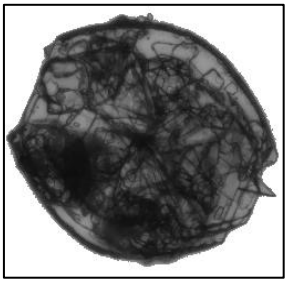

Figure C.3 Agglomerated QDMSO crystals shown on Morphologi G3 size measurement tool.

[1] P. Klitou, C. M. Pask, L. Onoufriadi, I. Rosbottom, and E. Simone, “Solid-State Characterization and Role of Solvent Molecules on the Crystal Structure, Packing, and Physiochemical Properties of Different Quercetin Solvates,” *Cryst. Growth Des.*, vol. 20, no. 10, pp. 6573–6584, Oct. 2020, doi: 10.1021/acs.cgd.0c00751.